Dissertation

# Cyclic di-adenosine monophosphate metabolism and functions in *Streptomyces venezuelae*

zur Erlangung des akademischen Grades

Doctor rerum naturalium
(Dr. rer. nat.)
im Fach Biologie

eingereicht an der Lebenswissenschaftlichen Fakultät
der Humboldt-Universität zu Berlin
von

**M. Sc. Andreas Latoscha**

Präsidentin der Humboldt-Universität zu Berlin

Prof. Dr.-Ing. Dr. Sabine Kunst

Dekan der Lebenswissenschaftlichen Fakultät

Prof. Dr. Dr. Christian Ulrichs

Gutachter/in: 1. Prof. Dr. Natalia Tschowri

2. Prof. Dr. Marc Erhardt

3. Prof. Dr. Fabian M. Commichau

Tag der mündlichen Prüfung: 19.04.2021

Diese Dissertation wurde in der Arbeitsgruppe von Dr. Natalia Tschowri an der Humboldt-Universität zu Berlin zwischen Dezember 2016 und Oktober 2020 angefertigt.

# Publikationen

Ein Teil der vorliegenden Dissertation ist in der folgenden Publikation enthalten:

**Latoscha, A.***, Drexler, D. J.*, Al-Bassam, M. M., Bandera, A. M., Kaever, V., Findlay, K. C., Witte, G., & Tschowri, N. (2020). c-di-AMP hydrolysis by the phosphodiesterase AtaC promotes differentiation of multicellular bacteria. *Proc Natl Acad Sci U S A*, 117(13), 7392-7400. https://doi.org/10.1073/pnas.1917080117

*) contributed equally

Weitere Publikationen:

**Latoscha, A.***, Wörmann, M. E.*, & Tschowri, N. (2019). Nucleotide second messengers in *Streptomyces*. *Microbiology (Reading)*, *165*(11), 1153-1165. https://doi.org/10.1099/mic.0.000846

*) contributed equally

**Latoscha, A.***, Drexler, D. J.*, Witte, G., & Tschowri, N (2021). Assessment of Diadenylate Cyclase and c-di-AMP-phosphodiesterase Activities Using Thin-layer and Ion Exchange Chromatography. *Bio Prot*, 11(1):e3870. https://doi.org/10.21769/BioProtoc.3870

*) contributed equally; corresponding authors

# Danksagung

An erster Stelle möchte ich mich bei meiner Betreuerin Prof. Dr. Natalia Tschowri für die Möglichkeit bedanken mit ihrer Unterstützung und Leitung dieses spannende Projekt bearbeiten zu können. Ich bedanke mich insbesondere für die gute Kommunikation, regelmäßige Projektbesprechungen und für vielfältige Möglichkeiten meine Arbeit selbständig zu gestalten und bei zahlreichen Konferenzen präsentieren zu können.

Des Weiteren gilt mein großer Dank den ehemaligen und aktuellen Mitgliedern der AG Tschowri für die angenehme, lockere Arbeitsatmosphäre und zahlreiche hilfreiche Diskussionen (oder auch einfach Gespräche) während der Kaffeepausen, welche natürlich ohne die Mitglieder der AG Hengge nur halb so spannend gewesen wären.

Ich danke PD Dr. Gregor Witte, Dr. David Drexler und Adrian Bandera für ihr Engagement und Mühe mit dem AtaC-Paper, welche den Umfang des Papers erheblich erweiterten und wertvolle Erkenntnisse lieferten. In diesem Zusammenhang bedanke ich mich auch bei Kim Findlay für die SEM Aufnahmen, PhD Mahmoud Al-Bassam für die PDE-Liste und weitere bioinformatische Analysen und Prof. Dr. Volkhard Kaever für die Nukleotidmessungen.

Ich bedanke mich bei Prof. Dr. Fabian Commichau für die genomische DNA zur Generierung des PgpH-Überexpressionskonstruktes, bei Prof. Dr. Jörg Stülke für den *E. coli* LB2003 Stamm und bei Prof. Dr. Thomas Eitinger für den T18-Antikörper.

Mein größter Dank und tiefste Liebe gilt meinen Kindern Alexej und Sophia und meiner Frau Sabine, die mich immer bedingungslos unterstützt und insbesondere während der letzten Monate des Schreibens viel Geduld mit mir gezeigt haben.

# Table of Content

# List of Figures

# List of Appendix Figures



# List of Tables

# List of Abbreviations

| | |
|---|---|
| **°C** | Degree Celsius |
| **α** | anti |
| **aa** | Amino acids |
| **A** | Ampere |
| **Amp** | Ampicillin |
| **Apr** | Apramycin |
| **APS** | Ammonium persulfate |
| **BACTH** | Bacterial Adenylate Cyclase Two-Hybrid assay |
| **bp** | Base pairs |
| **c-di-AMP** | bis-(3′,5′)-cyclic di-adenosine monophosphate |
| **$CaCl_2$** | Calcium chloride |
| **$Ca(NO_3)_2$** | Calcium nitrate |
| **CFU** | Colony forming units |
| **Cm** | Chloramphenicol |
| **d** | day |
| **DAC** | Diadenylate cyclase |
| **$ddH_2O$** | Double distilled water |
| **DMSO** | Dimethyl sulfoxide |
| **DNA** | Deoxyribonucleic acid |
| **DTT** | Dithiothreitol |
| **DRaCALA** | Differential Radial Capillary Action of Ligand Assay |
| **$FeCl_3$** | Iron(III) chloride |
| **g** | gram |
| **gDNA** | Genomic DNA |
| **$H^+$** | Proton / Hydrogen ion |
| **HCl** | Hydrochloric acid |
| **HEPES** | 4-(2-hydroxyethyl)-1-piperazineethanesulfonic acid |
| **HRP** | Horseradish peroxidase |
| **GST** | Glutathione S-transferase |
| **h** | hour |
| **His** | Histidine |
| **Hyg** | Hygromycin B |
| **IPTG** | Isopropyl-β-D-thiogalactopyranoside |
| **$K^+$** | Potassium ion(s) |
| **Kan** | Kanamycin |
| **kb** | Kilobase pairs |
| **KCl** | Potassium chloride |
| **$KH_2PO_4$** | Potassium dihydrogen phosphate |
| **l** | liter |
| ***lac*$_P$** | *lac* promoter |
| **LB** | Lysogeny Broth |
| **LMW** | Low molecular weight |

| | |
|---|---|
| **M** | Molar (mol/l) |
| **m** | milli |
| **M9** | Defined minimal medium |
| **MCS** | Multiple cloning site |
| **min** | minute |
| **$MgSO_4$** | Magnesium sulfate |
| **MYM** | Maltose-Yeast Extract-Malt Extract |
| **n. a.** | Not applicable |
| **NA** | Nutrient agar |
| **NaCl** | Sodium chloride |
| **$Na_2HPO_4$** | Sodium hydrogen phosphate |
| **$NaH_2PO_4$** | Sodium dihydrogen phosphate |
| **Nal** | Nalidixic acid |
| **nanoDSF** | Nano differential scanning fluorimetry |
| **NaOH** | Sodium hydroxide |
| **Ni-NTA** | Nickel nitrilotriacetic acid |
| **$NH_4Cl$** | Ammonium chloride |
| **nm** | nanometer |
| ***oriT*** | Origin of transfer |
| **$OD_{578}$** | Optical density at 578 nm |
| **PAGE** | (SDS) polyacrylamide gel electrophoresis |
| **PBS** | Phosphate-buffered saline |
| **PCR** | Polymerase chain reaction |
| **PDE** | Phosphodiesterase |
| **pH** | Power of hydrogen |
| **PVDF** | Polyvinylidene difluoride |
| **RCK_C** | C-terminal domain of regulator of conductance of $K^+$ |
| **rpm** | Revolutions per minute |
| **RT** | Room temperature |
| **s** | second |
| **SDS** | Sodium dodecyl sulfate |
| **TB** | Tryptone Broth |
| **TBST** | Tris-buffered saline with Tween 20 |
| **TEMED** | Tetramethylethylenediamine |
| **Tris** | 2-Amino-2-(hydroxymethyl)propane-1,3-diol |
| **TSS** | Transformation and storage solution |
| **µ** | micro |
| **µm** | micrometer |
| **UV** | ultraviolet |
| **V** | volt |
| **X-Gal** | 5-brom-4-chlor-3-indoxyl-β-D-galactopyranoside |

# Zusammenfassung

Alle Lebewesen verwenden nukleotid-basierte sekundäre Botenstoffe um extra- und intrazelluläre Signale weiterzuleiten und eine passende physiologische Zellantwort zu induzieren. Das zyklische Dinukleotid c-di-AMP ist ein Signalmolekül, welches verschiedene physiologische Prozesse steuert und für viele Bakterien unter bestimmten Wachstumsbedingungen essentiell ist. Dieser Botenstoff muss präzise reguliert werden, da eine Erhöhung des intrazellulären c-di-AMP-Spiegels oftmals toxisch ist. Diadenylatzyklasen mit konservierter DAC-Domäne synthetisieren c-di-AMP, welches von Phosphodiesterasen (PDE) mit einer DHH/DHHA1- oder HD-Domäne zu pApA und/oder AMP abgebaut wird.

Streptomyceten sind Boden bewohnende, Gram-positive Aktinobakterien mit einem komplexen Lebenszyklus, während welchem sie viele sekundäre Metabolite, wie bspw. Antibiotika, produzieren. Der Lebenszyklus besteht aus Wachstum als vegetatives Myzelium, Differenzierung zu reproduktiven Lufthyphen und anschließender Ausbildung von Exosporen. Die Regulierung und Bedeutung von c-di-AMP in der Biologie von Streptomyceten waren zu Beginn dieser Arbeit unbekannt. Während die c-di-AMP-Synthese durch die DAC DisA erfolgt, sind die typischen PDEs sowie die meisten der bekannten c-di-AMP-Effektoren nicht konserviert. Ziel dieser Arbeit war die Identifizierung von weiteren c-di-AMP-regulierenden Enzymen und c-di-AMP-bindenden Proteinen für die Signaltransduktion in Streptomyceten.

In dieser Arbeit zeigte ich, dass in *Streptomyces venezuelae* c-di-AMP primär durch DisA synthetisiert wird und präsentiere Daten, welche auf c-di-AMP-Produktion durch mindestens eine DAC-Domänen-unabhängige Synthetase hinweisen. Mit verschiedenen bioinformatischen und biochemischen Methoden, charakterisierte ich AtaC als den ersten Vertreter einer neuen Klasse von hochkonservierten c-di-AMP-spezifischen aktinobakteriellen PDEs, welche auch in Pathogenen konserviert sind. Die Detektion vom c-di-AMP-Abbauprodukt pApA in der *ataC*-Mutante deutet darauf hin, dass weitere c-di-AMP-PDEs in *S. venezuelae* vorhanden sein könnten.

*disA* und *ataC* werden konstitutiv exprimiert und sorgen für den Erhalt eines bestimmten c-di-AMP-Grundspiegels während des kompletten Lebenszyklus von *S. venezuelae*. Im Gegensatz zu vielen anderen Bakterien ist *disA* nicht essentiell für das Wachstum von *S. venezuelae* auf reichem Medium und kann ohne Schwierigkeiten deletiert werden. Die Deletion oder Inaktivierung von *disA* führt zu einer starken Reduktion von c-di-AMP während des vegetativen Wachstums und dem Verschwinden von detektierbarem c-di-AMP während der späteren Wachstumsphasen. Dieser Defekt in der c-di-AMP-Produktion wirkt sich negativ auf das Wachstum bei osmotischem Stress aus, welcher durch hohe extrazelluläre Konzentrationen von Kationen hervorgerufen wird, hat aber keinen Effekt auf das Wachstum oder Differenzierung auf reichem Medium ohne Stresseinwirkung. Im

Gegensatz dazu ist der c-di-AMP-Spiegel in der *ataC*-Mutante erhöht, was Wachstumsdefekte hervorruft und die Differenzierung behindert. In einem Stamm, welcher eine inaktive DisA-Variante exprimiert, stellt die Deletion von *ataC* den c-di-AMP-Spiegel nur während der späten vegetativen Wachstumsphase wieder her, was aber auszureichen scheint um das Wachstum auf Medien mit hohen Natrium- oder Kaliumkonzentrationen zu ermöglichen. Diese Ergebnisse deuten darauf hin, dass das c-di-AMP, welches durch DisA und die unbekannte Synthetase produziert wird, für verschiedene zelluläre Funktionen verwendet werden könnte und durch unterschiedliche PDEs abgebaut wird.

Bioinformatische Analysen und *in vitro* Bindungsversuche zeigen, dass die „regulator of conductance of $K^+$ C-terminal“ (RCK_C)-Domänen Proteine CpeA und CpeD die ersten Proteineffektoren sind, welche an c-di-AMP-regulierten Signaltransduktionswegen in Streptomyceten beteiligt sind. *cpeA* und *cpeD* befinden sich in Operons mit den putativen Kation/Proton-Antiportern *cpeB* bzw. *cpeE* und die jeweiligen Genprodukte interagieren miteinander *in vivo* in Anwesenheit von c-di-AMP. *In silico* Analysen prognostizieren, dass CpeB und CpeE strukturelle Homologe von charakterisierten Natrium/Proton-Antiportern sind. Zum anderen besitzen CpeAB und CpeDE eine gewisse Ähnlichkeit zu bekannten Kalium-exportierenden Transportern. Beides deutet darauf hin, dass die Cpe-Systeme das Ionen-Gleichgewicht in Streptomyceten regulieren könnten. Diese Annahme wird dadurch gestützt, dass die Expression des Transporters CpeABC das Wachstum von *Escherichia coli* in Flüssigmedien mit moderaten KCl-Konzentrationen in Abwesenheit von c-di-AMP verbessert. Dies deutet darauf hin, dass Cpe-Transporter die intrazelluläre Kalium-Konzentration in Abhängigkeit von c-di-AMP regulieren und zeigt einen potenziellen Zusammenhang mit dem Kation-sensitiven Phänotyp der *disA*-Mutante. Die exakte Funktion der Cpe-Transporter muss noch bestimmt werden und wahrscheinlich sind in *S. venezuelae* weitere c-di-AMP-abhängige Faktoren an der zellulären Stressantwort auf osmotischen Stress, welcher durch monovalente Kationen hervorhergerufen wird, beteiligt.

Zusammengefasst, verbessert diese Studie das allgemeine Verständnis der c-di-AMP Signaltransduktionswege in *Streptomyces spp*. Die biochemische Charakterisierung von DisA und Identifizierung von AtaC als Vertreter einer neuen Familie von c-di-AMP-PDEs sowie die Hinweise auf weitere c-di-AMP-metabolisierende Enzyme erlauben zum ersten Mal eine Erkenntnis darüber, wie intrazelluläres c-di-AMP in *S. venezuelae* reguliert wird. c-di-AMP ist in die Regulierung von Wachstum, Differenzierung und der Stressantwort auf erhöhte extrazelulläre Kalium- und Natrium-Konzentrationen involviert. Für letzteres könnten (zumindest zum Teil) die neu entdeckten c-di-AMP-bindenden Effektoren CpeA und CpeD verantwortlich sein, welche in Abhängigkeit von c-di-AMP die prognostizierten Kation/Proton-Antiporter CpeB und CpeE binden und somit wahrscheinlich deren Aktivität modulieren, um das Ionengleichgewicht in *S. venezuelae* zu regulieren.

# Summary

Nucleotide second messengers are used by all forms of life to transduce extra and intracellular signals and translate them into a physiological cell response. The cyclic dinucleotide c-di-AMP is a signaling molecule involved in diverse functions in bacterial physiology and is essential for many bacteria under certain growth conditions. However, this second messenger has to be tightly regulated since increased levels of c-di-AMP can be toxic. In many bacteria, diadenylate cyclases with a conserved DAC domain synthesize c-di-AMP and phosphodiesterases (PDEs) with a DHH/DHHA1 or HD domain degrade it to pApA and/or AMP.

*Streptomyces spp.* are soil-inhabiting gram-positive Actinobacteria well-known for their sophisticated developmental life cycle, which includes growth as vegetative mycelium, differentiation into reproductive aerial hyphae and formation of dormant exospores. During this life cycle *Streptomyces* produce a huge variety of secondary metabolites, including many antibiotics. The regulation and role of c-di-AMP is not well understood in *Streptomyces* biology. For c-di-AMP synthesis, streptomycetes utilize the DAC DisA but do not encode any canonical PDE. Moreover, most of the known effector proteins for c-di-AMP signal transduction are absent. Hence, the aims of this study were the identification of enzymes involved in regulation of c-di-AMP and c-di-AMP-binding components for signal transduction in streptomycetes.

In this work, I demonstrated that DisA is the primary c-di-AMP synthetase in *Streptomyces venezuelae* and provide evidence for c-di-AMP production in a DAC domain-independent manner, suggesting that *S. venezuelae* encodes at least one enzyme with a previously unrecognized domain capable to synthesize c-di-AMP. Using a combination of bioinformatic and biochemical methods, I characterized AtaC as the founding member of a novel class of highly conserved c-di-AMP-specific actinobacterial PDEs, which are also encoded in pathogens. Detection of the c-di-AMP cleavage product pApA in the *ataC* mutant suggests that additional c-di-AMP PDE(s) might be encoded in *S. venezuelae*. Thus, streptomycetes appear to possess a unique enzymatic set for c-di-AMP production and degradation.

In *S. venezuelae*, *disA* and *ataC* are constitutively expressed and maintain a basic level of c-di-AMP throughout the whole life cycle. In contrast to many other bacteria *disA* is not essential in *S. venezuelae* in rich media and can be readily deleted. *disA* deletion or inactivation strongly reduces c-di-AMP during vegetative growth and abolishes its production at late growth stages. The defect in c-di-AMP production affects bacterial survival under high cation osmotic stress conditions but does not influence growth or differentiation if grown in rich media without stress. On the other hand, deletion of *ataC* increases intracellular c-di-

AMP and causes growth defects and interferes with development without affecting spore viability. Interestingly, deletion of *ataC* in a strain producing an enzymatically inactive DisA variant restores c-di-AMP to wild-type levels during vegetative growth only, which however seems to be sufficient to permit growth in presence of high extracellular sodium or potassium chloride. These results suggest that c-di-AMP produced by DisA and the unknown synthetase is likely utilized for distinct cellular functions and regulated by different PDEs.

Using bioinformatic analyses and biochemical *in vitro* binding assays, I identify the regulator of conductance of $K^+$ C-terminal (RCK_C) domain-containing proteins CpeA and CpeD as first protein effectors involved in c-di-AMP signaling in *Streptomyces*. The genes *cpeA* and *cpeD* are encoded in operons with the predicted cation/proton antiporters *cpeB* and *cpeE*, respectively, and the gene products interact *in vivo* in a c-di-AMP-dependent manner. Strikingly, *in silico* analyses predict that CpeB and CpeE are structural homologs of characterized sodium/proton antiporters and CpeAB and CpeDE share similarity with known potassium efflux systems, suggesting that the Cpe transporters regulate ion homeostasis in *Streptomyces*. In support of this, expression of the transporter CpeABC in *Escherichia coli* improves the growth in liquid media supplemented with moderate KCl concentrations. Simultaneous production of c-di-AMP appears to inhibit this growth, indicating that Cpe transporters are likely involved in regulation of potassium homeostasis in response to c-di-AMP. Altogether, these findings provide an intriguing link to the cation-sensitive phenotype observed in Δ*disA*. However, the exact function of the Cpe transporters remains to be elucidated and likely other c-di-AMP-dependent factors with redundant functions are involved in the cellular response to osmotic stress induced by monovalent cations in *S. venezuelae.*

In summary, this study substantially facilitates the understanding of c-di-AMP signal transduction pathways in *Streptomyces spp.* The biochemical characterization of DisA and identification of AtaC as a member of a novel family of c-di-AMP PDE as well as the evidence for other c-di-AMP-producing and degrading enzymes provides for the first time an insight how intracellular c-di-AMP is regulated in streptomycetes. c-di-AMP is involved in growth, differentiation and the stress response to increased extracellular potassium and sodium concentrations. The latter process might be (at least partially) regulated by the novel c-di-AMP-binding effectors CpeA and CpeD as potential signal transduction components, which bind to the predicted cation/proton antiporters CpeB and CpeE in response to c-di-AMP, thus likely modulating the activity of the latter to control ion homeostasis in *S. venezuelae.*

# 1 Introduction

## 1.1 Nucleotide second messenger signaling in bacteria

Transduction of extra- and intracellular signals via nucleotide second messengers is a widespread concept throughout all kingdoms of life (Hengge et al., 2019). These signals are sensed by specific receptors, which can be fused as additional domains to the enzymes synthesizing or degrading the second messenger. Effectors, like so-called riboswitches or specific proteins, bind the second messenger, resulting in alterations of target gene expression and cellular processes, which ultimately lead to an appropriate cell response as an output to a perceived cue (Hengge, 2009).

Bacteria utilize different nucleotide second messengers derived from guanosine or adenosine triphosphate. Generally, these molecules are either modified mononucleotides such as guanosine pentaphosphate or tetraphosphate ((p)ppGpp), cyclic guanosine (3′,5′)-monophosphate (cGMP) and cyclic adenosine (3′,5′)-monophosphate (cAMP) or cyclic dinucleotides like bis-(3′,5′)-cyclic di-guanosine monophosphate (c-di-GMP), bis-(3′,5′)-cyclic di-adenosine monophosphate (c-di-AMP) and (3′,3′)-cyclic-AMP-GMP (cGAMP) (Gomelsky, 2011; Hengge et al., 2019). Recently, uridine-based cyclic di-nucleotides and mixed cyclic trinucleotides were identified in bacteria (Whiteley et al., 2019).

Nucleotide second messengers are involved in different physiological processes. (p)ppGpp is an alarmone, which is produced upon starvation and signals nutrient limitation to the cell (Hengge et al., 2019). Whereas function of cGMP is poorly understood in bacteria, cAMP is best known in its involvement in carbon catabolite repression as an activator of utilization of alternative carbon sources, when the preferred is absent (Brückner & Titgemeyer, 2002; Gomelsky, 2011). cGAMP is involved in virulence of *Vibrio cholerae* (Davies et al., 2012). c-di-GMP is an important life style switch regulator in both gram-negative and gram-positive bacteria, which determines whether bacteria live as planktonic, motile, single cells or form complex sessile biofilms (Hengge et al., 2019). Recently, a comparable function was demonstrated in gram-positive *Streptomyces*, where c-di-GMP controls the differentiation from vegetative, multicellular mycelium into unicellular spores (see paragraph 1.5) (Gallagher et al., 2020; Tschowri et al., 2014).

## 1.2 Regulation of intracellular c-di-AMP

Under standard growth conditions, i.e. generally in rich media, c-di-AMP is the only known nucleotide second messenger that is essential for many bacteria which produce it, but also toxic if accumulated. Hence, it was termed as an “essential poison” (Gundlach, Mehne, et al., 2015). Consequently, intracellular c-di-AMP balance has to be precisely maintained by dedicated synthases, known as diadenylate cyclases (DACs), that produce c-di-AMP by

condensation of two ATP molecules releasing a pyrophosphate as byproduct and specific phosphodiesterases (PDEs), which cleave it to 5'-pApA and/or two AMP (Figure 1A) (Commichau et al., 2019).

### 1.2.1 c-di-AMP is synthesized by diadenylate cyclase domain proteins

c-di-AMP was first identified after crystallization of *Thermotoga maritima* DNA integrity scanning protein (DisA) as a ligand bound within the crystal structure (Witte et al., 2008). Subsequent analyses showed that purified DisA from *T. maritima* and *Bacillus subtilis* produce c-di-AMP from two ATP molecules using the DUF147 domain, which was renamed to diadenylate cyclase domain (Figure 1B) (Witte et al., 2008). For enzymatic activity, formation of a DAC homodimer with the active sites of the protomers directed towards each other is required to form the minimal functional unit (Heidemann et al., 2019; Witte et al., 2008). Within the DAC domain, two amino acid motifs are of particular importance and conserved in all DACs: (i) DGA (Asp-Gly-Ala at positions 75 to 77 in *T. maritima* DisA) which is responsible for metal coordination, and thus catalytic activity. In agreement with this, a D77N DisA mutant from *B. subtilis* is inactive *in vitro*. (ii) The RHR (Arg-His-Arg at positions 108 to 110 in *T. maritima* DisA) motif is required for ATP binding (Bai et al., 2012; Müller et al., 2015; Witte et al., 2008). Additionally, a specific tyrosine (position 187 in *Listeria monocytogenes* CdaA) is suggested to lock ATP within the active site and thus play an important role in enzymatic activity of the CdaA-type DACs (Heidemann et al., 2019; Tosi et al., 2019).

DAC domains are encoded in Euryarchaeota and many bacterial phyla (Corrigan & Gründling, 2013; Yin et al., 2020). Many different types of DACs were identified and five of them were phenotypically and/or biochemically characterized: DisA, CdaA (or DacA), CdaS, CdaM and CdaZ (Figure 1B) (Corrigan & Gründling, 2013; Yin et al., 2020). Besides the DAC domain, these proteins contain distinct domains, which are often involved in regulation of enzymatic activity (Mehne et al., 2014; Witte et al., 2008; Zheng et al., 2015).

Many c-di-AMP-producing bacteria contain only one of the two most frequent DAC proteins, DisA or CdaA (Corrigan & Gründling, 2013; Yin et al., 2020). An interesting exception are *Bacilli* that contain DisA, CdaA as well as CdaS (Yin et al., 2020). Most Actinobacteria, including *Streptomyces spp.*, encode DisA as the sole DAC domain protein, which is also present in some spore-forming Firmicutes as well as in other minor bacterial phyla (Corrigan & Gründling, 2013; Yin et al., 2020). Initially, DisA was identified as a protein required for DNA integrity scanning at the onset of endospore formation in *B. subtilis* (Bejerano-Sagie et al., 2006). There, DisA forms a globular dynamic focus that moves through the bacterial cell. Upon addition of nalidixic acid or Mitomycin C, the movement stops

in response to DNA damage caused by these agents (Bejerano-Sagie et al., 2006). Bejerano-Sagie et al. (2006) further demonstrated that a *disA* deletion leads to premature sporulation resulting in fewer viable spores in presence of DNA-damaging agents. On the other hand, overexpression of DisA impairs sporulation efficiency when no DNA damage is present (Bejerano-Sagie et al., 2006). This led to the suggestion of a model in which DisA is a checkpoint for sporulation, scanning the DNA for damage and delaying sporulation until the damage was repaired. However, a later study showed that a functional DisA is also required during *B. subtilis* vegetative growth to counteract DNA-damaging stress induced by methyl methane sulfonate (Gándara & Alonso, 2015). Moreover, in *B.* subtilis, DisA is also expressed during spore germination and outgrowth, and has been shown to delay both processes in response to accumulation of oxidative DNA damage in spores (Campos et al., 2014). However, in non-sporulating Actinobacteria, DisA appears to control different cellular functions. Zhang and He (2013) observed that in *Mycobacterium smegmatis* DisA overexpression leads to a growth defect, cell swelling, cell aggregation and loss of motility.

The crystal structure of *T. maritima* DisA revealed that the protein consists of the N-terminal DAC domain which is connected to a DNA-binding Helix-hairpin-Helix (HhH) domain via a linker domain (Witte et al., 2008). For enzymatic activity, DisA forms a homooctamer, which consists of two tetramers interacting via their DAC domains and contain magnesium ions as enzymatic cofactors. Within a single tetramer, interaction is largely provided by the linker with minor contributions of the DAC and HhH domains (Witte et al., 2008). Interestingly, removal of the HhH domain strongly reduces the catalytic activity of DisA (Bai et al., 2012; Torres et al., 2019). Witte et al. (2008) demonstrated that *B. subtilis* DisA binds DNA via its HhH domain and that this binding regulates the diadenylate cyclase activity *in vitro.* Particularly, c-di-AMP synthesis was strongly inhibited when branched DNA (so-called Holliday junction), but not single- or double-stranded DNA (dsDNA), was added to the reaction. Since branched DNA can be a result of stalled replication forks or initiation of DNA double strand break repair, a potentially reduced c-di-AMP level within the cell was suggested to represent a DNA damage signal (Gándara et al., 2017; Witte et al., 2008).

Further studies revealed that DisA enzymatic activity is regulated by direct protein-protein interaction. In *M. smegmatis*, RadA (radio-sensitive gene A), which gene is encoded in the same operon with *disA* in many bacteria, directly interacts with DisA and inhibits its cyclase activity *in vitro* and *in vivo* (Zhang & He, 2013). Using *M. smegmatis* as a heterologous expression system, the authors also showed that among others *Streptomyces coelicolor* RadA has a similar effect on DisA (Zhang & He, 2013). In *B. subtilis*, DisA activity is inhibited by RadA as well, and this inhibition can be partially reversed in presence of dsDNA *in vitro* (Gándara et al., 2017).

The well-characterized cyclic di-AMP synthase A (CdaA, or DacA) is generally prevalent in the phylum Firmicutes and was extensively studied in *B. subtilis*, *Streptococcus spp.*, *Staphylococcus aureus* and *L. monocytogenes* (Bai et al., 2013; Corrigan et al., 2011; Gibhardt et al., 2020; Gundlach, Mehne, et al., 2015; Heidemann et al., 2019; Mehne et al., 2013; Woodward et al., 2010; Yin et al., 2020). In many bacteria, where CdaA is the only DAC domain protein, it is essential under standard growth conditions (Agostoni et al., 2018; Bai et al., 2013; Woodward et al., 2010). However, in some *Streptococci* and cyanobacteria *cdaA* can be readily deleted and growth conditions (such as cultivation in defined synthetic medium) have been identified, which allow to overcome the essentiality of *cdaA* and c-di-AMP in general (Fahmi et al., 2019; Gibhardt et al., 2019; Gundlach et al., 2017; Rørvik et al., 2020; Rubin et al., 2018; Whiteley et al., 2017; Zeden et al., 2020). Thus, *cdaA* mutants or strains where *cdaA* can be conditionally switched off were used to study the physiological role of this DAC. In general, depletion of c-di-AMP due to cyclase deletion or activity reduction causes growth defects in different bacteria (Agostoni et al., 2018; Fahmi et al., 2019; Rørvik et al., 2020; Witte et al., 2013; Zarrella et al., 2020). The exact cause of this defect appears to be rather species-specific since c-di-AMP-depleted bacteria show opposite reactions to different stresses. For example, growth of *L. monocytogenes* and *S. aureus cdaA* mutants in rich medium can be restored by supplementation with NaCl or KCl, whereas a *Streptococcus pyogenes cdaA* mutant fails to grow in rich medium upon addition of KCl or NaCl (Fahmi et al., 2019; Whiteley et al., 2017; Witte et al., 2013). These observations reveal a contribution of CdaA to osmotic regulation, which is supported by the fact that mutations in ion and compatible solute transporters can restore the growth defect of *cdaA* mutants (Gundlach et al., 2017; Gundlach et al., 2019; Whiteley et al., 2017; Zeden et al., 2020). Further analyses revealed that *cdaA* deletion alters the resistance to changes in medium acidity, renders the mutants more sensitive to oxidative stress and cell wall targeting antibiotics, and reduces virulence and biofilm formation (Fahmi et al., 2019; Gándara & Alonso, 2015; Rubin et al., 2018; Whiteley et al., 2017; Witte et al., 2013; Zarrella et al., 2020).

CdaA is a membrane-bound protein that consists of three N-terminal transmembrane domains (TM) followed by the C-terminal DAC domain, which is flanked by two coiled-coil domains of unknown function (Figure 1B) (Gibhardt et al., 2020; Gundlach, Mehne, et al., 2015; He et al., 2020). In *B. subtilis*, *cdaA* is the first gene in a constitutively expressed operon containing *cdaR* (cyclic di-AMP synthase A regulator) and *glmM* (phosphoglucosamine-6-phosphate mutase), which is essential for cell wall biosynthesis (Mehne et al., 2013). Additionally, *cdaA* expression is induced by high extracellular KCl concentrations, which results in enhanced c-di-AMP production (Gundlach et al., 2017). Interestingly, both CdaR and GlmM have been shown to regulate CdaA activity post-

translationally in a heterologous expression system, and all three proteins form a complex with CdaA as the central component (Gibhardt et al., 2020; Gundlach, Mehne, et al., 2015; Mehne et al., 2013; Tosi et al., 2019). The membrane-anchored, extracellular CdaR interacts with CdaA likely via the TM domains (Gibhardt et al., 2020; Gundlach, Mehne, et al., 2015; Mehne et al., 2013). Although a study involving *B. subtilis* CdaR demonstrated enhancement of CdaA cyclase activity when co-expressed in *Escherichia coli*, most studies showed rather an inhibition using a comparable experimental setup with CdaR and CdaA from *L. monocytogenes* or *S. aureus* (Gibhardt et al., 2020; Mehne et al., 2013; Tosi et al., 2019; Zhu et al., 2016). In agreement with the latter, CdaR negatively controls CdaA activity in dependence on osmotic stress in *L. monocytogenes.* Under similar conditions, the cytosolic GlmM inhibits c-di-AMP production by CdaA (Gibhardt et al., 2020). It has been further demonstrated that during co-expression of *Lactococcus lactis* and *S. aureus* GlmM in *E. coli* the enzymatic activity of the respective CdaA is reduced (Tosi et al., 2019; Zhu et al., 2016). Also, purified *S. aureus* GlmM directly inhibits CdaA activity *in vitro* (Tosi et al., 2019) In contrast, neither CdaR nor GlmM appear to be direct targets for c-di-AMP regulation (Gundlach et al., 2019; Tosi et al., 2019).

CdaS, the sporulation-specific DAC, has been so far only identified in endospore-forming *Bacilli.* It is exclusively expressed in the forespore and is required for proper sporulation in *Bacillus thuringiensis* and germination in *B. subtilis* (Mehne et al., 2013; Mehne et al., 2014; Yin et al., 2020; Zheng et al., 2015). CdaS is composed of a regulatory N-terminal YojJ and a C-terminal DAC domain (Figure 1B). The YojJ domain is required to form a hexamer in solution, but its regulatory function is not entirely feasible. A YojJ domain-deficient *B. thuringiensis* CdaS is inactive *in vitro*, whereas *B. subtilis* CdaS without the YojJ domain shows significantly increased c-di-AMP production compared to the wild-type protein when expressed in *E. coli* (Mehne et al., 2014; Zheng et al., 2015).

CdaM was identified in *Mycoplasma pneumoniae* and is composed of a single N-terminal TM domain, followed by the DAC domain (Figure 1B) (Blötz et al., 2017). It has been shown to be an active DAC as c-di-AMP could be detected after expression in *E. coli.* The *cdaM* gene is essential and the role of its gene product in *M. pneumoniae* is not clear, but presence of a c-di-AMP-binding protein, which is part of a low-affinity potassium uptake transporter, suggests that c-di-AMP produced by CdaM might be involved in osmoregulation (Blötz et al., 2017).

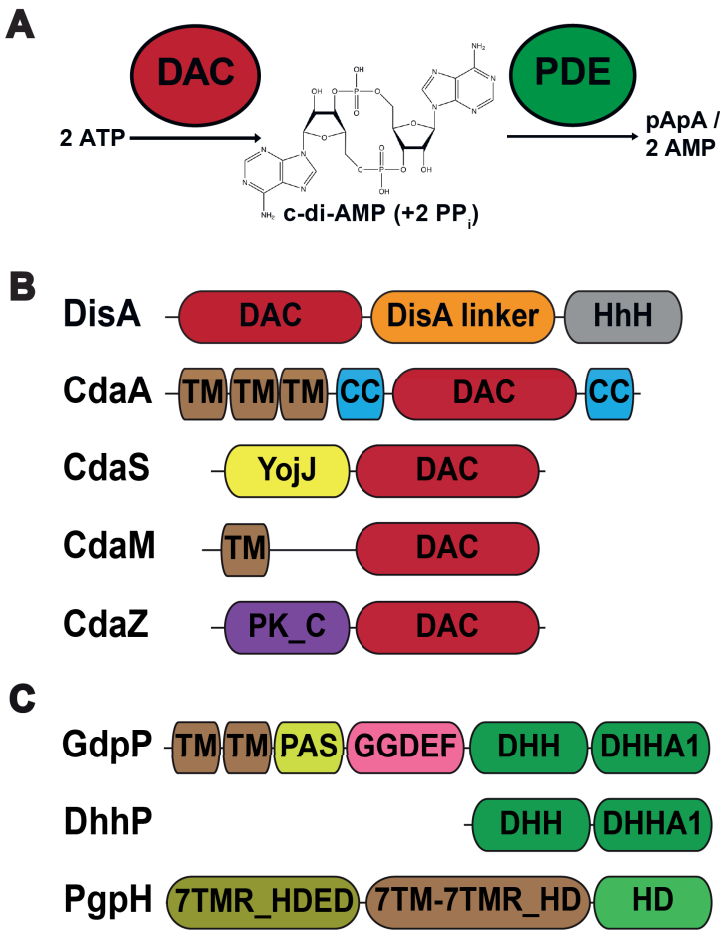


**Figure 1: c-di-AMP metabolism and schematic domain structures of c-di-AMP synthesizing and degrading enzymes.**

**(A)** c-di-AMP is synthesized by diadenylate cyclases (DACs) under release of pyrophosphate ($PP_i$) as a byproduct, whereas degradation to 5'-pApA or two AMP is catalyzed by specific phosphodiesterases (PDEs). **(B)** All biochemically characterized DACs contain the DAC domain for c-di-AMP synthesis and additional distinct domains which are presumably involved in regulation of enzymatic activity. HhH, helix-hairpin-helix domain; TM, transmembrane domain; CC, coiled-coil domain; YojJ, YojJ domain; PK_C, C-terminal pyruvate kinase domain. **(C)** PDEs containing the DHH-DHHA1 or HD domains degrade c-di-AMP. GdpP and PgpH are membrane-localized enzymes with additional domains presumably required for regulation of enzymatic activity, whereas DhhP is a soluble single-domain protein. PAS, Per-Arnt-Sim domain; GGDEF, degenerate GGDEF domain; 7TMR_HDED, extracellular domain of 7TRM_HD family PDEs; 7TMR_7TMR_HD, seven transmembrane domains of 7TRM_HD family PDEs. Protein domains are not drawn to scale. Figure reproduced after Gundlach, Mehne, et al. (2015) and He et al. (2020).

The last characterized DAC is CdaZ (or DacZ), which is encoded in Euryarchaeota and some bacteria (Yin et al., 2020). CdaZ contains an N-terminal pyruvate kinase C-terminal domain (PK_C), which is proposed to have a regulatory function and a C-terminal DAC domain (Figure 1B). Purified DacZ from the Euryarchaeon *Haloferax volcanii* produced c-di-AMP from ATP using manganese as a cofactor *in vitro* (Braun et al., 2019). Like DACs in

many bacteria, DacZ is essential for *H. volcanii* as it could not be deleted or overexpressed (Braun et al., 2019). Nevertheless, the authors could show that a reduction of DacZ expression improves growth in hypoosmotic medium, linking c-di-AMP to osmoregulation in Euryarchaeota (Braun et al., 2019).

To summarize, all characterized diadenylate cyclases rely on the DAC domain to produce c-di-AMP. c-di-AMP is utilized in many different physiological processes out of which osmoregulation appears to be the primary function.

### 1.2.2 Specific phosphodiesterases cleave c-di-AMP

To regulate the intracellular c-di-AMP level, bacteria evolved different types of PDEs capable of cleaving c-di-AMP to 5'-pApA, which can be further degraded to two AMP molecules (Figure 1A). In contrast to DACs, which utilize exclusively the DAC domain for c-di-AMP synthesis, PDEs use distinct domains such as DHH/DHHA1 and HD domains for enzymatic activity (see below), and frequently multiple types of PDEs are present within a single bacterial species (Yin et al., 2020). Note that some bacteria utilize multidrug efflux pumps to specifically export c-di-AMP from their cytosol, which can be subsequently cleaved by extracellular, cell wall-associated PDEs. However, this export appears rather to be relevant for virulence and biofilm formation than for control of intracellular c-di-AMP and will not be further described here (Andrade et al., 2016; Townsley et al., 2018; Woodward et al., 2010).

The first identified c-di-AMP-specific PDE is GdpP from *B. subtilis*, which is present in virtually all Firmicutes (Corrigan & Gründling, 2013; Rao et al., 2010; Yin et al., 2020). GdpP is a membrane-bound multi-domain protein, which consists of two N-terminal TMs, followed by a Per-Arnt-Sim (PAS) domain, a degenerate GGDEF domain and a DHH/DHHA1 domain (Figure 1C). The DHH/DHHA1 domain of GdpP is characterized by the presence of the conserved Asp-His-His motif in the active site, which is responsible for degradation of c-di-AMP to 5'-pApA (Corrigan et al., 2011; Rao et al., 2010). Two Asp residues at positions 420 and 499 coordinate manganese ions, which are required for catalytic activity. The PAS domain binds heme and has been proposed to sense nitric oxide (NO), whereas the degenerate GGDEF domain exhibits some ATPase activity (Rao et al., 2011; Rao et al., 2010). A study demonstrated that binding of NO to the PAS domain appears to stimulate PDE activity of the *B. subtilis* protein *in vitro*, however a recombinant protein from *Streptococcus pneumoniae* lacking the PAS domain showed no difference in activity *in vitro* (Bai et al., 2013; Rao et al., 2011). On the other hand, it remains unknown whether the ATPase activity of the GGDEF domain regulates the DHH/DHHA1 domain (Rao et al., 2011). Interestingly, *in vitro* activity of GdpP is inhibited by (p)ppGpp and 5'-pApA (Bowman et al., 2016; Rao et al., 2010). Deletion of *gdpP* results in a variable increase of intracellular c-di-AMP depending on the studied organism, demonstrating that GdpP also cleaves c-di-AMP *in*

*vivo.* This c-di-AMP increase is accompanied with a growth defect and/or smaller cell size in many species. Further phenotypes associated with *gdpP* deletion are increased resistance to acid stress, enhanced resistance to cell wall-targeting antibiotics and oxidative stress, deregulated biofilm formation, reduction of virulence and increased sensitivity to UV light and osmotic stress (Bai et al., 2013; Bowman et al., 2016; Corrigan et al., 2011; Devaux et al., 2018; Gándara & Alonso, 2015; Hu et al., 2020; Rao et al., 2010; Rørvik et al., 2020; Teh et al., 2019; Witte et al., 2013; Zhu et al., 2016).

The second type of c-di-AMP PDEs is a soluble protein, consisting of a single DHH/DHHA1 domain (Figure 1C). Depending on the organism, homologs of this protein have different names, but will be exclusively referred to as DhhP here. With only a few exceptions, virtually all c-di-AMP-producing organisms encode a DhhP homolog, which can occur in different combinations with the other PDEs (Yin et al., 2020). In contrast to GdpP, DhhP is also capable of degrading 5'-pApA to AMP. Interestingly in organisms, which possess multiple PDEs, 5'-pApA appears to be the preferred (or even exclusive) substrate *in vitro* (Bai et al., 2013; Bowman et al., 2016; Konno et al., 2018). However, similar to GdpP, enzymatic activity of DhhP is negatively regulated by ppGpp (Bowman et al., 2016). *In vivo, dhhP* deletion alone can cause and enhance the physiological defects observed in *gdpP* mutants. In particular, *dhhP* deletion or simultaneous deletions of both PDEs significantly increase the intracellular c-di-AMP pool and cause severe growth defects in rich media (Bowman et al., 2016; Konno et al., 2018; Wooten et al., 2020; Ye et al., 2014). As an interesting exception, *dhhP* is essential in the gram-negative pathogen *Borrelia burgdorferi* (Ye et al., 2014).

The third c-di-AMP PDE, PgpH, was initially identified in an affinity pull-down assay as a c-di-AMP-binding protein in *L. monocytogenes* (Sureka et al., 2014). This PDE is widely distributed across different bacterial phyla, but is absent in Actinobacteria as well as Euryarchaeota (Yin et al., 2020). PgpH is a membrane-associated, multi-domain protein composed of an extracellular domain, followed by seven TMs and a cytosolic HD domain (Huynh et al., 2015) (Figure 1C). The extracellular domain (7TMR_HDED) is proposed to be a receptor domain, but the extracellular signal perceived by this domain and thus the consequences for PDE activity of PgpH are not known (Huynh et al., 2015). The first biochemical study of the cytosolic HD domain of PgpH ($PgpH_{HD}$) revealed that it is the c-di-AMP binding domain and particularly the eponymous His-Asp (HD) motif is required for metal cofactor coordination and degradation of c-di-AMP to 5'-pApA (Huynh et al., 2015). Similar to the DHH/DHHA1 domain proteins, activity of $PgpH_{HD}$ was inhibited allosterically by ppGpp. Interestingly, 5'-pApA and c-di-GMP reduced c-di-AMP binding *in vitro*, but the consequences on the c-di-AMP-specific activity of PgpH were not studied (Huynh et al., 2015). In *L. monocytogenes*, a *pgpH* mutant does not show a growth defect, which however occurs if *gdpP* (*pdeA*) is deleted simultaneously. Interestingly, a *pgpH* mutant grown in broth

secretes more c-di-AMP than the wild type, which does not occur during infection, where the *pdeA* mutant appears to be the main PDE responsible for c-di-AMP cleavage *in vivo*. However, the double PDE mutant shows an additive effect in c-di-AMP overproduction and is strongly inhibited in virulence (Huynh et al., 2015). In *Bacillus anthracis*, which encodes *gdpP* and *pgpH*, the purified HD domain of PgpH has only weak activity against c-di-AMP. However *in vivo*, both single mutants showed increased c-di-AMP levels and this phenotype was additive in the double mutant (Hu et al., 2020). Similar to *L. monocytogenes*, the *B. anthracis* PDE double mutant has a growth defect and reduced virulence. Generally, increase in intracellular c-di-AMP was accompanied by enhanced sensitivity to salt and detergent (Hu et al., 2020).

In summary, c-di-AMP-producing bacteria rely on different types of PDEs, which regulate the intracellular c-di-AMP often in concert with each other. Their activity is required for optimal growth, virulence and osmotic stress resistance. Interestingly, many Actinobacteria, including *Streptomyces spp*., do not encode any GdpP, DhhP or PgpH-type PDEs, implicating presence of a novel mechanism for c-di-AMP degradation.

## 1.3 c-di-AMP is a major regulator of osmotic balance

As already pointed out (see paragraph 1.2), c-di-AMP is involved in many different cellular processes, which were studied in detail predominantly in Firmicutes (Stülke & Krüger, 2020). These processes include: monitoring of DNA integrity, sporulation and spore germination, cell wall homeostasis, virulence, resistance to acidic and oxidative stresses, metabolism, as well as biofilm formation (Figure 2). However, the main function, and thus very likely the reason for c-di-AMP essentiality, is osmoregulation since the great majority of so far identified c-di-AMP effectors is involved potassium homeostasis and uptake of compatible solutes (Stülke & Krüger, 2020). This is supported by the fact that essentiality of DACs can be overcome by growth in defined minimal medium, which is depleted for potassium, or supplementation of rich medium with salt (Gibhardt et al., 2019; Gundlach et al., 2017; Whiteley et al., 2017; Zeden et al., 2020).

As a second messenger, c-di-AMP binds different effectors, which in turn modulate respective targets to achieve an output as a cellular response to a specific signal (Figure 2). Up to date, two classes of c-di-AMP effectors were identified: the *ydaO* riboswitch and proteins. The *ydaO* riboswitch is an RNA structure that resides in the 5’ untranslated region (UTR) of the *ktrAB* and *kimA*, *kdpFABC*, and *rpfA* transcripts in *B. subtilis*, *B. thuringiensis* and *S. coelicolor*, respectively (Gundlach et al., 2017; Nelson et al., 2013; St-Onge et al., 2015; Wang et al., 2019). Binding of c-di-AMP to the riboswitch abolishes transcript elongation and thus expression of the respective genes. Therefore, c-di-AMP inhibits expression of potassium importers in *Bacilli spp.* and a cell wall hydrolase in *S. coelicolor*

(Figure 2). Regulation of potassium importer expression is not restricted only to riboswitches. In *S. aureus* and *L. monocytogenes*, c-di-AMP binds to the universal stress protein domain (USP) of KdpD (Corrigan et al., 2013; Gibhardt et al., 2019; Moscoso et al., 2016). KdpD is the histidine kinase of the two-component system KdpDE, which controls the expression of the potassium importer KdpFABC. Upon binding to KdpD, c-di-AMP impairs the expression of KdpFABC under high salt conditions *in vivo* (Moscoso et al., 2016).

Alternatively, Firmicutes exert direct control of the potassium homeostasis via binding of c-di-AMP to different potassium uptake proteins or exporters to modulate their activity (Stülke & Krüger, 2020). For example, the high-affinity potassium importers KimA from *B. subtilis*, and KupA and KupB from *L. lactis* are inactive upon c-di-AMP binding (Figure 2) (Gundlach et al., 2019; Quintana et al., 2019). However, the c-di-AMP binding region is not known for these proteins.

In contrast, the so-called C-terminal regulator of conductance of $K^+$ domain (RCK_C) is a well-established c-di-AMP-binding domain for different potassium transporters (Figure 2). The mode of c-di-AMP binding has been elucidated for the RCK_C domain of *S. aureus* KtrA by obtaining a crystal structure with the bound ligand (Kim et al., 2015). There, a single c-di-AMP molecule is bound in the interface of two interacting RCK_C monomers. Solving the crystal structure, the authors showed that an $II(X)_2D(X)R(X)_5NII$ motif is responsible for c-di-AMP binding, with the Ile residues providing hydrophobic interactions and Asp, Arg and Asn residues required for polar interactions with c-di-AMP (Kim et al., 2015). In *S. aureus*, the gating component KtrA interacts with the membrane channel KtrB, and binding of c-di-AMP to KtrA inhibits potassium uptake (Corrigan et al., 2013). A similar observation of activity regulation was reported for the KtrAB-related transporter CabP-TrkH from *S. pneumoniae*, where binding of c-di-AMP to CabP disturbs the interaction with the channel TrkH, thereby preventing potassium uptake (Bai et al., 2014). The general mechanism of potassium uptake inhibition by c-di-AMP seems to be conserved within Firmicutes since also the activity of the low-affinity potassium importer KtrCD in *L. monocytogenes* (KtrC is related to KtrA and contains an RCK_C domain) is negatively controlled by c-di-AMP (Gibhardt et al., 2019).

However, RCK_C domains are not only restricted to potassium importers. CpaA, which exports both potassium and sodium in exchange for protons, and the cytosolic component KhtT of the potassium/proton antiporter KhtTU bind c-di-AMP via their RCK_C domains (Chin et al., 2015; Gundlach et al., 2019). In contrast to the gating components of potassium importers, binding of c-di-AMP to the RCK_C domain of *S. aureus* CpaA reconstituted in proteoliposomes activates the antiporter, thus contributing to the potassium homeostasis by removal of excessive potassium ions from the cytosol (Figure 2) (Chin et al., 2015).

Additionally, an RCK_C domain is present in the GntR-type regulator BusR in *L. lactis* and *Streptococcus agalactiae*. In these bacteria, c-di-AMP binds to BusR and thereby represses the expression of the BusAB transporter, which is responsible for the uptake of the compatible solute glycine betaine (Devaux et al., 2018; Pham et al., 2018). Besides BusR, c-di-AMP has been shown to bind to RCK_C-unrelated transcription repressors: (i) DarR from *M. smegmatis*, regulator of the fatty acid metabolism and (ii) NrdR from *L. monocytogenes*, the repressor of ribonucleotide reductase expression (Borovok et al., 2004; Sureka et al., 2014; Zhang et al., 2013). Although c-di-AMP increases the binding affinity of DarR to its target DNA sequences, the consequences of this binding are not clear (Zhang et al., 2013).

The second largest group of c-di-AMP-binding effectors in Firmicutes contains a pair of cystathionine β synthase domains (CBS). These proteins are divided into transport proteins and signal transduction proteins (Figure 2). Interestingly, c-di-AMP binding to the magnesium transporter MgtE was demonstrated in *B. subtilis*, but was not present in *S. aureus* (Gundlach et al., 2019; Schuster et al., 2016). On the other hand, the c-di-AMP binding site within the CBS domain was identified in OpuCA, which is the ATPase subunit of the osmoprotectant uptake system OpuCABCD. Specifically, c-di-AMP binding to OpuCA results in inhibition of the uptake of the compatible solute carnitine in *L. monocytogenes* and *S. aureus* (Huynh et al., 2016; Schuster et al., 2016).

c-di-AMP binding of the CBS domain-containing signal transduction proteins CbpA and DarB (CbpB) has been independently shown in *L. monocytogenes* and *B. subtilis* (Gundlach et al., 2019; Sureka et al., 2014). A third signal transduction protein, DarA (or PstA), is abundant in Firmicutes but does not require a CBS domain for c-di-AMP binding (Choi et al., 2015; Corrigan et al., 2013; Gundlach, Dickmanns, et al., 2015; Sureka et al., 2014). The exact cellular functions of the three signal transduction proteins remain obscure, but a study in *L. monocytogenes* have shown that deletion of *darB* or *darA* restores the growth defect of a *cdaA* mutant in rich medium (Whiteley et al., 2017). Finally, c-di-AMP is involved in metabolism regulation in *L. monocytogenes* and *L. lactis.* c-di-AMP is an allosteric inhibitor of the pyruvate carboxylase (PycA), which catalyzes one of the first steps of amino acid *de novo* synthesis in these organisms (Choi et al., 2017; Sureka et al., 2014).

Summarized, c-di-AMP controls diverse physiological aspects in Firmicutes. In particular, osmoregulation appears to be the main function exerted by c-di-AMP since it directly and indirectly controls the expression or activity of several potassium transporters and osmoprotectant uptake systems. Interestingly, streptomycetes do not encode most of the c-di-AMP binding proteins or the c-di-AMP-binding sites are not well conserved, suggesting that these bacteria might involve a different set of effectors or that c-di-AMP regulates alternative physiological processes than in Firmicutes.

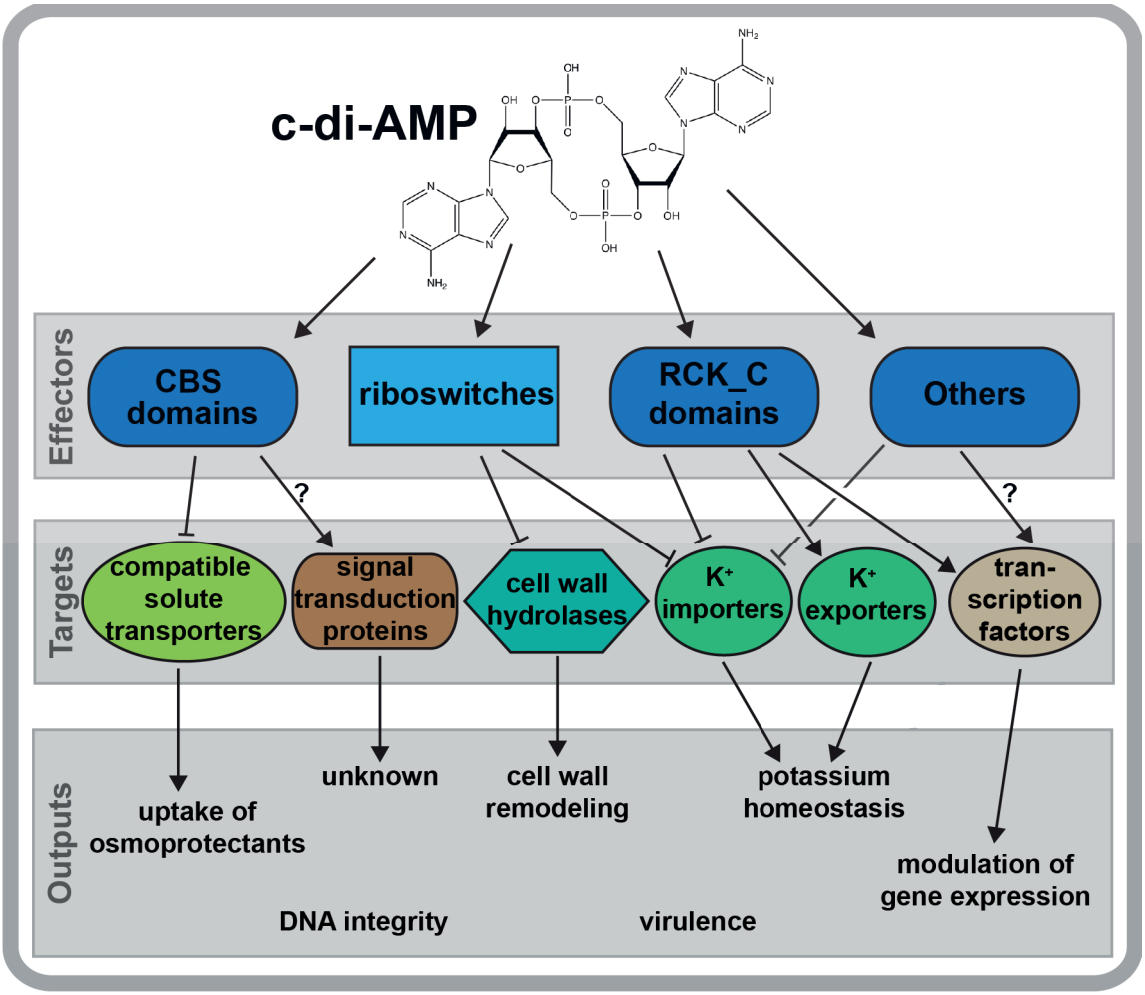


**Figure 2: Main cellular and physiological processes controlled by c-di-AMP.**

c-di-AMP binds to effectors, which can be riboswitches or proteins containing different domains. Upon c-di-AMP binding, effectors alter the expression or activity of different targets such as transporters, enzymes or transcription factors, resulting in specific cellular responses as outputs. Note that DNA integrity appears to be directly controlled by enzymatic activity of DisA, whereas virulence is a direct result of c-di-AMP secretion into the eukaryotic host cell or differential expression of virulence genes in c-di-AMP mutants via unknown mechanisms. Regulation of metabolism via PycA is not shown. CBS, cystathionine β synthase domain; RCK_C, C-terminal domain of the regulator of conductance of $K^+$ domain; $K^+$, potassium. “Others” include the unspecified or unknown c-di-AMP-binding domains of KimA, KupA, KupB, NrdR, DarA, DarR as well as the USP domain of KdpD. For references, see the text in paragraphs 1.2 and 1.3.

## 1.4 General responses to osmotic stress in bacteria

Maintenance of a certain cellular turgor is imperative for proper cellular functions in bacteria and their survival. In their habitats, bacteria are frequently exposed to osmotic stress, which can be divided into hyper and hypoosmotic stress. During hyperosmotic stress, the concentration of osmotically active components is increased in the extracellular space and causes extrusion of water from the cell by diffusion, which leads to dehydration and impairment of function of different bioactive molecules. In contrast, hypoosmotic stress is caused by dilution of extracellular solvents and leads to water influx, increasing the internal pressure, which can cause cell lysis (Bremer & Krämer, 2019).

Bacteria evolved strategies to counteract osmotic stress by passively regulating water flux across the membrane. Halophilic bacteria adapted to high salinity in their habitats by accumulation of potassium ions (salt-in strategy). In other bacteria, as a fast first response to an osmotic upshift, potassium ions are imported to reduce the concentration gradient between the intra and extracellular spaces and thus prevent water efflux (salt-out strategy) (Bremer & Krämer, 2019; Epstein, 2003). However, for a more enduring response, potassium is removed from the cytosol by dedicated exporters and replaced by synthesis or uptake of the so-called compatible solutes, which are highly water-soluble molecules and almost do not interfere with biochemical processes within the cell (Bremer & Krämer, 2019). For example, streptomycetes produce and import a variety of different molecules as compatible solutes, including the amino acids alanine, glutamine and proline and amino acid derivatives ectoine and hydroxyectoine (Bursy et al., 2008; Kol et al., 2010; Sadeghi et al., 2014; Shao et al., 2015). To counteract an osmotic downshift, bacteria encode mechanosensitive channels in the membrane, which open and release compatible solutes likely upon the increased turgor due to water influx, which exerts mechanical forces on the lipid bilayer (Cox et al., 2018; Epstein, 2003).

As described in the previous paragraph, c-di-AMP is strongly involved in regulation of expression and/or activity of multiple potassium importers and exporters as well as compatible solute transporters and thus appears to be an important regulator of osmotic stress response.

## 1.5 Differentiation of *Streptomyces venezuelae* and the potential role of c-di-AMP

Due to their multicellular lifestyle and complex differentiation, *Streptomyces spp.* are especially fascinating bacteria. They are members of gram-positive Actinobacteria with a high GC content in their DNA and play an important ecological role in recycling of cellulose and chitin in the soil. Due to the presence of a large number of biosynthetical gene clusters, streptomycetes have an outstanding potential to produce an overwhelming number of

secondary metabolites, including antibiotics. Intriguingly, secondary metabolite production is connected with morphological development. Both processes are directly or indirectly regulated by several nucleotide second messengers. To date, four nucleotide second messengers have been identified in *Streptomyces*: (p)ppGpp, cAMP, c-di-GMP and c-di-AMP (Chater, 2016; Latoscha et al., 2019; Liu et al., 2013; McCormick & Flärdh, 2012).

The *Streptomyces* life cycle includes vegetative growth as a multicellular, multigenomic mycelium, erection of reproductive aerial hyphae and their differentiation into chains of dormant unigenomic exospores. Due to the reduced water content, the spores are resistant to many physical and chemical stresses. By this means, spores are optimal vehicles to preserve genetic information during adverse growth conditions and to spread to new habitats (Bobek et al., 2017; McCormick & Flärdh, 2012).

Upon encountering a suitable environment, spores resuscitate and initiate germination. Germination is a complex process, which requires many components produced and stored before spore maturation. During germination, the spores lose their hydrophobicity and swell due to influx of water, which allows resumption of metabolic functions and nutrient uptake (Bobek et al., 2017). The germ tubes continue growth by apical tip extension as vegetative hyphae (Figure 3). A so-called polarisome, with the essential protein DivIVA at its core, drives the growth and peptidoglycan cell wall synthesis at the hyphal tip. Occasionally, a part of the polarisome separates from the whole machinery and initiates formation of a new tip, resulting in hyphal branching. This leads to formation of a complex vegetative mycelium, which is divided in multigenomic cells by irregularly emerging cross-walls (Figure 3) (Bush et al., 2015).

The second messenger c-di-GMP plays a central role during vegetative growth since it is essential for dimerization of the master regulator BldD. The $(BldD)_2$-$(c\text{-}di\text{-}GMP)_4$ complex represses expression of several *bld* and *whi* regulators (and many other genes) by binding to their promoter regions, confining the bacteria to the vegetative growth phase (Tschowri et al., 2014). Upon specific extra- or intracellular signals such as nutrient depletion, several *bld* regulators become relieved from repression, which results in cessation of vegetative growth and erection of unbranched, hydrophobic, sporogenic aerial hyphae. For example, the expression of the $(BldD)_2$-$(c\text{-}di\text{-}GMP)_4$-repressed sigma factor BldN drives the production and export of rodlin and chaplin proteins, which are essential to form the hydrophobic sheath and enable growth of aerial hyphae (Bobek et al., 2017; Bush et al., 2015; McCormick & Flärdh, 2012).

Differentiation of aerial hyphae to prespores and subsequent spore maturation are dependent on *whi* regulators. Activity of the early sporulation genes WhiA and WhiB (target of $(BldD)_2$-$(c\text{-}di\text{-}GMP)_4$) is required to halt growth of aerial hyphae and initiate septation. Among other targets, WhiA activates expression of FtsZ (repressed by BldD during

vegetative growth), which in concert with other proteins synchronously forms a ladder-like structure of regularly spaced rings (sporulation septa) within the hypha. Subsequently, these rings constrict, creating single genome-containing compartments (prespores) (Figure 3) (Bush et al., 2015; McCormick & Flärdh, 2012).

An important element in spore maturation is the sigma factor WhiG, which is repressed by BldD during vegetative growth and activated by WhiA. WhiG controls expression of WhiI, a transcription factor, which activates expression of late sporulation genes in cooperation with BldM, and is essential for spore maturation (Bush et al., 2015). Interestingly, WhiG is directly regulated by c-di-GMP, which binds to the anti-sigma factor RsiG and reduces WhiG activity (Gallagher et al., 2020). During spore maturation, thick spore walls form and the chromosome condensates within the spore. The production and accumulation of a polyketide spore pigment is one of the final steps and is dependent on the *whiE* gene locus which expression is controlled by WhiG via WhiI/BldM. Finally, activity of cell wall hydrolases releases single spores from the spore chain enabling dispersal to new environments and subsequent reinitialization of the developmental life cycle (Bobek et al., 2017; Bush et al., 2015).

In contrast to c-di-GMP, the involvement of the other nucleotide messengers in *Streptomyces* development is poorly understood (Gallagher et al., 2020; Latoscha et al., 2019; Tschowri et al., 2014). In *S. coelicolor*, (p)ppGpp is required for expression of genes associated with secondary metabolite production, including antibiotics (Latoscha et al., 2019). A strain harboring a deletion in a (p)ppGpp synthase (*relA*) is defective in formation of aerial mycelium and fails to produce the spore pigment, which is probably caused by down regulation of several *bld* and *whi* regulators (Hesketh et al., 2007; Sun et al., 2001). However, it is not clear how loss of (p)ppGpp leads to altered gene expression since no (p)ppGpp effectors were identified in streptomycetes so far (Latoscha et al., 2019).

cAMP production was reported to reach its maxima during germination and aerial hyphae formation in *S. coelicolor* (Süsstrunk et al., 1998). Interestingly under certain conditions (unbuffered minimal medium), a cAMP cyclase (*cya*) mutant is delayed in germination and fails to produce aerial hyphae, which is a result of increased sensitivity to low pH (Süsstrunk et al., 1998). In *Streptomyces*, cAMP is bound by the cAMP receptor protein (Crp) and the extension of sporogenic hyphal branches protein (EshA). Both proteins are required for antibiotic production during sporulation, which correlates with increased cAMP production (Latoscha et al., 2019; Saito et al., 2006; Süsstrunk et al., 1998). Interestingly, deletion of *eshA* impairs the formation of aerial hyphae due to reduced DNA synthesis in *Streptomyces griseus* (Saito et al., 2006). On the other hand, *crp* mutation impairs germination and leads to formation of smaller colonies and hypersporulation in *S. coelicolor* (Derouaux et al., 2004). The germination defect might be mediated via the

resuscitation promoting factor A (RpfA) since Crp has been shown to specifically bind the *rpfA* promoter and to induce *rpfA* expression (St-Onge et al., 2015). RpfA is a cell wall hydrolase involved in remodeling of the peptidoglycan to enable reinitialization of growth after dormancy (Haiser et al., 2009; Latoscha et al., 2019). Similar to mutants deficient in cAMP production or *crp*, deletion of *rpfA* significantly delays germination (Haiser et al., 2009). Furthermore, the *rpfA* mutant produces heat-sensitive spores, which have a reduced spore-wall thickness and vary in size (Haiser et al., 2009). This indicates that the gene product is required in multiple stages of bacterial development. Interestingly, *rpfA* overexpression interferes with germination as well but has no effect on subsequent growth and differentiation, which however might be caused by differential expression of other *rpf* genes or degradation of excessive RpfA by a (p)ppGpp-dependent metalloprotease (St-Onge et al., 2015).

Intriguingly, the transcript of *rpfA* contains an *ydaO*-like, c-di-AMP-responsive riboswitch in the 5' untranslated region, suggesting that c-di-AMP might be involved in the process of germination (St-Onge et al., 2015). Indeed, binding of c-di-AMP to the riboswitch inhibits transcript elongation (St-Onge & Elliot, 2017; St-Onge et al., 2015). Accordingly, removal of the riboswitch in *S. coelicolor* or abolishment of c-di-AMP production due to *disA* deletion in *S. venezuelae* strongly increases the amount of *rpfA* transcripts (St-Onge et al., 2015). Notably, *S. coelicolor* and *S. venezuelae* encode a total number of seven and six cell wall hydrolases, respectively, which are preceded by an *ydaO*-like riboswitch (Haiser et al., 2009; Latoscha et al., 2019). Besides RpfA, three riboswitch-containing hydrolases were studied in *S. coelicolor*. Whereas SwlA is required for proper germination, deletion of *swlB* or *swlC* results in aberrant branching of the vegetative mycelium. Similar to the *rpfA* mutant, single deletions in the *swl* genes lead to formation of defective, heat-sensitive spores (Haiser et al., 2009). However, whether c-di-AMP controls the expression of these genes via the riboswitch remains unknown.

Taken together, all nucleotide second messengers produced by *Streptomyces spp.* appear to be involved in regulation of the developmental life cycle. Whereas c-di-GMP is unequivocally in direct control of the transition from vegetative to reproductive growth (via complex formation with BldD) and spore maturation (regulation of the activity of the sigma factor WhiG via binding to RsiG), the mode of action by the other nucleotides is less evident. Potentially, c-di-AMP might directly control processes like germination and vegetative growth via binding to riboswitches, modulating expression of several cell wall hydrolases. Given the high number of c-di-AMP effectors involved in osmoregulation in Firmicutes (see paragraph 1.3), a similar function for c-di-AMP mediated by binding to yet unidentified protein effectors would be feasible in streptomycetes as well.

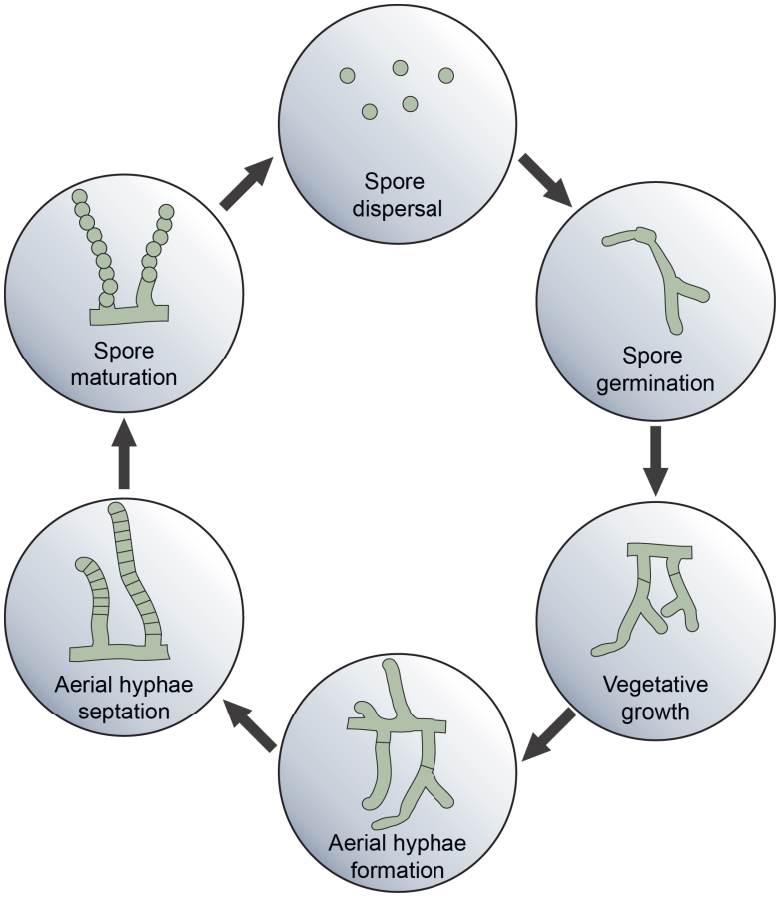


**Figure 3: Developmental life cycle of *Streptomyces spp*.**

Germination of dispersed spores is the first step in the developmental life cycle. After germination, vegetative growth leads to formation of a complex, branched, multicellular and multigenomic mycelium. The nucleotide second messenger c-di-GMP locks the cells in the vegetative phase by complex formation with BldD and repression of sporulation genes. When the growth conditions become unfavorable, erection of reproductive hydrophobic aerial hyphae is induced. During a synchronous cell division event (formation of aerial hyphae septa), single-genomic prespores emerge and subsequently differentiate to chains of mature, pigmented exospores. The spores are released into the environment and can spread to new habitats. For more details and references, see text.

# 2 Aims of the dissertation

c-di-AMP is a recently identified nucleotide second messenger predominantly found in gram-positive bacteria and Euryarchaeota (Yin et al., 2020). It is unique among other second messengers since it is often both essential and toxic to organisms if the intracellular levels are disturbed (Gundlach, Mehne, et al., 2015). Among the many physiological processes regulated by c-di-AMP, control of osmoregulation appears to be the most important and the vast majority of known c-di-AMP effectors regulate expression and/or activity of potassium transporters and osmoprotectant uptake systems (Stülke & Krüger, 2020). Precise balance of intracellular c-di-AMP via production by diadenylate cyclases (DACs) and degradation by specific phosphodiesterases (PDEs) is crucial to avoid toxic accumulation of potassium and uncontrolled water influx in the cytosol, which can both result in cell death.

At the beginning of this study it was known that *Streptomyces spp.* produce c-di-AMP using the sole DAC DisA but do not encode the canonical PDEs for degradation and most of the known c-di-AMP binding effectors, which could transmit the signal of this second messenger (Stülke & Krüger, 2020; Yin et al., 2020). Hence, the regulation and role of c-di-AMP in *Streptomyces* was generally obscure. This study attempted to elucidate the c-di-AMP signaling network in *S. venezuelae* by answering the following questions:

(i) Which enzymes does *S. venezuelae* utilize to produce and degrade c-di-AMP?

(ii) How are these enzymes expressed during the developmental life cycle and how do they influence intracellular c-di-AMP?

(iii) Are differentiation and/or resistance to osmotic stress the physiological processes regulated by c-di-AMP?

(iv) How is c-di-AMP signaling integrated in the respective cellular responses?

To answer the first question, *S. venezuelae* DisA and c-di-AMP degrading PDE(s) identified by bioinformatic means should be biochemically characterized for the first time. Subsequent evaluation of DAC/PDE(s) expression by immunoblot analysis and measurements of intracellular c-di-AMP in the respective mutants should confirm that the identified protein(s) are responsible for c-di-AMP regulation *in vivo* as well. Since all other nucleotide second messengers in *Streptomyces spp.* appear to be involved in differentiation (see paragraph 1.5) and c-di-AMP regulates osmotic balance in other bacteria (see paragraph 1.3), cultivation of *disA* and PDE mutant(s) on solid and in liquid media should demonstrate how changes in the intracellular c-di-AMP affect differentiation or general growth in presence of osmotic stress. For more detailed understanding how these physiological processes are regulated by c-di-AMP, identification of potential c-di-AMP binding proteins by bioinformatic

analyses should answer the fourth question. For this, deletion of candidate effectors, which showed c-di-AMP binding *in vitro*, and comparison to phenotypes of c-di-AMP mutants (*disA* and/or PDE) should be performed. Depending on the identity of the c-di-AMP effector proteins, further microbiological or biochemical analyses should dissect their exact function.

Altogether, this dissertation should lead to the first characterization of the c-di-AMP signaling network and its impact on development and physiology of *S. venezuelae*.

# 3 Material and Methods

## 3.1 Chemicals and materials

All relevant devices are listed in Table 1:

**Table 1:** List of used devices.

| Device | Model | Supplier / Manufacturer |
|---|---|---|
| Agarose gel electrophoresis chambers | EasyPhor mini and midi | Biozym |
| Autoclaves | DX-45; DX-150 | Systec |
| Bead Beater | BeadBlaster 24 | Benchmark |
| Biomolecular imager | Typhoon FLA 7000 | GE Healthcare |
| Centrifuges | 5810 R; MiniSpin plus; Heraeus Megafuge 16R; Heraeus Fresco 21; Sorvall Lynx 4000 | Eppendorf; Thermo Scientific |
| CCD imager | ImageQuant LAS 4000 | GE Healthcare |
| Digital camera | EOS 1300D (W) | Canon |
| Electroporator | GenePulser Xcell with PC and CE modules | Bio-Rad |
| French Press | HTU-DIGI-F-Press | G. Heinemann Ultraschall- und Labortechnik |
| French Pressure Cell | French Pressure Cell (FA-032) | Thermo |
| Gel documentation | AlphaImager HP, Mutliimage II | AlphaInnotech |
| Heat blocks | Mixing Block MB-102; Rotilabo-Block-Heater H 250 | BIOER; Roth |
| Lyophilizator with refrigerated vapor trap | Savant SpeedVac Plus SC110A; Savant Refrigerated Vapor Trap RVT100 | Thermo Scientific |
| Magnetic stirrer | MR 2000 | Heidolph |
| Microplate reader | Synergy H1 | BioTek |
| Nano fluorescence reader | Tycho NT.6 | NanoTemper |
| Orbital shaker | Celloshaker | Renner |
| PCR machine | Arktik Thermal Cycler | Thermo Scientific |
| Photospectrometer | GeneQuant100 | GE Healthcare |
| Power supplies | PowerPac HC; EPS 600 | Bio-Rad; Pharmacia Biotech |
| SDS gel electrophoresis and Wet Blot chamber | Mini-PROTEAN Tetra System | Bio-Rad |
| SemyDry Western Blotter | Trans-Blot Turbo | Bio-Rad |
| Shaking Incubators | innova43, innova44 | New Brunswick Scientific |
| Spectrophotometer | NanoDrop 2000 | Thermo Scientific |
| UV crosslinker | UV Stratalinker 1800 | Stratagene |
| Vortexer | Vortex-Genie 2 | Scientific Industries |
| Water bath | 1002 | GFL |

If not stated differently, all chemicals, kits or media components were obtained from AppliChem, Bio-Rad, Biolog, Biozym, Carl Roth, Difco, Hartmann Analytic, GE Healthcare, iba, Merck Millipore, New England Biolabs, Promega, Qiagen, roboklon, Sigma-Aldrich, Thermo Fisher Scientific and VWR.

## 3.2 Media and supplements

All media and heat-resistant supplements were sterilized by autoclaving for 20 min at 121 °C. Heat-sensitive supplements like antibiotics, amino acids, casein hydrolysate, galactose, glucose, IPTG, maltose, sucrose, thiamine · HCl and trace elements as well as $CaCl_2$, $Ca(NO_3)_2$ and $FeCl_3$ solutions were sterile filtered through a 0.2 µm filter and added to the media after sufficient cooling.

### 3.2.1 Liquid media

| | | |
|---|---|---|
| **Lysogeny Broth (LB)** | 10 g | Bacto tryptone |
| | 5 g | Bacto yeast extract |
| | 10 g | NaCl |
| | ad 1 l | $ddH_2O$ |
| **LB without salt (LBon)** | 10 g | Bacto tryptone |
| | 5 g | Bacto yeast extract |
| | ad 1 l | $ddH_2O$ |
| **LBon with 87 mM KCl (LBK)** | 10 g | Bacto tryptone |
| | 5 g | Bacto yeast extract |
| | 6.48 g | KCl |
| | ad 1 l | $ddH_2O$ |
| **LBon with 200 mM NaCl** | 10 g | Bacto tryptone |
| **and 50 mM HEPES, pH 7.5 (LB200N)** | 5 g | Bacto yeast extract |
| | 2.92 g | NaCl |
| add | 210 ml | $ddH_2O$ |
| adjust to pH 7.5 with | | 5 M NaOH |
| add | 25 ml | 0.5 M HEPES, pH 7.5 |
| adjust to pH 7.5 with | | 5 M NaOH |
| | ad 250 ml | $ddH_2O$ |

| | | |
|---|---|---|
| **20 x defined potassium-free minimal medium base (M9 base)** (modified from Gibhardt et al. (2019)) | 140 g | $Na_2HPO_4 \cdot 2\ H_2O$ |
| | 60 g | $NaH_2PO_4 \cdot H_2O$ |
| | 20 g | $NH_4Cl$ |
| | ad 1 l | $ddH_2O$ |

| | | |
|---|---|---|
| **M9 defined minimal medium**[1] (modified from Gibhardt et al. (2019)) | 10 ml | 20 x M9 base |
| | 0.2 ml | 1 M $MgSO_4$ |
| | 0.2 ml | 0.1 M $CaCl_2$ |
| | 0.1 ml | 1 mM $FeCl_3$ |
| | 0.2 ml | 1 mg/ml thiamine · HCl |
| | 2 ml | 4 mg/ml L-proline |
| | 13.2 ml | 10 % casein hydrolysate |
| | 0.625 ml | 80 % glycerol |
| | ad 200 ml | sterile $ddH_2O$ |

[1] To achieve M9 + 50 mM KCl and M9 + 10 mM KCl add 2.5 ml or 0.5 ml autoclaved 4 M KCl, respectively, before filling up with $ddH_2O$.

| | | |
|---|---|---|
| **Maltose-Yeast Extract-Malt Extract (MYM)** | 1 g | maltose (Roth) |
| | 1 g | yeast extract (Difco) |
| | 2.5 g | malt extract (Difco) |
| | 125 ml | de-ionized $H_2O$ |
| | 125 ml | tap $H_2O$ |
| after autoclaving: | 0.5 ml | trace elements |

## 3.2.2 Solid media

For **LB** and **LBK agar**, 1 l medium (paragraph 3.2.1) was supplemented with 18 g Span agar prior to autoclaving. For **MYM agar**, 250 ml MYM (paragraph 3.2.1) was supplemented with 5 g Difco Bacto agar.

| | | |
|---|---|---|
| **Nutrient agar (NA)** | 5.75 g | Nutrient agar (Roth) |
| | 250 ml | $ddH_2O$ |

| | | |
|---|---|---|
| **NA + 0.5 M NaCl** | 5.75 g | Nutrient agar (Roth) |
| | 7.3 g | NaCl |
| | 250 ml | $ddH_2O$ |

| | | | |
|---|---|---|---|
| **NA + 0.4 M KCl (0.5 M KCl)** | | 5.75 g | Nutrient agar (Roth) |
| | | 7.46 g | KCl (or 9.33 g for 0.5 M) |
| | | 250 ml | dd$H_2O$ |
| **NA + 0.5 M Sucrose** | | 5.75 g | Nutrient agar (Roth) |
| | | 187.5 ml | dd$H_2O$ |
| | after autoclaving: | 62.5 ml | 2 M sucrose |
| **NA-Ca$(NO_3)_2$** | | 4.6 g | Nutrient agar (Roth) |
| | | 200 ml | dd$H_2O$ |
| | after autoclaving: | 5 ml | 20 % glucose |
| | | 2 ml | 1 M $MgSO_4$ |
| | | 2 ml | 1 M $Ca(NO_3)_2$ |
| **MacConkey agar / 1% maltose** | | 15 g | MacConkey Agar Base (Difco) |
| | | 300 ml | dd$H_2O$ |
| | after autoclaving: | 15 ml | 20 % maltose |
| **MacConkey agar / 1% galactose** | | 15 g | MacConkey Agar Base (Roth) |
| | | 300 ml | dd$H_2O$ |
| | after autoclaving: | 15 ml | 20 % galactose |
| **Soy Flour Mannitol (SFM) agar** | | 20 g | soy flour |
| | | 20 g | mannitol |
| | | 20 g | Bacto agar |
| | | 1 l | tap $H_2O$ |

| | | |
|---|---|---|
| **Tryptone broth (TB) soft agar** | 2 g | Bacto tryptone |
| | 1 g | NaCl |
| | 1.4 g | Span agar |
| | ad 200 ml | tap $H_2O$ |

## 3.2.3 Supplements

**Table 2:** Stock and working concentrations of antibiotics and other media supplements.

| **Media supplements** | **Stock concentration** | **Working concentration** |
|---|---|---|
| Ampicillin (Amp) | 100 mg/ml in $ddH_2O$ | 100 µg/ml |
| Apramycin (Apr) | 50 mg/ml in $ddH_2O$ | 50 µg/ml |
| Chloramphenicol (Cm) | 15 mg/ml in 70 % ethanol | 15 µg/ml |
| Hygromycin B (Hyg) | 50 mg/ml in $ddH_2O$ | 22 µg/ml (LBon); 16 µg/ml (NA) |
| Kanamycin (Kan) | 50 mg/ml in $ddH_2O$ | 50 µg/ml[a] |
| Nalidixic acid (Nal) | 25 mg/ml in 0.3 M NaOH | 25 µg/ml |
| Isopropyl-β-D-thiogalactopyranoside (IPTG) | 1 M in $ddH_2O$ | 0.05 – 0.5 mM |
| Trace elements | 40 mg/l $ZnCl_2$, 120 mg/l $FeCl_3$, 7.9 mg/l $CuCl_2$, 6.4 mg/l $MnCl_2$, 5.3 mg/l $Na_2B_4O_7$, 9.4 mg/l $(NH_4)_6Mo_7O_{24}$ | 1:500 (e.g. 2 ml per liter MYM) |
| 5-brom-4-chlor-3-indoxyl-β-D-galactopyranoside (X-Gal) | 10 mg/ml in dimethylformamide | 40 µg/ml |

[a] For protein overexpression or *E. coli* ET12567/pUZ8002 liquid cultures, working concentration was reduced to 25 µg/ml; for selection of $Kan^S$ transconjugants Kan concentration was reduced to 5 µg/ml.

## 3.3 Bacterial strains, phages, cosmids and plasmids

**Table 3:** List of *S. venezuelae* strains.

| | **Genotype or comments** | **Source or reference** |
|---|---|---|
| NRRL B-65442 | Wild type | NCBI Reference Sequence: NZ_CP018074.1 |
| *disA::apr* | ATCC 10712 *SVEN_3211::aac(3)IV*; $Apr^R$ | (St-Onge et al., 2015) |
| Wild type + pIJ10257 | $attB_{\Phi BT1}$::pIJ10257; $Hyg^R$ | Tschowri lab collection |
| SVAL5 | Δ*disA::apr,* $attB_{\Phi BT1}$::p3xFLAG-*disA*; $Apr^R$, $Hyg^R$ | (Latoscha et al., 2020) |
| SVAL8 | *disA::*$disA_{D86A}$ | (Latoscha et al., 2020) |
| SVAL19 | Δ*disA::apr* (SV1 transduction); $Apr^R$ | (Latoscha et al., 2020) |
| SVAL20 | Δ*vnz_27310* (*ataC*)*::apr* (Redirect); $Apr^R$ | (Latoscha et al., 2020) |

| | | |
|---|---|---|
| SVAL22 | Δ*ataC::apr* (SV1 transduction from SVAL20); $Apr^R$ | (Latoscha et al., 2020) |
| SVAL24 | Δ*disA::apr, attB*$_{\Phi BT1}$::pIJ10770-*disA*; $Apr^R$, $Hyg^R$ | (Latoscha et al., 2020) |
| SVAL26 | Δ*ataC::apr, attB*$_{\Phi BT1}$::pIJ10770-*vnz_27305prom-ataC*; $Apr^R$, $Hyg^R$ | (Latoscha et al., 2020) |
| SVAL27 | Δ*ataC::apr, attB*$_{\Phi BT1}$::pIJ10770-*vnz_27305prom-ataC*$_{D269N}$; $Apr^R$, $Hyg^R$ | (Latoscha et al., 2020) |
| SVAL28 | Δ*vnz_31290::apr*; $Apr^R$ | This study |
| SVAL29 | *disA::disA*$_{D86A}$, Δ*ataC::apr;* $Apr^R$ | This study |
| SVAL30 | *disA::disA*$_{D86A}$, Δ*ataC::apr*, *attB*$_{\Phi BT1}$::pIJ10770-*vnz_27305prom-ataC*; $Apr^R$, $Hyg^R$ | This study |
| SVAL31 | *disA::disA*$_{D86A}$, Δ*ataC::apr*, *attB*$_{\Phi BT1}$::pIJ10770-*vnz_27305prom-ataC*$_{D269N}$; $Apr^R$, $Hyg^R$ | This study |
| SVAL40 | Δ*vnz_28055::apr* (*cpeA*); $Apr^R$ | This study |
| SVAL41 | Δ*vnz_28520::hyg* (*cpeD*); $Hyg^R$ | This study |
| SVAL42 | Δ*cpeA::apr*, Δ*cpeD::hyg*; $Apr^R$, $Hyg^R$ | This study |
| SVAL43 | Δ*vnz_28050::apr* (*cpeB*); $Apr^R$ | This study |
| SVAL44 | Δ*vnz_28520::hyg* (*cpeE*); $Hyg^R$ | This study |
| SVAL45 | Δ*cpeB::apr*, Δ*cpeE::hyg*; $Apr^R$, $Hyg^R$ | This study |
| SVAL62 | Δ*vnz_28040::apr*; $Apr^R$ | This study |
| SVAL63 | Δ*vnz_14905::hyg*; $Hyg^R$ | This study |
| SVAL64 | *attB*$_{\Phi BT1}$::pIJ10257-*cpeABC*; $Hyg^R$ | This study |
| SVAL65 | Δ*disA::apr*, *attB*$_{\Phi BT1}$:: pIJ10257-*cpeABC*; $Apr^R$, $Hyg^R$ | This study |
| SVAL66 | Δ*ataC::apr*, *attB*$_{\Phi BT1}$:: pIJ10257-*cpeABC*; $Apr^R$, $Hyg^R$ | This study |
| SVAL67 | Δ*vnz_12665::apr*; $Apr^R$ | This study |

**Table 4:** List of *E. coli* strains.

| | **Genotype or comments** | **Source or reference** |
|---|---|---|
| W3110 | K-12 derivative; *F-, λ-, rpoS(Am), rph-1, Inv(rrnD-rrnE)* | (Hayashi et al., 2006) |
| W3110 Δ*cya* | W3110 derivative with deleted adenylate cyclase | (Herbst et al., 2018) |
| DH5α | *fhuA2 lac(del)U169 phoA glnV44 Φ80' lacZ(del)M15 gyrA96 recA1 relA1 endA1 thi-1 hsdR17* | ThermoFisher Scientific |

| | | |
|---|---|---|
| ET12567/pUZ8002 | *dam*, *dcm*, *hsd*; $Kan^R$, $Cm^R$ | (Paget et al., 1999) |
| BW25113/pIJ790 | (Δ(*araD-araB*)*567*, Δ*lacZ4787*(::*rrnB-4*), *lacIp-4000*($lacI^Q$), λ-, *rpoS369*(Am), *rph-1*, Δ(*rhaD-rhaB*)568, *hsdR514*; $Cm^R$ | (Datsenko & Wanner, 2000) |
| BL21 (DE3) pLysS | F- *ompT hsdS*($r_{B^-}$ $m_{B^-}$) *gal dcm* λ(DE3), $Cm^R$ | Promega |
| HME68 | W3110Δ (*argF-lac*)*U169* $galK_{tyr145UAG}$ *mutS<>cat* | (Thomason et al., 2014) |
| Rosetta (DE3) pET28-$disA_{Bsu}$ | Overexpression of *Bacillus subtilis* DisA; $Kan^R$, $Cm^R$ | (Witte et al., 2008) |
| Rosetta 2 (DE3) | F- *ompT* $hsdS_B$($r_{B^-}$ $m_{B^-}$) *gal dcm* (DE3) pRARE2; $Cm^R$ | Novagen |
| EP432 | *mel*BLid, Δ*nhaA1*::*kan*, Δ*nhaB1*::*cat*, Δ*lacZY*, *thr1*; $Kan^R$, $Cm^R$ | (Pinner et al., 1993) |
| LB2003 | *F- kup1(trkD1)* Δ*kdpABC5 aroE rpsL metE thi rha gal* Δ*trkA aroE*$^+$ | (Stumpe & Bakker, 1997) |

**Table 5:** List of *S. venezuelae* phages.

| | **Genotype or comments** | **Source or reference** |
|---|---|---|
| SV1 | Temperate *S. venezuelae*-specific wild type phage | (Stuttard, 1982) |
| phSVAL1 | SV1 Δ*disA::apr* | (Latoscha et al., 2020) |
| phSVAL2 | SV1 Δ*ataC::apr* | (Latoscha et al., 2020) |

**Table 6:** List of *S. venezuelae* cosmids.

| | **Genotype or comments** | **Source or reference** |
|---|---|---|
| Sv-4-B12 | Contains wild-type *disA*; $Amp^R$, $Kan^R$ | John Innes Centre, Norwich, UK |
| PI1_F15 | Contains wild-type *ataC*; $Amp^R$, $Kan^R$ | John Innes Centre, Norwich, UK |
| PI2_N1 | Contains wild-type *vnz_31290*; $Amp^R$, $Kan^R$ | John Innes Centre, Norwich, UK |
| 4B02 | Contains wild-type *cpeA*, *cpeB* and *vnz_28040*; $Amp^R$, $Kan^R$ | John Innes Centre, Norwich, UK |
| PI2_A22 | Contains wild-type *cpeD* and *cpeE*; $Amp^R$, $Kan^R$ | John Innes Centre, Norwich, UK |
| 4I14 | Contains wild-type *vnz_14905*; $Amp^R$, $Kan^R$ | John Innes Centre, Norwich, UK |
| Sv-3-C02 | Contains wild-type *vnz_12665*; $Amp^R$, $Kan^R$ | John Innes Centre, Norwich, UK |

| | | |
|---|---|---|
| pSVAL1 | Sv-4-B12 *neo::apr-oriT*; $Amp^R$, $Apr^R$ | (Latoscha et al., 2020) |
| pSVAL3 | Sv-4-B12 *neo::apr-oriT disA::disA$_{D86A}$*; $Amp^R$, $Apr^R$ | (Latoscha et al., 2020) |
| pSVAL8 | PI1_F15 *ataC::apr-oriT*; $Amp^R$, $Apr^R$, $Kan^R$ | (Latoscha et al., 2020) |
| pSVAL13 | PI2_N1 *vnz_31290::apr-oriT*; $Amp^R$, $Apr^R$, $Kan^R$ | This study |
| pSVAL17 | 4B02 *cpeB::apr-oriT*; $Amp^R$, $Apr^R$, $Kan^R$ | This study |
| pSVAL18 | PI2_A22 *cpeE::hyg-oriT*; $Amp^R$, $Hyg^R$, $Kan^R$ | This study |
| pSVAL19 | 4B02 *cpeA::apr-oriT*; $Amp^R$, $Apr^R$, $Kan^R$ | This study |
| pSVAL20 | PI2_A22 *cpeD::hyg-oriT*; $Amp^R$, $Hyg^R$, $Kan^R$ | This study |
| pSVAL21 | 4B02 *vnz_28040::apr-oriT*; $Amp^R$, $Apr^R$, $Kan^R$ | This study |
| pSVAL22 | 4I14 *vnz_14905::hyg-oriT*; $Amp^R$, $Hyg^R$, $Kan^R$ | This study |
| pSVAL23 | Sv-3-C02 *vnz_12665::apr-oriT*; $Amp^R$, $Apr^R$, $Kan^R$ | This study |

**Table 7:** List of plasmids

| | **Genotype or comments** | **Source or reference** |
|---|---|---|
| pIJ773 | Plasmid template for amplification of the *apr-oriT* cassette for 'Redirect' PCR-targeting; $Apr^R$ | (Gust et al., 2003) |
| pIJ10700 | Plasmid template for amplification of the *hyg-oriT* cassette for 'Redirect' PCR-targeting; $Hyg^R$ | John Innes Centre, Norwich, UK |
| pIJ790 | Modified λRED recombination plasmid [*oriR101*] [*repA101*(ts)] *araBp-gam-be-exo*; $Cm^R$ | (Gust et al., 2003) |
| pIJ10257 | pMS81 derivative, which contains the constitutive *ermE** promoter and allows integration at the *attB$_{\Phi BT1}$* site; $Hyg^R$ | (Hong et al., 2005) |
| pIJ10770 | pMS82 derivative, which allows integration at the *attB$_{\Phi BT1}$* site; $Hyg^R$ | (Schlimpert et al., 2017) |
| pUZ8002 | RP4 derivative with defective *oriT*; $Kan^R$ | (Paget et al., 1999) |
| p3xFLAG | pIJ10770 derivative containing *3xFLAG* sequence downstream of MCS; $Hyg^R$ | (Al-Bassam et al., 2018) |
| pGEX-6P-1 | T7 expression vector (modified MCS); $Amp^R$ | GE Healthcare |
| pET15b | T7 expression vector; $Amp^R$ | Novagen |
| pKNT25 | Low copy vector encoding the T25 fragment of *Bordetella pertussis cyaA* downstream of the MCS; $Kan^R$ | Euromedex |
| pUT18 | High copy vector encoding the T18 fragment of *B. pertussis cyaA*; $Amp^R$ | Euromedex |

| | | |
|---|---|---|
| pECAL1 | pET15b-*disA*; $Amp^R$ | (Latoscha et al., 2020) |
| pECAL4 | pET15b-$disA_{D86A}$; $Amp^R$ | (Latoscha et al., 2020) |
| pECAL7 | pGEX-6P-1-$pgpH_{HD}$ (HD domain of *L. monocytogenes* PgpH); $Amp^R$ | This study |
| pECAL10 | pET15b-*vnz_27460*; $Amp^R$ | This study |
| pECAL12 | pET15b-*ataC*; $Amp^R$ | (Latoscha et al., 2020) |
| pECAL13 | pET15b-*vnz_31010*; $Amp^R$ | (Latoscha et al., 2020) |
| pECAL16 | pET15b-$ataC_{Mlu}$; $Amp^R$ (insert codon-optimized for *E. coli*) | (Latoscha et al., 2020) |
| pECAL17 | pET15b-*cpeA*; $Amp^R$ | (Latoscha et al., 2020) |
| pECAL18 | pKNT25-$cpeB^a$; $Kan^R$ | (Latoscha et al., 2020) |
| pECAL19 | pUT18-$cpeA^a$; $Amp^R$ | (Latoscha et al., 2020) |
| pECAL20 | pUT18-*cpeA-disA-FLAG*; $Amp^R$ | (Latoscha et al., 2020) |
| pECAL21 | pUT18-*cpeA*-$disA_{D86A}$-*FLAG*; $Amp^R$ | (Latoscha et al., 2020) |
| pECAL22 | pET15b-*vnz_28520* (*cpeD*; 5 N-terminal aa missing); $Amp^R$ | This study |
| pECAL23 | pET15b-$ataC_{Cbo}$; $Amp^R$ (insert codon-optimized for *E. coli*) | This study; generated by GenScript |
| pECAL24 | pET15b-$ataC_{Mtub}$; $Amp^R$ (insert codon-optimized for *E. coli*) | This study; generated by GenScript |
| pECAL27 | pKNT25-$cpeE^a$; $Kan^R$ | This study |
| pECAL28 | pUT18-$cpeD^a$; $Amp^R$ | This study |
| pECAL31 | pKNT25-$vnz\_28045^a$ (*cpeC*); $Kan^R$ | This study |
| pECAL32 | pUT18-$cpeC^a$; $Amp^R$ | This study |
| pECAL33 | pET15b-$cpeD_{extended}$ (full length *cpeD*; *sven15_5647* annotation); $Amp^R$ | This study |
| pECAL34 | pUT18-*cpeD-disA-FLAG*; $Amp^R$ | This study |
| pECAL35 | pUT18-*cpeD*-$disA_{D86A}$-*FLAG*; $Amp^R$ | This study |
| pECAL36 | p*cpeABC-disA-FLAG*; $Amp^R$ | This study |
| pECAL37 | p*cpeABC*-$disA_{D86A}$-*FLAG*; $Amp^R$ | This study |
| pECAL41 | pIJ10257-*cpeABC*; $Hyg^R$ | This study |
| pECAL42 | pET15b-$vnz\_12665_{183-380}$ (codon-optimized cytosolic domain of Vnz_12665); $Amp^R$ | This study; generated by GenScript |
| pECAL43 | pET15b-$vnz\_14905_{390-506}$ (codon-optimized cytosolic domain of Vnz_14905); $Amp^R$ | This study; generated by GenScript |

| | | |
|---|---|---|
| pECAL44 | pET15b-*vnz_28040*$_{380\text{-}507}$ (codon-optimized cytosolic domain of Vnz_28040); Amp$^R$ | This study; generated by GenScript |
| pECAL45 | pGEX-6P-1-*vnz_12665*$_{183\text{-}380}$; Amp$^R$ | This study |
| pECAL46 | pGEX-6P-1-*vnz_14905*$_{390\text{-}506}$; Amp$^R$ | This study |
| pECAL47 | pGEX-6P-1-*vnz_27460*; Amp$^R$ | This study |
| pECAL48 | pGEX-6P-1-*vnz_28040*$_{380\text{-}507}$; Amp$^R$ | This study |
| pSVAL6 | pIJ10770-*disA*; Hyg$^R$ | (Latoscha et al., 2020) |
| pSVAL11 | pIJ10770-*vnz_27305prom-ataC* (200 bp upstream of *vnz_27305* start codon fused to *ataC*); Hyg$^R$ | (Latoscha et al., 2020) |
| pSVAL12 | pIJ10770-*vnz_27305prom-ataC*$_{D269N}$ (pSVAL11 derivative); Hyg$^R$ | (Latoscha et al., 2020) |
| pSVNT-10 | p3xFLAG-*disA*; Hyg$^R$ | (Latoscha et al., 2020) |

[a] ORF cloned without start and stop codons; for cloning of *cpeA and cpeD* the *sven15* annotations were used.

## 3.4 Microbiological methods

### 3.4.1 *Escherichia coli* growth conditions

If not stated otherwise, all *E. coli* strains were grown aerobically at 37 °C.

#### 3.4.1.1 *E. coli* general cultivation and storage

*E. coli* strains were grown in Lysogeny Broth (LB) liquid culture or on LB agar supplemented with antibiotics if required. For strains containing a Hygromycin B resistance (Hyg$^R$), LB was replaced with LBon (LB without salt) and LB agar was replaced with nutrient agar (NA). Growth on plates containing X-Gal was conducted at 30 °C and incubation on MacConkey plates supplemented with 1% maltose was performed at 26 °C. Strains EP432 and LB2003 were cultivated in LBon + 87 mM KCl (LBK) or grown on LBK agar supplemented with Amp if required. For long-term storage, 930 µl of overnight cultures were mixed with 70 µl DMSO in screw cap cryotubes and stored at -80 °C.

#### 3.4.1.2 Growth of strain EP432 in LB200N

Pre-cultures were grown overnight in 5 ml LBK supplemented with Amp (LBK/Amp) in a rotor at 26 °C. For complementation experiments with *cpeABC*, EP432 strains were diluted to an $OD_{578}$ (optical density at 578 nm) 0.05 in 5 ml LBK/Amp or LBon supplemented with Amp, 200 mM NaCl and 50 mM HEPES, pH 7.5 (LB200N/Amp) and grown in a rotor at 37 °C until final $OD_{578}$ was measured.

#### 3.4.1.3 Growth of strain LB2003 in defined minimal liquid medium

The protocol was modified from Gibhardt et al. (2019). Single colonies of LB2003 strains were inoculated into 5 ml LBK/Amp and grown at 37 °C and 220 rpm for 7-9 h. 10 µl of each culture were used to inoculate 5 ml M9 supplemented with Amp and 50 mM KCl (M9/Amp/50 mM KCl) and incubated at 37 °C and 220 rpm overnight. The cultures were diluted to $OD_{578}$ 0.1 in fresh 10 ml M9/Amp/50 mM KCl and grown at 37 °C and 220 rpm for 4 h. After centrifugation at 4000 x g for 10 min, pellets were resuspended in equal volume of potassium-free M9 and incubated at 37 °C and 220 rpm for 30 min. The washed cultures were split into two equal volumes, which were pelleted at 4000 x g for 10 min and resuspended in 4 ml of M9/Amp/50 mM KCl or M9/Amp/10 mM KCl supplemented with 50 µM IPTG. Cultures were diluted to $OD_{578}$ 0.05 in 10 ml M9/Amp/50 mM KCl/50 µM IPTG or M9/Amp/10 mM KCl/50 µM IPTG main cultures, respectively. Main cultures were stored statically at 12 °C in the programmed incubator until automated heating to 37 °C and shaking at 220 rpm started. Starting at 4 h of growth, every hour 500 µl of each culture were mixed with 500 µl M9 and used to assess growth by measuring the $OD_{578}$.

### 3.4.2 *Streptomyces venezuelae* growth conditions

*S. venezuelae* strains were grown aerobically at 30 °C, with the exception of cultures designated for genomic DNA (gDNA) isolation, which were grown for 2-3 days in a rotor at 26 °C.

#### 3.4.2.1 *S. venezuelae* standard cultivation and storage

For determination of growth, immunoblot analysis and nucleotide extraction, 50-100 ml of Maltose-Yeast Extract-Malt Extract supplemented with trace elements (MYM) were filled in baffled flasks and inoculated with *S. venezuelae* spores to a final concentration of $10^6$ CFU/ml. If samples needed to be gathered at defined time points, inoculated cultures were stored statically at 12 °C in the programmed incubator until automated heating to 30 °C and shaking at 170 rpm started.

For storage of spores, sporulated single colonies were streaked as a lawn on MYM agar. After growth for 3-5 days at 30 °C, 2 ml of sterile 20 % glycerol were pipetted atop of bacteria. A sterile cotton pad was used to carefully detach spores from colony surface. Spores were gathered into a 5 ml syringe by filtering the glycerol/spore suspension through the cotton pad. Gathered spores (spore stocks) were stored in screw cap cryotubes at -20 °C.

For Colony forming units (CFU) determination, spore stocks were serially diluted in 20 % glycerol and 10 µl of appropriate dilution steps were spread-plated on LB agar in

duplicates. After 2 days at 30 °C, CFU were counted and used for calculation of the CFU/µl of the spore stock.

#### 3.4.2.2 Analysis of *S. venezuelae* development

To compare differentiation between strains, spore stocks were thawed on ice and diluted in 20 % glycerol. 12 µl of $10^5$ CFU/µl were spotted and patched with a sterile cotton swab on MYM agar. Development of bacteria at 30 °C was monitored regularly and pictures were taken at appropriate time points using a Canon EOS 1300D (W) camera.

For scanning electron microscopy (SEM), *S. venezuelae* strains were grown on MYM agar for up to 7 days and imaging of single colonies was conducted by K. C. Findlay at the John Innes Centre, UK, as described in Tschowri et al. (2014).

In case of strains overexpressing *cpeABC*, spores were also streaked on NA supplemented with 16 µg/ml Hyg and grown for 3 d at RT. Single colonies of approximately the same size were streaked on MYM agar or MYM agar supplemented with 16 µg/ml Hyg. Development of strains was assessed after 4 d at 30 °C.

#### 3.4.2.3 Growth on nutrient agar supplemented with osmolytes

For analysis of growth in presence of 0.4 M (or 0.5 M) KCl, 0.5 M NaCl and 0.5 M sucrose, spore stocks were serially diluted in 20 % glycerol and $10^5$ to $10^2$ CFU (10 µl of $10^4$ to $10^1$ CFU/µl) were spotted on square nutrient agar (NA) plates without (control) or with supplemented osmolytes. After 2 days growth at 30 °C, plates were photographed using a Canon EOS 1300D (W) camera. If 0.5 M KCl was used as supplement, incubation of the KCl plate was extended to 4 days.

In case of strains overexpressing *cpeABC*, spores were streaked on NA supplemented with 16 µg/ml Hyg and grown for 3 d at RT. Single colonies of approximately the same size were streaked on NA, NA + 0.5 M NaCl or 0.4 M KCl. Growth of strains was assessed after 3 d at 30 °C.

### 3.4.3 Conjugation of *E. coli* with *S. venezuelae*

Introduction of cosmids or plasmids into *S. venezuelae* was performed using a modified protocol from (Gust et al., 2003; Gust et al., 2004). For conjugation, overnight cultures of *E. coli* ET12567/pUZ8002 containing mutated cosmids or plasmids (Table 6 and Table 7, respectively) were diluted 1:20 in LB or LBon containing required antibiotics. Cultures were grown at 37 °C until an $OD_{578}$ 0.4-0.8, pelleted in 50 ml reaction tubes for 15 min at 7000 rpm and washed twice with 50 ml LB to remove antibiotics. Pellets were resuspended in LB and ~200 µl ET12567/pUZ8002 suspension were plated with 10 µl *S. venezuelae* spores on Soy Flour Mannitol (SFM) agar. After overnight incubation at RT, SFM plates were overlaid with 2

ml dd$H_2O$ containing 20 µl of 25 mg/ml Nal and 20 µl of 50 mg/ml Apr (cosmids with *apr-oriT* cassette) or 20 µl of 50 mg/ml Hyg (cosmids with *hyg-oriT* cassettes and pIJ10770/pIJ10257 derivatives). Plates dried at RT and were incubated at 30 °C for 2-3 days until colonies appeared.

#### 3.4.3.1 Conjugation of cosmids for chromosomal gene inactivation

*Deletion of genes*: Single clones from conjugations with cosmids for gene deletion were picked from SFM plates and streaked in parallel on NA/Nal supplemented with 5 µg/ml Kan and NA/Apr/Nal or NA/Hyg/Nal. Clones sensitive to Kan, i.e. clones where a double cross-over occurred and the cosmid was lost, were passaged 1-2 times on fresh NA/Apr/Nal or NA/Hyg/Nal. Spore stocks were generated as described above after extraction of gDNA and verification of the integration of the resistance cassette at the intended site using site-specific primers for each deleted gene.

*Introduction of the chromosomal D86A point mutation into disA*: Cosmid Sv-4-B12 *neo::apr-oriT disA::disA*$_{D86A}$ was generated via single-stranded DNA recombineering (paragraph 3.5.5). It was conjugated via ET12567/pUZ8002 with *S. venezuelae* wild-type spores, and selected on SFM as described above. Single colonies from the SFM plate were passaged twice on NA/Apr/Nal, followed by 3 passages on NA without antibiotics to achieve loss of the cosmid. Colonies were streaked on NA/Apr and Apr$^S$ clones were verified for successful *disA*$_{D86A}$ mutation via Polymerase Chain Reaction (PCR) with allele-specific primers and sequencing of the *disA* allele. Spore stock was prepared as described above.

#### 3.4.3.2 Complementation with plasmids

Single colonies from conjugations with derivatives of vectors pIJ10770 or pIJ10257 were picked from SFM plates and passaged twice on NA/Hyg/Nal before preparing spore stocks.

### 3.4.4 Chromosomal gene inactivation via SV1 transduction and storage of phage lysates

For transduction of the *disA::apr* and *ataC::apr* alleles into a new wild type background, *S. venezuelae*-specific SV1 phages were used. The protocol was modified from Tschowri et al. (2014). Wild-type SV1 lysate from the Tschowri lab collection was serially diluted in LB and 100 µl of $10^{-2}$, $10^{-4}$, $10^{-6}$ dilutions were mixed with 6 µl spores of *S. venezuelae* Δ*disA* or Δ*ataC* to generate SV1 *disA::apr* and SV1 *ataC::apr*, respectively. The suspension was mixed with 800 µl TB soft agar, plated on NA-Ca$(NO_3)_2$ and incubated overnight at 30 °C. The plates containing $10^{-6}$ dilutions of SV1 phages were overlaid with 2.5 ml LB for 3-4 h at RT since they produced the best plaques. Liquid was gathered into syringes and filtered through 0.45 µm filters. Phage lysates were stored in screw cap glass tubes at 4 °C.

To transduce the *disA::apr* and *ataC::apr* alleles, 100 µl of respective phage lysates were mixed with 5 µl of *S. venezuelae* wild-type spores, plated on MYM agar and incubated overnight at RT. Plates were overlaid with 2 ml dd$H_2O$ containing 20 µl of 50 mg/ml Apr and incubated at 30 °C until colonies appeared. Single colonies were streaked on NA/Apr to test for successful allele transduction. Integration of the antibiotic cassettes at the correct site was verified via PCR using site-specific primers. Spore stocks were prepared and stored as described in paragraph 3.4.2.1.

A similar approach for the transduction of the *cpeA::apr*, *cpeB::apr*, *cpeD::hyg* and *cpeE::hyg* alleles failed since the respective phage lysates could not be generated.

### 3.4.5 Heat shock of *S. venezuelae* spores

To assess viability of spores of *S. venezuelae* Δ*disA*, $disA_{D86A}$ and Δ*ataC* in comparison to the wild type, a modified protocol from Tschowri et al. (2014) was used. Spores were diluted to ~$10^9$ CFU/ml in 300 µl 20 % glycerol. 20 µl were serially diluted and 10 µl of $10^{-5}$ and 3 µl of $10^{-4}$ dilutions were plated in duplicates on LB agar. After 2 d at 30 °C, CFU were counted and used to assess the “CFU/ml at 0 min”. 250 µl of the $10^9$ CFU/ml dilution were incubated in 1.5 ml reaction tubes in a water bath at 50 °C for 1 h, diluted and plated similarly as above. The CFUs were counted and the “CFU/ml at 60 min” was calculated. To determine survival in % the ratio of the CFU/ml at 60 min to CFU/ml at 0 min multiplied by 100 was determined.

### 3.4.6 Spore viability after UV light stress

Spore stocks were diluted in 20 % glycerol to ~8 x $10^8$ CFU/ml. 100 µl suspensions were exposed to UV light (254 nm) at intensities of 100 to 400 J $m^{-2}$ in sterile, transparent PCR tubes. After treatment, spore suspensions were serially diluted and 10 µl of $10^{-5}$ and $10^{-4}$ dilutions were plated in duplicates on LB agar for CFU determination. The survival rate was calculated as described for the heat shock (paragraph 3.4.5) setting not exposed spores (0 J $m^{-2}$) as 100 % survival.

### 3.4.7 Sterilization and decontamination of materials

All heat-resistant materials, as well as liquid and solid waste, were sterilized by autoclaving for 20 min at 121 °C. Heat-sensitive materials, contaminated glass pipettes and centrifugation cups were decontaminated with 1% Mucocit T (schülke) at least overnight.

## 3.5 Biomolecular methods

### 3.5.1 DNA isolation

Cosmids and plasmids were isolated from 5-10 ml *E. coli* overnight cultures using the innuPREP Plasmid Mini Kit 2.0 (Analytik Jena) and *S. venezuelae* gDNA was isolated from

5 ml MYM cultures using innuPREP Bacteria DNA Kit (Analytik Jena) according to manufacturer's instructions. Quality and concentration of DNA were assessed with the NanoDrop 2000 spectrophotometer.

## 3.5.2 Used oligonucleotides

**Table 8:** List of used oligonucleotides.
Underlined nucleotides show restriction sites (specified in primer names or description), nucleotides in bold indicate introduced mutations and nucleotides in italics represent sequences to overlapping genes.

| **Oligonucleotide** | **Sequence** | **Purpose/Description and reference where applicable** |
|---|---|---|
| disA_D86Achr_rev | TCTTGGTGATGTCCTTGTCGAGGACGAGCGC GCC**CG**CGAGCTTGCACAGCTCCCGCAGCCG CGTGGCGGC | Introduction of the D86A point mutation into *disA* in Sv-4-B12 (Latoscha et al., 2020) |
| Oligo 100 | AAGTCGCGGTCGGAACCGTATTGCAGCAGCT TTATCATCTGCCGCTGGACGGCGCACAAATC GCGCTTAA | Restoration of *galK* gene in HME68 (Costantino & Court, 2003) |
| disA_D86A_check_fwd | GGAGCTGTGCAAGCTCGCG | $disA_{D86A}$ allele-specific PCR with disA_rev_XhoI as reverse primer (Latoscha et al., 2020) |
| disA_fwd_NdeI | TATCATATGGTGGCAGCCAAGGAC | Amplification of *disA* for sequencing; cloning of *disA* into pET15b (pECAL1) (Latoscha et al., 2020) |
| disA_rev_XhoI | TATCTCGAGCTAGACGTACCGCTCAAG | |
| neo_H1-P1-fw | AGATCTGATCAAGAGACAGGATGAGGATCGT TTCGCatg*ATTCCGGGGATCCGTCGACC* | Amplification of *apr-oriT* cassette with flanks homologous to *neo* (Kan resistance cassette); pIJ773 used as template (sequence overlapping to antibiotic cassette in italics) |
| neo_H2-P2-rev | TCGCTTGGTCGGTCATTTCGAACCCCAGAGT CCCGCtca*TGTAGGCTGGAGCTGCTTC* | |
| neo_test-fw | GTTTTATGGACAGCAAGCG | Verification of *neo* replacement by *apr-oriT* |
| neo_test-rev | GAATCGAAATCTCGTGATG | |
| disA_test_f | GTGGTTCACTCACGCCGCATGAACGGTTC | Primers for *disA* site-specific PCR from *S. venezuelae* gDNA (St-Onge et al., 2015) |
| disA_test_r | GGCACGTACCTGGTGGAGGCGAAGGTG | |
| 3142_NdeI-for | GCTGCATATGGGCCGGCGGGTCG | Amplification of 528 bp upstream of *disA* and *disA* without stop codon for generation of pSVNT-10 (Latoscha et al., 2020) |
| 3142_XhoI-rev | GCAGCCTCGAGGACGTACCGCTCAAGGATC | |
| disA_rev_XhoI | TATCTCGAGCTAGACGTACCGCTCAAG | In combination with 3142_NdeI-for: amplification of 528 bp upstream of *disA* and *disA* with stop codon for generation of pSVAL6 (Latoscha et al., 2020) |
| pSS170_seq_f | GCTCAGTGGAACGAAAACTC | Test primers for verification of successful cloning into pIJ10770 |
| pSS170_seq_r | CTGATGTGCTCAGTATCACC | |
| 27310_fwd_Apra | CGAAGCGATCGCGGCCACCGCCGCGCCCAC CCGCTGATG*ATTCCGGGGATCCGTCGACC* | Deletion of *vnz_27310* (*ataC*) on PI1_F15; pIJ773 used as template (sequence overlapping to antibiotic cassette in italics) (Latoscha et al., 2020) |
| 27310_rev_Apra | GGTCGTGGGGGGGGAGGAGACGGGTGAGGA GTGGGCTCA*TGTAGGCTGGAGCTGCTTC* | |
| 27310_test_f | ACACCGTGCGGCAGACCC | Primers for *ataC* site-specific PCR |

| | | |
|---|---|---|
| 27310_test_r | TTCCCGCAGTCCATGGTTCC | from *S. venezuelae* gDNA (Latoscha et al., 2020) |
| 27305prom_f_NdeI | TATCATATGGGTGTCCCGGCTCGTCGAC | Amplification of 200 bp upstream of *vnz_27305* (sequence in italics indicate introduced overlap to *ataC*) (Latoscha et al., 2020) |
| 27305prom_r_OL_ataC | *GCTGCACCAT*GGACTCCATCCTACGGGGCT | |
| ataC_f_OL_27305prom | *GATGGAGTCC*ATGGTGCAGCCGACCGCCGT | Amplification of *ataC* for fusion to *vnz_27305prom* (sequence in italics indicate introduced overlap to *vnz_23705prom*) (Latoscha et al., 2020) |
| 5409_rev_XhoI | TATACTCGAGTCAGGTGCGGACTTCGAG | |
| D269N_backbone_f | CGGCGCTGTACGTCACGGCC**A**ACCACGGCAT GGTCGACAT | Used to generate pSVAL12 with pSVAL11 as template |
| D269N_backbone_r | ATGTCGACCATGCCGTGGT**T**GGCCGTGACGT ACAGCGCCG | |
| 31290_fwd_Apra | GCTTGGGACAGGAAACGGGCGAAAGGTGAA GCGGGCGTG*ATTCCGGGGATCCGTCGACC* | Deletion of *vnz_31290* on PI2_N1; pIJ773 used as template (sequence overlapping to antibiotic cassette in italics |
| 31290_rev_Apra | CGCCGCCACGGGCGGCGACAACTCCGGCGG GGACAGCAG*TGTAGGCTGGAGCTGCTTC* | |
| 31290_test_f | ATGCCGACGGCGGGCTAC | Primers for *vnz_31290* site-specific PCR from *S. venezuelae* gDNA |
| 31290_test_r | CCGGTAGTGCCGAACAGGCG | |
| 28050_fwd_apr | GCCGCTGCCTCCATACTCGGACGGGAGTGAT CGCCTGTG*ATTCCGGGGATCCGTCGACC* | Deletion of *vnz_28050* (*cpeB*) on 4B02; pIJ773 used as template (sequence overlapping to antibiotic cassette in italics) |
| 28050_rev_apr | TCTCCCGGCTGGTGATCGCCGCCCAGGTGTC CTCACTCA*TGTAGGCTGGAGCTGCTTC* | |
| 28050_test_f | ACGGAGACCGGTGTCTCGAT | Primers for *cpeB* site-specific PCR from *S. venezuelae* gDNA |
| 28050_test_r | GCGCCGCCGAGGTAGACA | |
| 28525_fwd_hyg | CGGCCGCCGCGATACTCGGTCGGGAGTGAG GGCGTCGTG*ATTCCGGGGATCCGTCGACC* | Deletion of *vnz_28525* (*cpeE*) on PI1_A22; pIJ10700 used as template (sequence overlapping to antibiotic cassette in italics) |
| 28525_rev_hyg | GGGAGTCCGTCGAGATCGCGGACTGAGGGA CCGCGGTCA*TGTAGGCTGGAGCTGCTTC* | |
| 28525_test_f | AGGCGGGCGCCTCCATC | Primers for *cpeE* site-specific PCR from *S. venezuelae* gDNA |
| 28525_test_r | GGAGCTTCTGTCGTCCGCGA | |
| 28055_fwd_apr | GCGTCACGTAGGAAAGCGAACACGAGGGGG ACAGCTGTG*ATTCCGGGGATCCGTCGACC* | Deletion of *vnz_28055* (*cpeA*) on 4B02; pIJ773 used as template (sequence overlapping to antibiotic cassette in italics) |
| 28055_rev_apr | GAACTCGATCAGGAACAGAGCGGAATGCACA GGCGATCA*TGTAGGCTGGAGCTGCTTC* | |
| 28055_test2_f | ACACGCGGAAAGTGGCACGAT | Primers for *cpeA* site-specific PCR from *S. venezuelae* gDNA |
| 28055_test2_r | AGGCCGGCCAGGAGGTACAG | |
| 28520_fwd_hyg | ATCACCCTTCGACACGACCATAGGAGGGACG GGCCCTTG*ATTCCGGGGATCCGTCGACC* | Deletion of *vnz_28520* (*cpeD*) on PI1_A22; pIJ10700 used as template (sequence overlapping to antibiotic cassette in italics) |
| 28520_rev_hyg | AATTCGATCAGGAAGACCGCGGAGTGCACGA CGCCCTCA*TGTAGGCTGGAGCTGCTTC* | |
| 28520_test2_f | AGGATCCGGCGGCTTGTCCAT | Primers for *cpeD* site-specific PCR from *S. venezuelae* gDNA |
| 28520_test2_r | AGGGGTATCGGGGAGAAGCT | |

| | | |
|---|---|---|
| 12665_fwd_apr | TCACATTTCGCCCAGATTGGGCGAGGTGACG GCGGATGG*ATTCCGGGGATCCGTCGACC* | Deletion of *vnz_12665* on Sv-3-C02; pIJ773 used as template (sequence overlapping to antibiotic cassette in italics) |
| 12665_rev_apr | GATGTTCCGGTCGAGGAATTCGATCATTGCGT CCCCTCA*TGTAGGCTGGAGCTGCTTC* | |
| 12665_test_f | GTTCGGGCGAGGCGTTGATC | In combination with e.g. 28040_rev_apr verification of *vnz_12665* deletion |
| 14905_fwd_hyg | CACCAGCTCAACGAACTCCTGCTCATCAGCTC CCTCGTG*ATTCCGGGGATCCGTCGACC* | Deletion of *vnz_14905* on 4I14; pIJ10700 used as template (sequence overlapping to antibiotic cassette in italics) |
| 14905_rev_hyg | CCTGAATTAATGCCTCGGATTAACGGGATGTT CACGTCA*TGTAGGCTGGAGCTGCTTC* | |
| 14905_test_f | GCCATGACGGCCGCTGGAA | In combination with e.g. 28040_rev_apr verification of *vnz_14905* deletion |
| 28040_fwd_apr | CGCCGCCTGCGCCGGCGCAGGCCCTAGGGG CGCGCTGTG*ATTCCGGGGATCCGTCGACC* | Deletion of vnz_28040 on 4B02; pIJ773 used as template (sequence overlapping to antibiotic cassette in italics) |
| 28040_rev_apr | TCGCACAGGTCTCCCGCCCGTCGAACAGCTC CTAGGTCA*TGTAGGCTGGAGCTGCTTC* | |
| 28040_test_f | TGGCGGCGGGCCTGATCAT | In combination with e.g. 14905_rev_hyg verification of *vnz_28040* deletion |
| disA_D86A_fwd | GCAAGCTCG**CG**GGCGCGCTC | Used in combination with disA_rev_XhoI and disA_fwd_NdeI to generate the insert for pECAL3; Used to generate pECAL21 (Latoscha et al., 2020) |
| disA_D86A_rev | GAGCGCGCC**CG**CGAGCTTGC | |
| 5409_fwd_NdeI | TATCATATGATGGTGCAGCCGACCG | In combination with 5409_rev_XhoI used to amplify full length *ataC* for cloning into pET15b (Latoscha et al., 2020) |
| 6143_fwd_NdeI | TATCATATGGTGATCGTCATCGCCCATGT | Amplification of full length *vnz_31010* for cloning into pET15b (Latoscha et al., 2020) |
| 6143_rev_BamHI | TATGGATCCTCAGACCGGCACGGTC | |
| 6202_fwd424_NdeI | TATCATATGCGCGACGACGACGCCTA | Amplification of the cytosolic domain of *vnz_31290* for cloning into pET15b |
| 6202_rev_BamHI | TATGGATCCTCAGCGGTTTTTGTCCTGTG | |
| 28055_fwd_NdeI | TATCATATGGTGCCTGCTCCACGGATG | Amplification of full length *cpeA* (*sven15_5557* annotation) for cloning into pET15b (Latoscha et al., 2020) |
| 28055_rev_XhoI | TATACTCGAGTCACTCCCGTCCGAGTATGG | |
| 28520_f_NdeI | TATCATATGATGAGAACGACACCCCTGC | Amplification of N-terminally truncated *cpeD* (*vnz_28520* annotation) for cloning into pET15b |
| 28520_r_XhoI | TATACTCGAGTCACTCCCGACCGAGTATCG | |
| pET15b_28520ext_f | *TTGCCTGCTCCGCGG*ATGAGAACGACACCCC TGC | Generation of pECAL33 containing full length *cpeD* (*sven15_5647* annotation) from pECAL22*;* sequences introducing the missing N-terminal aa are in italics |
| pET15b_28520ext_r | *CCGCGGAGCAGGCAA*CATATGGCTGCCGCG CGG | |
| trkAext_fwd_NdeI | TATCATATGGTGCACATCGTCATCATG | Cloning of full-length *vnz_27460* into pET15b |
| trkAext_rev_XhoI | TATACTCGAGTCAGTGACCGCCCTC | |
| T7prom | taatacgactcactataggg | Colony PCR of pET15b constructs and sequencing of inserts |
| T7term | Gctagttattgctcagcgg | |

| | | |
|---|---|---|
| pgpH_HD_f_BamHI | TATGGATCCGCTAATCCAAACCATCCATT | Cloning of the HD domain of *pgpH* from *L. monocytogenes* into pGEX-6P-1 |
| pgpH_HD_r_SmaI | TCCCGGGTCAATCTTTGTCATCAGGAT | |
| vnz_12665_fwd | cctgggatccATGCGTATCAACCTGCGTG | Cloning of codon-optimized cytosolic domain of *vnz_12665* into pGEX-6P-1 (BamHI/SmaI) |
| vnz_12665_rev | aattcccgggTTAATCGTTTTTAACCACCGC | |
| vnz_14905_fwd | cctgggatccGCGGCGGATCTGGGTGTG | Cloning of codon-optimized cytosolic domain of *vnz_14905* into pGEX-6P-1 (BamHI/SmaI) |
| vnz_14905_rev | aattcccgggTTAGCCGCTGCTACGACG | |
| vnz_27460_fwd | cctgggatccGTGCACATCGTCATCATGGG | Cloning of full-length *vnz_27460* into pGEX-6P-1 (BamHI/SmaI) |
| vnz_27460_rev | aattcccgggTCAGTGACCGCCCTCCTC | |
| vnz_28040_fwd | cctgggatccGCGCGTCCGGGTGCGGTG | Cloning of codon-optimized cytosolic domain of *vnz_28040* into pGEX-6P-1 (BamHI/SmaI) |
| vnz_28040_rev | aattcccgggTTATTCGGTACCGCCACCCACCGG | |
| pGEX_seq_f | ggctggcaagccacgtttg | Colony PCR of pGEX-6P-1 constructs |
| pGEX_seq_r | cgggagctgcatgtgtcag | |
| GEX-F | CTTTGCAGGGCTGGCAAG | Sequencing of inserts in pGEX-6P-1 |
| GEX-R | GAGCTGCATGTGTCAGAGG | |
| 28050_NT25f_XbaI | TATTCTAGACGTGCATTCCGCTCTGTTCCT | Amplification of *cpeB* for cloning into pKNT25 (Latoscha et al., 2020) |
| 28050_NT25r_KpnI | TATGGTACCCGCGCGCGGCCGGCCGGATCCT | |
| 28055_T18f_KpnI | TATGGTACCGCCTGCTCCACGGATGAGC | Amplification of *cpeA* for cloning into pUT18 (Latoscha et al., 2020) |
| 28055_T18r_EcoRI | TAGCAGAATTCGACTCCCGTCCGAGTATGGAGG | |
| 28045_T18_f | *ccgggtaccg*AGTGAGGACACCTGGGCG | Amplification of *cpeC* for cloning into pUT18 via Gibson Assembly; PCR product can be digested with KpnI and EcoRI |
| 28045_T18_r | *ctgaattcga*GGAGCTGTTCGACGGGCG | |
| T18_28045_f | *gaacagctcc*TCGAATTCAGCCGCCAGC | Amplification of pUT18 for *cpeC* insertion |
| T18_28045_r | *tgtcctcact*CGGTACCCGGGGATCCTC | |
| 28045_T25_f | gactctagagAGTGAGGACACCTGGGCG | Amplification of *cpeC* for cloning into pKNT25 via Gibson Assembly; PCR product can be digested with XbaI and KpnI |
| 28045_T25_r | tc*ggtacc*cgGGAGCTGTTCGACGGGCG | |
| T25_28045_f | gaacagctccCGGGTACCGAGCTCGAATTC | Amplification of pKNT25 for *cpeC* insertion |
| T25_28045_r | tgtcctcactCTCTAGAGTCGACCTGCAG | |
| 28525_NT25_f | *gactctagag*CACTCCGCGGTCTTCCTGATCGAATTCGG | Amplification of *cpeE* for cloning into pKNT25 via Gibson Assembly; PCR product can be digested with XbaI and KpnI |
| 28525_NT25_r | *tcggtacccg*CGCCCGCTCGGAGGCGGA | |
| NT25_28525_f | *cgagcgggcg*CGGGTACCGAGCTCGAATTC | Amplification of pKNT25 for *cpeE* insertion |
| NT25_28525_r | *ccgcggagtg*CTCTAGAGTCGACCTGCAG | |
| T18disA_28520_f | *cggtcgggag*TCGAATTCAGCCGCCAGC | Amplification of pUT18 for *cpeD* insertion |
| T18_28520_r | *gcggagcagg*CGGTACCCGGGGATCCTC | |

| | | |
|---|---|---|
| 28520_T18_f | *ccgggtaccg*CCTGCTCCGCGGATGAGA | Amplification of *cpeD* for cloning into pUT18 via Gibson Assembly; PCR product can be digested with KpnI and EcoRI |
| 28520_T18disA_r | *ctgaattcga*CTCCCGACCGAGTATCGC | |
| T18RCKC_disAFLAG_f | *cgacaagtag*TATGGTGCACTCTCAGTAC | Amplification of pUT18-*cpeA* and pUT18-*cpeD* with sequences complementary to *disA-FLAG* and $lac_P$ at the 5' and 3' end, respectively (for pECAL20 and pECAL34) (Latoscha et al., 2020) |
| T18RCKC_lacp_r | *gtgccagctg*TTACTTAGTTATATCGATTGGC | |
| lacp_T18RCKC_f | *aactaagtaa*CAGCTGGCACGACAGGTTTC | Amplification of $lac_P$ from pUT18 with sequences complementary to T18-fragment and *disA-FLAG* at the 5' and 3' end, respectively (for pECAL20 and pECAL34) (Latoscha et al., 2020) |
| lacp_disAFLAG_r | *ccttggctgc*CATAGCTGTTTCCTGTGTGAAATTGTTATC | |
| disAFLAG_lacp_f | *aacagctatg*GCAGCCAAGGACGGGGCA | Amplification of *disA-FLAG* with sequences complementary to $lac_P$ and pUT18 at the 5' and 3' end, respectively (for pECAL20 and pECAL34) (Latoscha et al., 2020) |
| disAFLAG_T18RCKC_r | *gtgcaccata*CTACTTGTCGTCATCGTCCTTGTAGTCG | |
| cpeA-disAFLAG_f_BC | *cagctcctag*CAGCTGGCACGACAGGTTTC | Amplification of pUT18-*cpeA-disA-FLAG* for *cpeBC* insertion |
| cpeA-disAFLAG_r_BC | *caggcgatca*CTCCCGTCCGAGTATGGAG | |
| cpeBC_f_A_disAFLAG | *cggacgggag*TGATCGCCTGTGCATTCC | Amplification of *cpeBC* for cloning into pUT18-*cpeA-disA-FLAG* via Gibson Assembly |
| cpeBC_r_A_disAFLAG | *gtgccagctg*CTAGGAGCTGTTCGACGG | |
| T18RCKC_testFLAG_f | gagcggacgttcgaagttct | Sequencing of *disA-FLAG* and $disA_{D86A}$-*FLAG* in all respective pUT18 constructs (Latoscha et al., 2020) |
| T18RCKC_testFLAG_r | cggtcacagcttgtctgtaa | |
| disA_D86A_fwd2 | GCGGGAGCTGTGCAAGCTCG**CG**GGCGCGCTCGTCCTCGAC | Used to generate pECAL35 and pECAL37 from pECAL34 and pECAL36, respectively |
| disA_D86A_rev2 | GTCGAGGACGAGCGCGCC**CG**CGAGCTTGCACAGCTCCCGC | |
| pIJ10257_fwd_ABC | cagctcctagAAGCTTGGATCCTAGGTTC | Amplification of pIJ10257 for *cpeABC* insertion |
| pIJ10257_rev_ABC | gagcaggcacCATATGGGGCCTCCTGTTC | |
| cpeABC_fwd_pIJ10257 | gccccatatgGTGCCTGCTCCACGGATG | Amplification of *cpeABC* for cloning into pIJ10257 via Gibson Assembly |
| cpeABC_rev_pIJ10257 | atccaagcttCTAGGAGCTGTTCGACGG | |
| pIJ10257-seq-fw | acgtccatgcgagtgtcc | Test PCR and sequencing of pIJ10257-*cpeABC* |
| pIJ10257-seq-rev | Ccaaacggcattgagcgtc | |

## 3.5.3 Polymerase chain reaction (PCR)

Generally, Q5 DNA polymerase (NEB) was used for amplification of DNA for cloning and in some cases for test PCRs with *S. venezuelae* gDNA. Opti*Taq* DNA polymerase (roboklon) was used for test PCRs with *S. venezuelae* gDNA and Colony PCRs of *E. coli*.

### 3.5.3.1 PCR using Q5 polymerase

Generally, a master mix without template DNA was prepared. Composition of a single reaction is given in Table 9 and reaction conditions are listed in Table 10.

**Table 9:** Components used in a 50 µl Q5 polymerase reaction.

| Component | Volume [µl] | Final concentration |
|---|---|---|
| 5x Q5 Reaction Buffer | 10 | 1x |
| 5x High GC Enhancer | 10 | 1x |
| 10 mM dNTPs (NEB) | 1 | 200 µM |
| 10 µM Forward Primer | 2.5 | 0.5 µM |
| 10 µM Reverse Primer | 2.5 | 0.5 µM |
| Q5 High-Fidelity DNA Polymerase | 0.5 | 0.02 U/µl |
| dd$H_2O$ | 22.5 | |
| Template DNA | 1 | < 1000 ng |
| Total volume | 50[a] | |

[a] For test PCRs, reaction volume was reduced to 25 µl by using half of the volume of all components except template DNA.

**Table 10:** Reaction conditions for Q5 polymerase PCR.

| | |
|---|---|
| Initial denaturation | 30 s at 98 °C |
| **35 cycles:** | |
| Denaturation | 10 s at 98 °C |
| Primer annealing | 30 s at X °C[a] |
| Extension | X min at 72 °C[b] |
| Final Extension | 2 min |

[a] Annealing temperature (Ta) for each primer pair was calculated by evaluation of the gene-specific primer sequences with "Q5 settings" in NEB Tm Calculator (https://tmcalculator.neb.com/#!/main). Generally, the formula was: Ta = lowest Tm + 1 °C (max. 72 °C).

[b] Extension time: 30 s per 1 kb fragment + 3 s.

### 3.5.3.2 PCR and Colony PCR using Opti*Taq* polymerase

A master mix without template DNA was prepared for all reactions. Composition of a single reaction is given in Table 11 and reaction conditions are listed in Table 12. For Colony PCR, a single colony was picked from solid medium, suspended in 1 ml sterile dd$H_2O$ and 1 µl of this suspension was used as template DNA.

**Table 11:** Components used in a 25 µl Opti*Taq* polymerase reaction.

| Component | Volume [µl] | Final concentration |
|---|---|---|
| 10x Pol Buffer C | 2.5 | 1x |
| 10 mM dNTPs (NEB) | 0.5 | 200 µM |
| 10 µM Forward Primer | 1.25 | 0.5 µM |
| 10 µM Reverse Primer | 1.25 | 0.5 µM |
| Opti*Taq* DNA Polymerase, 5 U/µl | 0.25 | 1.25 U/µl |
| dd$H_2O$ | 18.25 | |
| Template DNA | 1 | |
| Total volume | 25 | |

**Table 12:** Reaction conditions for Opti*Taq* polymerase PCR.

| Initial denaturation | 2 min at 95 °C[a] |
|---|---|
| **35 cycles:** | |
| Denaturation | 10 s at 95 °C |
| Primer annealing | 30 s at X °C[b] |
| Extension | X min at 72 °C[c] |
| Final Extension | 2 min |

[a] Initial denaturation extended to 5 min for Colony PCRs.

[b] Annealing temperature for each primer pair was calculated by evaluation of the gene-specific primer sequences with "Taq DNA polymerase" settings in NEB Tm Calculator (https://tmcalculator.neb.com/#!/main). Generally, the formula was: Ta = lowest Tm - 5 °C.

[c] Extension time: 60 s per 1 kb + 3 s.

### 3.5.3.3 Overlap PCR

An Overlap PCR with Q5 DNA Polymerase was used to amplify the insert for the construct pET15b-*disA*$_{D86A}$ (pECAL3). For that, two separate PCRs were performed. Fragment 1 (F1) was amplified with primers disA_fwd_NdeI/disA_D86A_rev and F2 was amplified with disA_D86A_fwd/disA_rev_XhoI from *S. venezuelae* gDNA; primers disA_D86A_fwd and disA_D86A_rev are complementary to each other and carry the D86A mutation. The PCR products (F1 and F2) were gel purified (paragraph 3.5.6) and used as templates in the same PCR with the flanking primers disA_fwd_NdeI/disA_rev_XhoI. The resulting fragment of 1143 bp was gel purified and used for cloning into pET15b.

In a similar way, full length *ataC* was fused to *vnz_27305prom*. F1 (promoter region 200 bp upstream of *vnz_27305* start codon) and F2 (*ataC*) were amplified separately and fused in a second PCR via overlapping sequences at their 3' and 5' end, respectively. The resulting promoter-*ataC* product was gel purified and cloned into pIJ10770.

### 3.5.3.4 Primer-based site-directed mutagenesis in plasmids

The primers were designed to introduce point mutations in pIJ10770-*vnz_27305prom-ataC* (primers: D269N_backbone_f/D269N_backbone_r); pUT18-*cpeA-disA-FLAG* (primers: disA_D86A_fwd/disA_D86A_rev); pUT18-*cpeD-disA-FLAG* and p*cpeABC-disA-FLAG* (primers: disA_D86A_fwd2/disA_D86A_rev2). The respective primer pairs are complementary to each other and allow amplification of a circular PCR product when the plasmids above were used as template DNA. Q5 PCRs were purified using the Monarch PCR & DNA Cleanup Kit (NEB) and digested for ~2 h at 37 °C with FastDigest DpnI (Thermo Fisher Scientific) according to manufacturer's instructions. DpnI is a methylation-sensitive restriction enzyme, which digests only the methylated template DNA, but not the methylation-free PCR product. The circular PCR product was dialyzed on a cellulose membrane (Merck Millipore) against dd$H_2O$ and used for electroporation of electro-competent *E. coli* W3110 or

DH5α. Plasmids were isolated (paragraph 3.5.1) and the mutations were verified via Sanger sequencing (paragraph 3.5.13).

Similarly, the construct pET15b-*cpeD*$_{extended}$ was generated. 15 bp missing in the *vnz_28520* annotation on StrepDB were introduced via PCR into pET15b-*cpeD* directly downstream of the NdeI restriction site. The primers pET15b_28520ext_f/ pET15b_28520ext_r were designed that the 15 bp on their 5' termini were complementary to each other and thus generated a circular PCR product. Further handling was performed as described above.

## 3.5.4 PCR targeting of cosmids

Gene deletion via replacement with antibiotic cassette was conducted using a modified Redirect PCR targeting protocol (Gust et al., 2003; Gust et al., 2004). A full list of cosmids with the encoded genes of interest is given in Table 6. Generally, cosmids were diluted and electroporated into electrocompetent *E. coli* BW25113/pIJ790 (paragraph 3.5.11). *oriT* containing Apr resistance (*aac(3)IV-oriT*) or Hyg resistance (*hyg-oriT*) cassette was PCR amplified and extended with 39 bp regions homologous to the locus of the gene of interest. This PCR product was introduced into L-arabinose-induced BW25113/pIJ790 containing the respective cosmid for λ Red mediated recombination. Transformants were plated on LB agar containing Apr, Cm and Kan or NA supplemented with Hyg, Cm and Kan and incubated overnight at 30 °C. Single clones were tested in Colony PCR (paragraph 3.5.3.2) for correct resistance cassette integration using site-specific test primers flanking the recombination site. Cosmids showing only the correct fragment size for antibiotic resistance insertion were isolated and transformed into strain ET12567/pUZ8002 for conjugation with *S. venezuelae* (paragraph 3.4.3). PI1_F15 *ataC::apr* contained traces of wild-type cosmid (as indicated by PCR) and was transformed into *E. coli* W3110, which was subsequently plated on LB/Apr agar to select for the mutated cosmid only. The loss of wild-type PI1_F15 was confirmed by PCR and pure PI1_F15 *ataC::apr* was isolated, transformed into strain ET12567/pUZ8002 for conjugation with wild-type *S. venezuelae.*

## 3.5.5 Single-stranded DNA recombineering in cosmids

To introduce the D86A point mutation into *disA* encoded on Sv-4-B12 a modified protocol from Tschowri et al. (2014) was used. First, the Kan resistance cassette (*neo*) in Sv-4-B12 was recombined with *apr-oriT* extended with homologous regions to *neo* as described for gene deletions in paragraph 3.5.4. The resulting cosmid SV-4-B12 *neo::apr-oriT* was transformed into mismatch repair-deficient *E. coli* HME68 and plated on LB agar containing Amp, Apr and Cm for selection. HME68/SV-4-B12 *neo::apr-oriT* was made electrocompetent including a heat shock at 42 °C for 15 min in a water bath to induce λ Red prior to

electroporation or storage. Induced bacteria were then electroporated with 1 µl of 100 µM mutagenic oligonucleotide disA_D86Achr_rev and oligo100 (Costantino & Court, 2003). oligo100 restores the *galK* gene in HME68 and allows utilization of galactose, which leads to pH decrease and red color of the indicator dye. Thus, screening for red clones on MacConkey agar containing 1% galactose and Apr indicates a successful recombineering event and facilitates identification of recombinant cosmids. Red, $Apr^R$ clones were analyzed by PCR using a primer pair specific for the $disA_{D86A}$ allele and sequenced to verify the presence of the point mutation. The purified cosmid SV-4-B12 *neo::apr-oriT disA::*$disA_{D86A}$ was electroporated into ET12567/pUZ8002 for conjugation with wild-type *S. venezuelae*.

## 3.5.6 Agarose gel electrophoresis

PCR products were separated on 0.8 or 1 % agarose gels at 90-120 V (dependent on the gel size). For 1 % agarose gels, 1 g agarose was dissolved per 100 ml 1x Tris acetate EDTA buffer (TAE; 40 mM Tris, 20 mM acetic acid, 1 mM EDTA). Agarose gels were stained in a GelRed solution (Genaxxon; 1:10000 diluted in $ddH_2O$) until nucleic acid bands were detectable. Gel images were digitized using the AlphaImager.

If using a preparative gel, stained bands were cut out from the gel using a clean scalpel and extracted using the Monarch DNA Gel Extraction Kit (NEB) according to manufacturer's instructions. PCR products were eluted in $ddH_2O$ and concentration and quality were assessed via NanoDrop 1000 spectrophotometer.

## 3.5.7 Enzymatic restriction digestion of DNA

For restriction digestion of vectors and PCR products, High-Fidelity (HF) or FastDigest (FD) restriction enzymes from NEB or Thermo Fisher Scientific, respectively, were used according to manufacturer's instructions. PCR products were digested with both enzymes for 2 h at 37 °C and heat-inactivated under required conditions. Plasmids were digested with the first enzyme for 2 h at 37 °C and the second was added after heat inactivation and incubated at the same conditions. Typical reaction recipes for HF and FD enzymes are given in Table 13 and Table 14, respectively. If enzymes were used, which could not be heat inactivated, digestion was stopped by purification with the Monarch PCR & DNA Cleanup Kit. Plasmids were dephosphorylated with rSAP (recombinant shrimp alkaline phosphatase, NEB) for 1 h at 37 °C (Table 15). rSAP was heat-inactivated for 5 min at 65 °C.

**Table 13:** Components in 20 µl restriction digestion assay with High-Fidelity restriction enzymes.

| Component | Amount | Final concentration |
|---|---|---|
| PCR product or plasmid | Up to 1 µg | Up to 50 ng/µl |
| HF restriction enzyme | 1 µl | 1 U/µl |
| 10x CutSmart Buffer | 2 µl | 1x |
| $ddH_2O$ | up to 20 µl | |

**Table 14:** Components in restriction digestion assay with FastDigest restriction enzymes.

| Component | Amount | Final concentration |
|---|---|---|
| PCR product / plasmid | 0.2 µg / up to 1 µg | 10 ng/µl / up to 50 ng/µl |
| FD restriction enzyme | 1 µl | n. a. |
| 10x FastDigest Buffer | 2 µl | 1x |
| $ddH_2O$ | up to 20 µl[a] | |

[a] Increase reaction volume to 30 µl for (unpurified) PCR product.

**Table 15:** Components in 20 µl dephosphorylation assay with rSAP.

| Component | Amount | Final concentration |
|---|---|---|
| Digested plasmid DNA | 17 µl | Up to 50 ng/µl |
| rSAP | 1 µl | 0.05 U/µl |
| 10x CutSmart Buffer | 2 µl | 1x |

## 3.5.8 Ligation of digested fragments

Restriction enzyme-digested PCR products (inserts) and plasmids were ligated using T4 DNA ligase from NEB or Thermo Fisher Scientific. In both cases inserts were used in a ~3-fold higher concentration than the vectors in 20 µl reactions; in cases with suboptimal ligation, the molar ratios were calculated using the NEBioCalculator (http://nebiocalculator.neb.com/#!/ligation) and used in 3:1 or 5:1 ratios of inserts to plasmids. Ligations with T4 DNA ligase from NEB were performed for ~2 h at RT with subsequent heat inactivation for 10 min at 65 °C. If T4 DNA ligase from Thermo Fisher Scientific was used, the incubation was performed in the PCR machine for 30 min at 22 °C with subsequent inactivation for 5 min at 70 °C. The components for both ligation reactions are given in Table 16. For electroporation, 1-2 µl of ligation reactions were used. Alternatively, ligations were dialyzed on a cellulose membrane (Merck Millipore) against $ddH_2O$ and used completely for electroporation (paragraph 3.5.12).

**Table 16:** Components in 20 µl ligation reactions with NEB or Thermo Fisher Scientific T4 DNA ligase.

| Component | Amount |
|---|---|
| Insert | 3-10 µl |
| Plasmid | 1 µl |
| T4 DNA ligase | 1 µl |
| 10x T4 DNA ligase buffer | 2 µl |
| $ddH_2O$ | up to 20 µl |

## 3.5.9 Gibson Assembly

Gibson Assembly was used as an alternative method to restriction digestion and ligation-based cloning. Here, all components including vectors are amplified via PCR using primers, which introduce overlapping sequences into PCR products. Primers were designed with the NEBuilder Assembly Tool (http://nebuilder.neb.com/#!/). All PCR products required to assemble a full construct were agarose gel purified, mixed with 2x Gibson Assembly Master Mix (NEB) on ice and incubated for 15-20 min at 50 °C. The Master Mix contains all enzymes

and buffers required for assembly. For components and amounts used see Table 17. 1.5 µl or whole reactions (after dialysis) were used for electroporation (paragraph 3.5.12).

**Table 17:** Components in Gibson Assembly reactions.

| Component | Amount |
|---|---|
| Plasmid (PCR amplified) | 50-100 ng |
| Insert(s) (PCR amplified) | 3-fold amount[a] |
| 2x Gibson Assembly Master Mix | 10 µl |
| dd$H_2O$ | up to 20 µl[b] |

[a] In case of *lac*$_P$ (generation of pECAL20 and pECAL34), 5-fold amount compared to plasmid amount was used because the fragment was smaller than 200 bp.

[b] Total reaction volume was reduced to 10 µl to save reagents if fragments for assembly had high concentrations.

## 3.5.10 TSS transformation

TSS transformation was used to introduce plasmids into *E. coli* W3110 Δ*cya*. ~3 single colonies were picked from LB agar plate, inoculated in 2 ml LB and grown for ~2 h in a rotor at 37 °C. 200 µl of culture were mixed with equal volume of 2x TSS (LB containing 20 % PEG-6000, 100 mM $MgSO_4$, 10 % DMSO) and 1 µl of plasmid(s). After 30-60 min on ice, the mixture was incubated for 30-60 min in a rotor at 37 °C. The suspension was plated on LB agar supplemented with required antibiotics and incubated overnight at 30 °C.

## 3.5.11 Generation and storage of electro competent cells

Generally, up to 1000 ml LB (containing antibiotics if required) were inoculated 1:100 with overnight *E. coli* cultures and grown at 37 °C and 150 rpm until the exponential phase ($OD_{578}$ ~0.4-0.8). Strains EP432 and LB2003 were grown in LBK. For strains HME68 and BW25113/pIJ790 culturing conditions were adjusted to 30 °C. BW25113/pIJ790 cultures containing cosmids for PCR targeting were supplemented with 10 mM L-arabinose to induce λ Red. HME68 containing pSVAL1 was heat shocked for 15 min at 42 °C in a water bath after exponential growth was reached. Cultures were incubated on ice for at least 30 min and then centrifuged for 15 min at 6000 rpm and 4 °C. Pellets were washed twice with cold sterile dd$H_2O$ using the same and the half culture volume during the first and the second wash step, respectively. Finally, pellets were washed with 10 ml 10 % glycerol per 500 ml culture. Pellets were resuspended in 1 ml 10 % glycerol (per 500 ml culture), aliquoted and stored at -80 °C.

## 3.5.12 Electroporation

Electrocompetent cells were thawed on ice and 50 µl aliquots were mixed with DNA. Suspensions were transferred to cold electroporation cuvettes and an electric pulse of 2500 V, 25 µF and 200 Ω was applied for 5 ms. Immediately after the pulse, electroporated

cells were mixed with 500 µl cold LB (or LBK) and incubated for ~1-1.5 h at 37 °C or 26 °C (BW25113/pIJ790 and HME derivatives) in a rotor. Transformants were plated on LB, LBK or nutrient agar supplemented with required antibiotics and incubated overnight at appropriate temperatures.

### 3.5.13 DNA sequencing

Sanger sequencing was performed by LGC Genomics. Plasmids were isolated and directly sent for sequencing. pET15b and pGEX-6P-1 constructs were sequenced with T7prom/T7term and GEX-F/GEX-R primers, respectively, available at LGC. pIJ10770 derivatives were sequenced with primers pSS170_fwd_seq/pSS170_rev_seq. pKNT25 and pUT18 constructs were sequenced with standard primers from the Tschowri lab. *disA-FLAG* and *disA*$_{D86A}$*-FLAG* introduced in some pUT18 constructs were sequenced with T18RCKC_testFLAG_f and T18RCKC_testFLAG_r. pIJ10257-*cpeABC* was sequenced with primers pIJ10257-seq-fw, pIJ10257-seq-rev and 28050_test_f.

For sequencing of the *disA* allele on pSVAL3 and in chromosome of *S. venezuelae disA*$_{D86A}$, the *disA* allele was PCR-amplified using Q5 DNA polymerase with primers disA_fwd_NdeI and disA_rev_XhoI. The PCR product was gel purified and sent to LGC Genomics for sequencing with disA_fwd_NdeI.

All obtained sequencings were compared to sequences of theoretical constructs using SerialCloner 2.6.1 (http://serialbasics.free.fr) and the chromatograms of critical positions (e.g. D86A mutation) were inspected in detail using the 4Peaks software (https://nucleobytes.com).

## 3.6 Protein-based and biochemical methods

### 3.6.1 SDS polyacrylamide gel electrophoresis (SDS-PAGE)

Routinely, purified proteins or bacterial lysates were separated on 12 % SDS polyacrylamide gels (recipe and buffer compositions are given in Table 18). Samples were boiled for 10 min at 70 °C or 5 min at 95 °C in 1x SDS sample buffer (10 % glycerol, 60 mM Tris-HCl pH 6.8, 2 % SDS, 0.01 % bromophenol blue, 1.25 % β-mercaptoethanol) and loaded with variable total protein amounts into the wells of the stacking gel. Electrophoresis was performed in 1x SDS PAGE running buffer (25 mM Tris, 190 mM glycine, 0.1 % SDS) at 25 mA per gel for ~45 min. Separated proteins were detected via staining with Coomassie (25 % 2-propanol, 25 % acetic acid, 0.05 % Coomassie blue R250). Coomassie solution was added to the gel and boiled in the microwave with subsequent incubation for ~5 min at RT on an orbital shaker. Coomassie was removed and the gel de-stained by boiling in 10 % acetic acid followed by incubation for 15 min at RT on an orbital shaker. Gels were digitized by scanning with ImageQuant LAS 4000. Alternatively, gels were used for immunoblot analysis.

**Table 18:** Recipe for 4 stacking (4 %) and 2 separating (12 %) SDS polyacrylamide gels.

| Component | Stacking gel | Separating gel |
|---|---|---|
| Lower gel buffer[a] | - | 2.5 ml |
| Upper gel buffer[b] | 1.25 ml | - |
| Rotiphorese Gel 30 (37.5:1) | 0.65 ml | 4 ml |
| dd$H_2O$ | 3.07 ml | 3.45 ml |
| 2,2,2-chloroethanol (TCE), optional | - | 50 µl |
| 10 % APS | 100 µl | 50 µl |
| TEMED | 10 µl | 10 µl |

[a] 36.34 g Tris, 0.4 % SDS, ad 200 ml dd$H_2O$, pH 8.8

[b] 6.06 g Tris, 0.4 % SDS, ad 100 ml dd$H_2O$, pH 6.8.

## 3.6.2 Immunoblot analysis of protein expression

To detect expression of specific proteins, immunoblot analysis was performed on SDS-PAGE-separated lysates from *S. venezuelae* and *E. coli* using specific antibodies.

*Detection of AtaC expression.* To analyze the expression of AtaC, wild-type *S. venezuelae* was grown in MYM at 30 °C and 170 rpm. Beginning at 10 h of growth 2 ml samples were taken every 2 h and pelleted in a swing rotor for 15 min at 3000 rpm and 4 °C. Pellets were washed once with 2 ml 1x phosphate-buffered saline (PBS; 137 mM NaCl, 2.7 mM KCl, 4.3 mM $Na_2HPO_4$, 1.5 mM $KH_2PO_4$, pH 7.3). 300 µl of lysis buffer (10-15 ml PBS with 1 protease inhibitor cocktail tablet, EDTA-free [Roche]) were used to suspend the pellets. The suspensions were transferred into screw cap tubes filled with ~300 µl 0.1 mm silica beads (Roth) and lysed in a Bead Beater using a program with 4 cycles with a pulse of 6 m/s for 30 s and a 60 s interval between pulses. Lysed samples were centrifuged for 15 min at 13000 rpm and 4 °C and supernatant was transferred into 1.5 ml reaction tubes. Total protein concentration of each sample was determined using Roti-Quant (Roth) and a bovine serum albumin standard curve according to manufacturer's instruction. 10 µg total protein per sample and 1.5 ng purified AtaC (positive control) were loaded on two 12 % SDS gels and separated by electrophoresis. One gel was used as loading control and stained with Coomassie, the other was used for Wet Blot transfer on a polyvinylidene difluoride (PVDF) membrane. First, the PVDF membrane was washed in 100 % ethanol for 15 s with subsequent washing in de-ionized water for 2 min. Afterwards, filter papers (Whatman) and the PVDF membrane were soaked in the transfer buffer (25 mM Tris, 192 mM glycine, 20 % ethanol) for 5 min. The SDS gel was shortly equilibrated in the transfer buffer and all components were placed into a Wet blotting cassette. Transfer from gel to PVDF membrane was performed for 75 min at 100 V. The PVDF membrane was blocked in M-TBST (5 % skim milk powder in TBST) for 1 h at RT. Rabbit α-AtaC antiserum (from immunization day 115; generated by Pineda AG using purified 6xHis-AtaC) was diluted 1:2000 in TBST (Tris-buffered saline with 1 % Tween 20; 10 mM Tris, 150 mM NaCl, pH 7.5) and applied to

the blocked membrane for 80 min at RT. Membrane was washed 3x with TBST for 5 min before applying the secondary antibody donkey α-rabbit coupled to horseradish peroxidase (HRP; GE Healthcare) diluted 1:2000 in TBST for 75 min at RT. The membrane was washed again 3x with TBST for 5 min. ECL detection reagent (Perkin-Elmer) was used for detection of AtaC with ImageQuant LAS 4000.

*Detection of DisA-FLAG expression. S. venezuelae* Δ*disA* strain complemented with *disA-FLAG* under control of a *disA* promoter integrated at the $attB_{\Phi BT1}$ site (SVAL5) was grown and sampled as described above. For immunoblotting 5 µg total protein was used. The Wet Blot and detection were performed similar to AtaC detection. Monoclonal mouse α-FLAG antibody (Sigma-Aldrich) was used at a dilution of 1:10000 in TBST overnight at 4 °C. Goat α-mouse-HRP (Thermo Fisher Scientific) was diluted 1:40000 and used as secondary antibody for 1 h at RT.

*Detection of DisA-FLAG and T18 fusion protein expression in E. coli.* To detect expression of CpeA or CpeD fused to the T18 fragment of *B. pertussis* Cya and DisA-FLAG or $DisA_{D86A}$-FLAG expressed from pUT18 derivatives, 5 ml cultures of *E. coli* W3110 Δ*cya* containing different combinations of pKNT25 and pUT18 vectors were grown overnight in a rotor at 26 °C. The $OD_{578}$ was measured and a bacterial pellet containing 30 µg total protein was collected using the formula:

$$\text{x µl} = \frac{30\ \text{µg} * 1000\ \text{µl} * 1\ \text{OD at 578 nm}}{107\ \text{µg} * \text{measured OD at 578 nm}}$$

Pellets were resuspended in 1x SDS sample buffer and boiled for 5 min at 95 °C. 2 µg total protein per strain were loaded in duplicates on a 12 % SDS gel containing 0.5 % TCE (Table 18). The gel was separated as usual and exposed to UV light for 5 min in the UV Stratalinker 1800 (Stratagene). The gel was then used to evaluate protein loading by visualization using the AlphaImager. The proteins were transferred from the gel to a PVDF membrane by semi-dry blotting using a ready-to-use Trans-Blo Turbo Mini PVDF Transfer Pack and the Trans-Blot Turbo Transfer System (Bio-Rad) at 1 A and 25 V for 30 min. Blocking and detection of proteins were performed as described above. After blocking, the membrane was cut in two pieces and one half was incubated with monoclonal mouse α-FLAG antibody and the other with monoclonal mouse 3D1 antibody (Santa Cruz Biotechnology), which specifically binds to the T18 fragment and will be referred to as “α-T18 antibody” from here on. Both antibodies were used at a dilution of 1:10000 in TBST overnight at 4 °C. As secondary antibody 1:20000 goat α-mouse-HRP was used at RT for 1 h.

## 3.6.3 Protein overexpression

For protein overexpression pET15b and pGEX-6P-1 constructs were electroporated into *E. coli* BL21 (DE3) pLysS or Rosetta 2 (DE3). *E. coli* Rosetta (DE3) pET28-*disA*$_{Bsu}$ was used for overexpression of *B. subtilis* DisA. 500 or 1000 ml LB cultures were grown in presence of required antibiotics until exponential phase, induced with 0.1-0.2 mM IPTG and incubated at 16 °C overnight or in some cases at 28 °C for 3.5 h. In case of strains expressing PDEs (AtaC, Vnz_31010 and PgpH$_{HD}$) cultures were supplemented with 0.2 % glucose and upon induction with 0.35 mM $MnCl_2$ (Huynh et al., 2015). Cultures were gathered by centrifugation (6000 rpm, 15 min, 4 °C) and pellets were lysed immediately or stored at -20 °C until lysis.

## 3.6.4 Protein purification

### 3.6.4.1 Purification of 6xHis-tagged proteins

Pellets of cultures, which overexpressed DisA variants, CpeA and CpeD were suspended in DisA lysis buffer (20 mM Tris HCl, pH 8, 300 mM NaCl, 10% glycerol, 20 mM imidazole, 0.05% Triton X-100, 0.5 mM DTT, 5 mM $MgCl_2$). Pellets of cultures with overexpressed PDEs (except PgpH$_{HD}$) were suspended in PDE lysis buffer, which was similar to DisA lysis buffer but contained 20 mM Tris HCl, pH 7.5 instead of pH 8 and 10 mM $MnCl_2$ instead of $MgCl_2$. Suspensions were supplemented with 1 EDTA-free protease inhibitor cocktail tablet and filled up to at least 20 ml with respective lysis buffers. Suspensions were transferred into a French Press cell and 4-6 lysis cycles were performed using a FrenchPress. If multiple pellets were lysed, the FrenchPress cell was washed once with $ddH_2O$ and once with the lysis buffer between pellets. Lysed suspensions were centrifuged for 40 min at 17000 rpm and 4 °C to remove cell debris and insoluble components. Samples of the pellet and the soluble supernatant (lysate) were taken after centrifugation and stored at -20 °C. The lysate was incubated with 0.5-1 ml Ni-NTA (iba or Macherey-Nagel) overnight at 4 °C. Incubated lysate was removed by gravity flow and a sample was taken (column flow through). The matrix was washed with up to 140 ml of the respective lysis buffers and a sample of the last wash step was taken. DisA variants were eluted 5x in 0.5-1 ml DisA elution buffer (50 mM Tris HCl, pH 8; 300 mM NaCl; 10% glycerol; 250 mM imidazole; 0.5 mM DTT; 5 mM $MgCl_2$). CpeA and CpeD were eluted in the same buffer but DTT was replaced by 5 mM β-mercaptoethanol. For elution of PDEs, Tris HCl, pH 8 and $MgCl_2$ were substituted with 50 mM Tris HCl, pH 7.5 and 10 mM $MnCl_2$, respectively. Samples of each elution fraction were taken and all samples were analyzed via SDS-PAGE and Coomassie staining. Eluates of DisA variants, CpeA and CpeD effectors containing the highest amounts of purified proteins were dialyzed twice in 2 l DisA cyclase buffer (25 mM Tris HCl, pH 8, 250 mM NaCl, 10 mM $MgCl_2$, 5 mM β-mercaptoethanol, 10% glycerol; modified from Christen et al. (2005)) at 4 °C.

PDEs were dialyzed in PDE buffer supplemented with 5-10 % glycerol (20 mM Tris, pH 7.5, 50 mM NaCl, 10 mM $MnCl_2$; modified from Huynh et al. (2015)). For AtaC variants from pathogenic organisms, $MnCl_2$ in all purification buffers was reduced to 1 mM and omitted in the PDE buffer to avoid protein precipitation and manganese oxidation. Dialyzed proteins were stored at -20 °C.

### 3.6.4.2 Purification of GST-tagged proteins

The pellet of BL21 (DE3) pLysS pGEX-6P-1-*pgpH*$_{HD}$ was resuspended in 1x PBS without protease inhibitors and lysed as described in paragraph 3.6.4.1. Clarified lysate was split equally into two gravity flow columns filled with 0.5 ml Glutathione Sepharose 4B slurry (GE Healthcare) and incubated overnight at 4 °C. Both columns were washed subsequently 4x with 20 ml PreScission cleavage buffer (50 mM Tris HCl, 150 mM NaCl, 1 mM EDTA, 1 mM DTT, pH 7.5) supplemented with 10 mM $MnCl_2$. The column dedicated for cleavage of $PgpH_{HD}$ was incubated with 40 µl PreScission protease (GE Healthcare) + 960 µl PreScission cleavage buffer for 4 h at 4 °C (elution fraction 1) and the remaining cleaved $PgpH_{HD}$ was eluted 4x with 1 ml PreScission cleavage buffer containing 10 mM $MnCl_2$. The column dedicated for elution of the fusion protein was washed with 20 ml PBS and eluted 5x with 0.5 ml GST elution buffer (50 mM Tris HCl, 10 mM reduced glutathione, pH 8) supplemented with 10 mM $MnCl_2$. Elution fractions with highest protein amount were dialyzed in PDE buffer and stored as described in paragraph 3.6.4.1.

Rosetta 2 (DE3) strains containing cytosolic domains of Vnz_12665, Vnz_14905, Vnz_24760 and Vnz_28040 were purified similarly but only involving the elution with glutathione approach. GST-Vnz_28040$_{390\text{-}506}$ was dialyzed in the DisA cyclase buffer as described in paragraph 3.6.4.1. The other RCK_C domain proteins were buffer exchanged and concentrated as described in paragraph 3.6.4.3.

### 3.6.4.3 Buffer exchange and concentration of purified proteins

For buffer exchange and concentration of GST-Vnz_12665$_{183\text{-}380}$, GST-Vnz_27460 and GST-Vnz_14905$_{380\text{-}507}$ all elution fractions (~5 ml) were applied to VIVASPIN 6 Columns 10,000 MWCO (Merck) columns and concentrated at least to 1 ml according to manufacturer's instructions. 5 ml DisA cyclase buffer were added to the concentrate and concentrated again to at least 1 ml. This step was repeated twice. The buffer exchanged and concentrated proteins were aliquoted and stored on ice in the cold room or at -20 °C.

### 3.6.4.4 Determination of the concentration of purified proteins

0.5-1.5 µl of dialyzed (and if required diluted) proteins were loaded together with defined amounts of the Low Molecular Weight (LMW) marker (GE Healthcare) on an SDS

polyacrylamide gel, separated via SDS PAGE and Coomassie stained as described above. Gels were scanned using ImageQuant LAS4000 and protein concentrations were determined using the 1D gel analysis of the ImageQuantTL software.

## 3.6.5 Enzymatic *in vitro* activity assays with purified proteins

Protocols for enzymatic *in vitro* activity assays were modified from Christen et al. (2005).

### 3.6.5.1 Diadenylate cyclase assay

Purified 6xHis-DisA, 6xHis-DisA$_{D86A}$ and 6xHis-DisA$_{Bsu}$ were diluted to 5 µM with DisA cyclase buffer and incubated with 83 nM [$^{32}$P]-ATP (Hartmann Analytik) in a total reaction volume of 20 µl for 30 and 60 min at 30 °C. Buffer containing only [$^{32}$P]-ATP served as negative control for diadenylate cyclase (DAC) activity. 5 µl of reactions were mixed with 5 µl 0.5 M EDTA (pH 8) to stop the reaction. Samples were spotted on a thin-layer chromatography (TLC) plate (Macherey-Nagel). After the spots dried the TLC plate was placed in a tank containing the TLC running buffer (saturated $(NH_4)_2SO_4$ and 1.5 M $KH_2PO_4$ pH 3.6 in a ratio of 1:1.5) and TLC was performed until the liquid front reached ~1 cm before the top of the TLC plate. The TLC plate was removed, air-dried and exposed to BAS-IP SR 2025 imaging plates (Fujifilm), which were scanned in Typhoon FLA 7000 (GE Healthcare). A detailed protocol for diadenylate cyclase assay can be found in Latoscha et al. (2021).

### 3.6.5.2 Phosphodiesterase assays

For PDE assays, appropriate concentrations for the proteins were determined. AtaC$_{Sven}$ and AtaC$_{Mlu}$ were finally used at concentrations of 100 nM, whereas AtaC$_{Cbo}$ was used at a concentration of 5 µM and AtaC$_{Mtub}$ was undiluted since the protein concentration was too low to determine. Vnz_31010 and PgpH$_{HD}$ were used at a concentration of 8 µM and 3-10 µM, respectively.

Proteins were diluted in PDE buffer containing 10 mM $MnCl_2$ (for AtaC$_{Mlu}$, AtaC$_{Cbo}$ and AtaC$_{Mtub}$ reduced to 1 mM) and incubated with 2-4 nM [$^{32}$P]-c-di-AMP (synthesized by Hartmann Analytik using purified 6xHis-DisA$_{Bsu}$) for 1 h at 30 °C. For competition PDEs were incubated on ice with 100 µM of unlabeled nucleotides before starting the reaction with [$^{32}$P]-c-di-AMP. Reactions were inactivated for 10 min at 95 °C and 5 µl were spotted on TLC plates. TLC and detection of reaction products was performed as described in paragraph 3.6.5.1. A detailed protocol for phosphodiesterase assay with competition can be found in Latoscha et al. (2021).

### 3.6.6 *In vitro* binding assays with purified proteins

#### 3.6.6.1 Differential Radial Capillary Action of Ligand Assay (DRaCALA)

Protocol for DRaCALAs was modified from Roelofs et al. (2011). Purified proteins were incubated with 42 nM [$^{32}$P]-c-di-AMP in a total reaction volume of 20 µl for 10 min at RT. For competition, [$^{32}$P]-c-di-AMP was added to 5 µg purified CpeA for 5 min at RT and subsequently incubated with 100 µM unlabeled nucleotides for 10 min at RT. To evaluate ATP-binding by CpeA, purified CpeA was incubated with 83 nM [$^{32}$P]-ATP for 10 min at RT. 10 µl of the reaction were spotted on nitrocellulose, air-dried and exposed to imaging plates, which were scanned in Typhoon FLA 7000. [$^{32}$P]-c-di-AMP binding to the RCK_C domain proteins (including CpeD) was evaluated using 10 µg of purified proteins.

#### 3.6.6.2 Nano differential scanning fluorimetry (nanoDSF)

Purified proteins were diluted to 5 µM and incubated with 1 mM nucleotides in a total reaction volume of 30 µl on ice. Samples were loaded by capillary force into glass capillaries (NanoTemper) and placed into Tycho NT.6 (NanoTemper). The machine heated the sample gradually and measured the internal fluorescence at 330 and 350 nm. Analysis of data and calculation of melting and derivative curves were performed automatically by the Tycho NT.6 software.

## 3.7 Evaluation of protein-protein interactions via Bacterial Adenylate Cyclase Two-Hybrid Assay (BACTH)

*E. coli* W3110 Δ*cya* containing different combinations of pKNT25 and pUT18 derivatives were streaked for single colonies on LB/X-Gal/Amp/Kan and incubated overnight at 30 °C. Three single colonies per strain were picked and suspended in 1 ml of sterile PBS. 3 µl suspensions were spotted on square plates containing Difco MacConkey agar supplemented with 1 % maltose, Amp and Kan. W3110 Δ*cya* pKT25/pUT18 and W3110 Δ*cya* pKT25-zip/pUT18C-zip were used as negative and positive control, respectively. Plates were incubated at 26 °C up to 45 h and interaction was evaluated by the red color of macrocolonies. The color change of the pH indicator in the medium indicates cAMP-dependent fermentation of maltose due to reconstituted Cya via physical interaction of T25 and T18-fused proteins. Plates were placed agar-up on a light table and colonies were documented with a Canon EOS 1300D (W) camera.

## 3.8 Nucleotide extraction

### 3.8.1 Sampling

*S. venezuelae* strains were grown under standard conditions in liquid MYM (paragraph 3.4.2.1). After 10 h of growth, every 2 h a 5 ml (nucleotide extraction) and two 1 ml samples (cellular protein determination) were taken. The 5 ml samples were pelleted for 15 min at 4000 rpm and 4 °C in a swing rotor, shock frozen in liquid nitrogen and subsequently stored at -80 °C. The 1 ml samples were pelleted for 15 min at maximal speed and stored at -20 °C.

### 3.8.2 Extraction procedure

The nucleotide extraction protocol from Gundlach, Mehne, et al. (2015) was modified for usage in *Streptomyces*. Pellets from the 5 ml samples were thawed on ice and suspended in 800 µl Extraction mixture II (acetonitrile/methanol/water [2:2:1]). The suspensions were pipetted into 2 ml screw cap tubes prefilled with 0.1 mm silica beads (Biozym). Before boiling for 10 min at 95 °C, the samples were fast frozen in liquid nitrogen for 15 s. To complete lysis, suspensions were disrupted in the Bead Beater at 4 °C with 2 pulses at 6 m/s for 45 s with a 2 min interval. After cooling on ice for 15 min, tubes were centrifuged for 15 min at maximal speed and 4 °C. Supernatants were carefully pipetted into a 2 ml reaction tube and 600 µl Extraction mixture I (acetonitrile/methanol [1:1]) were added to the beads. Subsequently, a lysis step with 2 pulses for 30 s at 6 m/s with a 60 s interval was performed followed by incubation on ice and centrifugation as above. Supernatants were saved and the extraction step with Extraction mixture I was repeated. Finally, all three supernatants per sample were combined and incubated for 2 days at -20 °C for protein precipitation. Samples were centrifuged for 30 min at max. speed and 4 °C and the supernatant was subjected to a second protein precipitation step. Finally, samples were lyophilized using a SpeedVac Plus SC110A connected to Refrigerated Vapor Trap RVT100 (Thermo Scientific) and stored at -80 °C until sent for analysis.

The pellets from 1 ml samples dedicated for protein quantification were suspended in 800 µl 0.1 M NaOH. The suspensions were boiled for 10 min at 98 °C in screw cap tubes prefilled with 0.1 mm silica beads (Biozym). Cells were lysed in the Bead Beater at 4 °C with 2 pulses for 30 s at 6 m/s and an interval of 2 min. The lysate was centrifuged for 15 min at max. speed and 4 °C and the lysis step with 800 µl 0.1 M NaOH was repeated. Supernatants were combined and used for determination of total protein using Roti-Quant (Roth).

### 3.8.3 Analysis of extracted nucleotides

Nucleotide extraction samples were sent to V. Kaever and H. Bähre (ZFA Metabolomics, Institute for Pharmacology, Hannover Medical School), who determined c-di-AMP and pApA concentrations as described in Gundlach, Mehne, et al. (2015).

For comparability between strains, nucleotide concentrations were normalized to the total protein amount using the following formula:

$$\frac{nucleotide\ [nM] \cdot 200\ \mu l}{cV\ [ml] \cdot c590\ [\frac{\mu g}{ml\ cells}]} = \frac{nucleotide\ [pmol]}{protein\ [mg]}$$

## 3.9 Data bases and bioinformatic analyses

The main source for *S. venezuelae* nucleotide and amino acid sequences was StrepDB (http://strepdb.streptomyces.org.uk). Since there are three different annotations (*sve*, *sven15*, *vnz*) of the *S. venezuelae*, which occasionally possess mis-annotated translational start sites, sequences of all used genes were compared within the respective annotations and the longest annotation was considered as the correct one. Amino acid sequences of proteins from other species were obtained from UniProtKB (https://www.uniprot.org/). BLAST analyses were performed using the BLASTp tool on StrepDB or on NCBI (https://blast.ncbi.nlm.nih.gov/Blast.cgi).

For identification of putative PDEs in *S. venezuelae* a list generated by M. Al-Bassam was used (M. Al-Bassam and N. Tschowri, unpublished). The *S. venezuelae* genbank file was obtained from NCBI and used to generate a FASTA file comprising all the potential proteins in the cell. The proteins in the FASTA file were functionally annotated with the command line Conserved Domain Database (CDD) tool (Lu et al., 2020). Following CDD command was used: *s.ven.fasta | parallel -S: --block 100k --recstart '>' --pipe /home/jk/NCBI/ncbi-blast-2.8.1/bin/rpsblast -query - -db ~/CDD/cdd-outfmt 6 -max_target_seqs 1 >sven_CDD_outfmt6.txt 2>/dev/null*. CDD generated a list of protein annotations and annotations with the lowest e-values were finally selected using the keyword "phosphodiesterase". The resulting table was analyzed using the Python module "pandas" and a total of 13 potential PDEs, including Vnz_27310, Vnz_31010 and Vnz_31290 were finally reported.

For identification of RCK_C proteins, an InterProScan annotated *S. venezuelae* genome was searched for “Regulator of K+ conductance, C-terminal domain” (PF02080) (Latoscha et al., 2020).

Multiple sequence alignments were performed using the latest version of Clustal Omega with default settings (https://www.ebi.ac.uk/Tools/msa/clustalo/) (Madeira et al., 2019).

Protter was used for prediction of protein features like transmembrane and cytosolic domains (http://wlab.ethz.ch/protter) (Omasits et al., 2014).

HHpred was used with default settings to predict structural homologs of CpeB, CpeE and *S. venezuelae* RCK_C domain proteins (https://toolkit.tuebingen.mpg.de/tools/hhpred) (Hildebrand et al., 2009; Zimmermann et al., 2018).

Identification of conserved domains in CpeB and CpeE was performed with the CD-Search function at CDD on NCBI (https://www.ncbi.nlm.nih.gov/Structure/cdd/wrpsb.cgi).

# 4 Results

## 4.1 Enzymes controlling c-di-AMP in *S. venezuelae*

The c-di-AMP regulation in *Streptomyces* is poorly understood. As a member of the phylum Actinobacteria, *Streptomyces spp.* encode DisA as the sole protein containing a DAC domain for c-di-AMP production. It has been shown previously that deletion of *disA* leads to loss of detectable c-di-AMP production in *S. venezuelae* (St-Onge et al., 2015). However, direct biochemical evidence for DAC activity is missing. Hence, one of the main objectives in this thesis was the biochemical characterization of purified DisA.

On the other hand, GdpP, DhhP and PgpH homologs responsible for c-di-AMP cleavage in Firmicutes and some other Actinobacteria are absent in streptomycetes (Corrigan & Gründling, 2013; Yin et al., 2020). Thus, it is not clear how *Streptomyces* remove excessive c-di-AMP from the cytosol.

Using a combination of biochemical and bioinformatic methods, I showed that DisA is a *bona fide* DAC *in vitro* and identified AtaC as a novel family of c-di-AMP-specific PDEs in Actinobacteria. These results demonstrate for the first time how c-di-AMP is regulated in *S. venezuelae* during growth in liquid rich sporulation medium.

### 4.1.1 DisA synthesizes c-di-AMP *in vitro*

To prove that DisA, the sole DAC domain protein encoded in *Streptomyces* (Corrigan & Gründling, 2013; Yin et al., 2020), is an active DAC *in vitro*, I overexpressed and purified the N-terminally 6xHis-tagged full-length protein. Purified *B. subtilis* DisA ($DisA_{Bsu}$) served as a positive control in the following experiment. It has been shown that the residue D77 within the conserved DGA motif in $DisA_{Bsu}$ is crucial for enzymatic activity (Witte et al., 2008), hence I mutated the corresponding D86 in *S. venezuelae* DisA ($DisA_{Sven}$) and used the resulting purified $DisA_{D86A}$ as a negative control.

The purified proteins were incubated with [$^{32}$P]-ATP in a DAC assay, with subsequent separation of the reaction products by thin-layer chromatography (TLC). $DisA_{Sven}$ successfully produced [$^{32}$P]-c-di-AMP as indicated by formation of a reaction product, which migrates at the same size as [$^{32}$P]-c-di-AMP synthesized by $DisA_{Bsu}$ (Figure 4). Confirming that the residue D86 is essential for DAC activity, $DisA_{D86A}$ failed to synthesize [$^{32}$P]-c-di-AMP. Interestingly, although similar concentrations of all reagents were used in the DAC assay, $DisA_{Bsu}$ was much more active than $DisA_{Sven}$. However, a similar result was observed for purified DisA from *Mycobacterium tuberculosis* (Bai et al., 2012), which likely reflects a species-specific demand for c-di-AMP.

In summary, these data show that $DisA_{Sven}$ is a functional DAC *in vitro*, which requires an intact DGA motif for enzymatic activity.

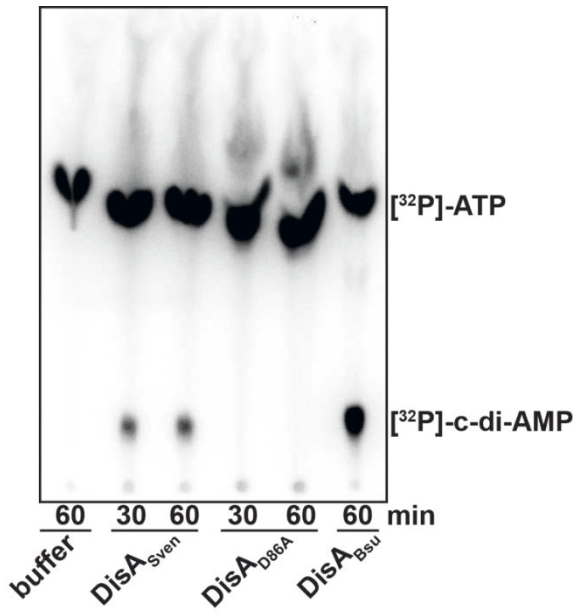


**Figure 4: *in vitro* diadenylate cyclase (DAC) activity of *S. venezuelae* DisA (DisASven).**
5 µM purified proteins were incubated with 83 nM [$^{32}$P]-ATP up to 1 h at 30 °C. Nucleotides were separated by thin-layer chromatography (TLC) and visualized by exposing to an imaging plate. $DisA_{Sven}$ synthesized [$^{32}$P]-c-di-AMP out of [$^{32}$P]-ATP, whereas the variant carrying a point mutation in the active site failed ($DisA_{D86A}$). DisA from *B. subtilis* was used as a positive control for DAC activity. The buffer lane shows migration of [$^{32}$P]-ATP.


## 4.1.2 Vnz_27310 (AtaC) specifically degrades c-di-AMP to AMP

*S. venezuelae* does not encode any characterized phosphodiesterases (PDEs) of the GdpP, DhhP or PgpH-type, suggesting that this organism relies on an alternative PDE to remove c-di-AMP from the cytosol. To identify the c-di-AMP-specific PDE in *S. venezuelae*, I obtained a list of predicted PDEs in *S. venezuelae* (for details, see paragraph 3.9; M. M. Al-Bassam and N. Tschowri, unpublished) for which a function was not shown experimentally yet. Out of this list, I selected candidate PDEs and successfully purified 6xHis-tagged Vnz_27310 and Vnz_31010, which belong to the phosphodiesterase and metallophosphatase superfamilies, respectively. Both proteins were tested for [$^{32}$P]-c-di-AMP cleavage activity in PDE assays and the cleavage products were separated by TLC. The cytosolic HD domain of *L. monocytogenes* PDE PgpH ($PgpH_{HD}$) was used as a stand-alone domain or fused to the GST tag as positive control for PDE activity (Huynh et al., 2015).

In the first PDE assay, I used all proteins at a final concentration of 3 µM, except Vnz_31010, which was used at a concentration of 8 µM, and added [$^{32}$P]-c-di-AMP as

substrate. Vnz_27310 degraded [$^{32}$P]-c-di-AMP completely, whereas Vnz_31010 as well as the positive control showed weaker activity (Figure 5A). Since PgpH degrades c-di-AMP to 5'-pApA (Huynh et al., 2015) and the cleavage product of Vnz_27310 ran higher in the TLC, Vnz_27310 likely cleaves [$^{32}$P]-c-di-AMP to [$^{32}$P]-AMP.

To assess specificity of c-di-AMP degradation by the tested PDEs, I repeated the experiment including 100 µM unlabeled c-di-AMP and c-di-GMP as competitors for radiolabeled c-di-AMP. Cold c-di-AMP inhibited the [$^{32}$P]-c-di-AMP-cleavage by both proteins, but Vnz_27310 still converted almost the complete radioactively labeled c-di-AMP to AMP suggesting that a concentration of 3 µM protein was too high (Appendix Figure A1A). To determine the optimal protein concentration for PDE competition assays, I titrated the proteins against a constant concentration of [$^{32}$P]-c-di-AMP. Even 100 nM Vnz_27310 were sufficient to cleave 2 nM [$^{32}$P]-c-di-AMP (Figure 5B). Usage of lower protein concentrations revealed that Vnz_27310 degrades c-di-AMP to AMP with 5'-pApA as an intermediate cleavage product, indicated by appearance of an additional spot corresponding to the size of [$^{32}$P]-pApA generated by Vnz_31010 and $PgpH_{HD}$ (Figure 5 A and B). The highly conserved Asp residue at position 269 was identified as critical for enzymatic activity by our collaboration partners in Munich modelling the Vnz_27310 structure on the crystal structure of PhnA from *Sinorhizobium meliloti*, the closest structural Vnz_27310 homolog. Accordingly, purified $Vnz\_27310_{D269N}$ was able to bind but not cleave c-di-AMP *in vitro* due to loss of manganese binding (Latoscha et al., 2020). In contrast to Vnz_27310, Vnz_31010 showed almost no activity already at a concentration of 2.8 µM suggesting that c-di-AMP is not its physiological substrate (Figure 5B).

The competition experiment was repeated with the optimized concentration of 100 nM Vnz_27310 and only unlabeled c-di-AMP inhibited the cleavage of the radioactive substrate, demonstrating that Vnz_27310 specifically degrades c-di-AMP (Figure 5C). This finding led to the renaming of Vnz_27310 to AtaC (actinobacterial PDE targeting c-di-AMP).

Generally, most AtaC homologs are found within the phylum of Actinobacteria, including *Micrococcus luteus* and contigs of eight *M. tuberculosis* strains (Latoscha et al., 2020). However, although AtaC is absent in the complete genome of *M. tuberculosis* H37Rv, it is encoded in many other mycobacteria, including *Mycobacterium avium* 104 and *M. smegmatis* MC2 155 (Latoscha et al., 2020). On the other hand, pathogenic Firmicutes like *Clostridium botulinum* also contain AtaC homologs (Latoscha et al., 2020). To evaluate whether these proteins are involved in c-di-AMP metabolism as well, I purified 6xHis-tagged AtaCs from *C. botulinum* ($AtaC_{Cbo}$, sequence ID: WP_049179360.1), *M. tuberculosis* ($AtaC_{Mtub}$, sequence ID: CNE38097.1) and *M. luteus* ($AtaC_{Mlu}$, sequence ID: CVN04004.1) and tested them in c-di-AMP PDE assays. Whereas $AtaC_{Cbo}$ and $AtaC_{Mtub}$ had only weak activity against [$^{32}$P]-c-di-AMP, $AtaC_{Mlu}$ showed an activity and substrate specificity

comparable to *S. venezuelae* AtaC (Figure 5D and Appendix Figure A1 B and C). However due to solubility issues $AtaC_{Mtub}$ had only a very low concentration, which could not be determined using RotiQuant and was potentially insufficient to show proper PDE activity.

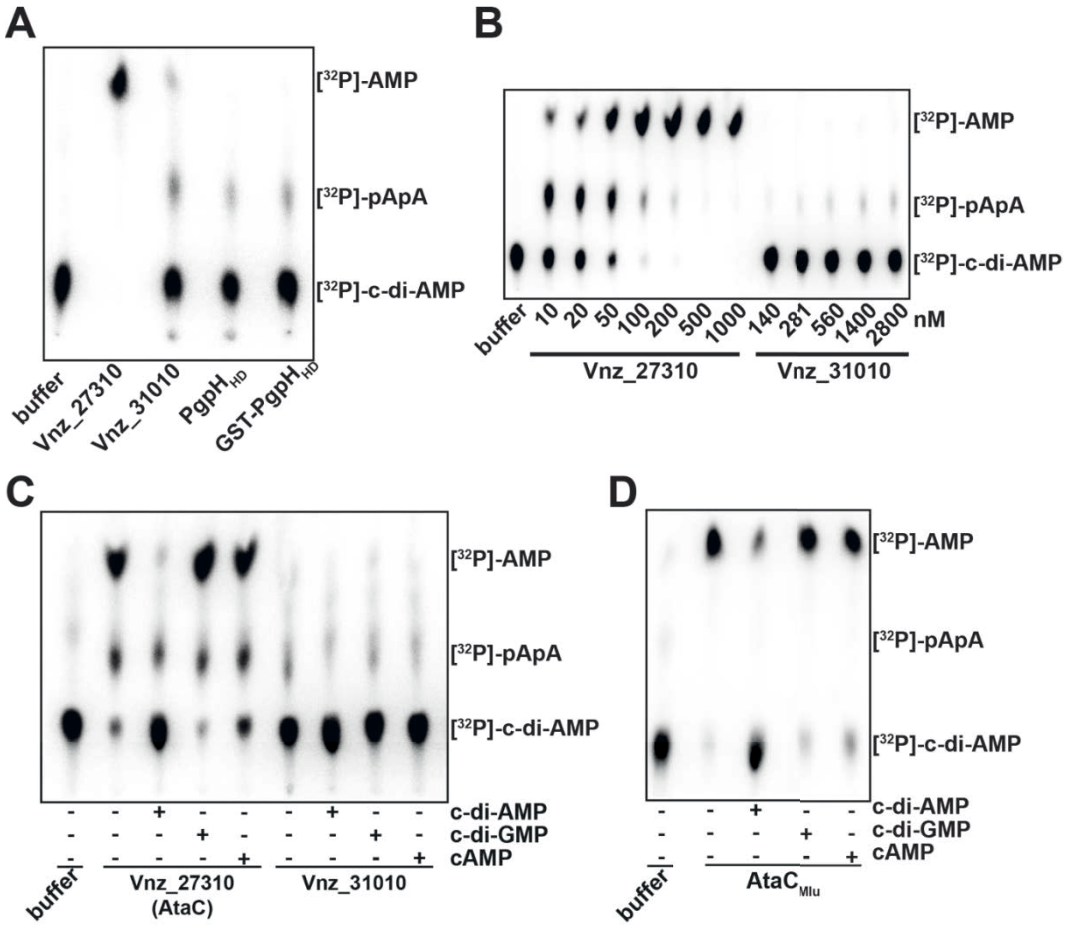


**Figure 5: c-di-AMP-directed phosphodiesterase (PDE) activity of Vnz_27310 (AtaC), Vnz_31010 and AtaC from *Micrococcus luteus* ($AtaC_{Mlu}$).**

All proteins were incubated for 1 h at 30 °C with 2 nM [$^{32}$P]-c-di-AMP. The buffer lanes show migration of [$^{32}$P]-c-di-AMP in the TLC. **(A)** Visualization of the reaction of 3 µM of Vnz_27310 and 8 µM of Vnz_31010 with [$^{32}$P]-c-di-AMP. Vnz_27310 cleaved [$^{32}$P]-c-di-AMP to [$^{32}$P]-AMP with high efficiency. Vnz_31010 showed only weak activity. 3 µM of the purified HD domain of PgpH ($PgpH_{HD}$) and GST-fused $PgpH_{HD}$ from *L. monocytogenes* were used as positive controls for c-di-AMP cleavage. **(B)** Titration of Vnz_27310 and Vnz_31010. 100 nM Vnz_27310 were sufficient to cleave [$^{32}$P]-c-di-AMP almost completely to [$^{32}$P]-pApA and finally [$^{32}$P]-AMP, whereas Vnz_31010 showed barely detectable activity already at 2800 nM. **(C)** Cleavage of [$^{32}$P]-c-di-AMP in competition with 100 µM unlabeled nucleotides. Unlabeled nucleotides were added on ice before starting the reaction with 2 nM [$^{32}$P]-c-di-AMP. Only unlabeled c-di-AMP significantly interfered with cleavage of [$^{32}$P]-c-di-AMP by 100 nM AtaC, demonstrating c-di-AMP specificity. **(D)** Competition PDE assay with 100 nM of $AtaC_{Mlu}$ under the same conditions as in (C). Unlabeled c-di-AMP but not c-di-GMP or cAMP inhibited cleavage of [$^{32}$P]-c-di-AMP.

Altogether, these data demonstrate that under conditions tested, AtaC homologs from non-pathogenic Actinobacteria degrade c-di-AMP with high specificity and efficiency to 5'-pApA and finally to AMP.

### 4.1.3 DisA and AtaC regulate intracellular c-di-AMP *in vivo*

The intracellular c-di-AMP levels were measured in *disA* and *ataC* mutants to demonstrate that DisA and AtaC are important components of c-di-AMP regulation in *S. venezuelae.* For that, the wild-type strain, Δ*disA* and Δ*ataC* were grown in liquid sporulation medium (MYM) at 30 °C and samples were gathered every two hours to assess the intracellular c-di-AMP level during all developmental stages. Generally, *S. venezuelae* grows as vegetative mycelium until 12 h. At 14 h of growth first fragments separate from the vegetative mycelium, indicating the onset of sporulation. From 18 h on, fragmentation of hyphae accelerates and first spores become visible. Since sporulation is asynchronous in liquid MYM, some vegetative hyphae exist simultaneously with fragments and spores in the late growth phases. I extracted intracellular nucleotides and c-di-AMP levels were quantified by V. Kaever and H. Bähre at Hannover Medical School. Measured c-di-AMP was normalized to the total cell protein gathered at the respective time points to allow direct comparison between strains.

Both, Δ*disA* and Δ*ataC* showed altered c-di-AMP levels compared to the wild type (Figure 6A). In the *disA* mutant, intracellular c-di-AMP was overall strongly reduced, and not detectable upon onset of sporulation (14 and 16 h) and during ongoing sporulation (18 and 20 h). Surprisingly, although DisA is the sole DAC domain protein encoded in *Streptomyces*, a low and rapidly sinking level of c-di-AMP was still detectable in the late vegetative phase (10 and 12 h), suggesting presence of a DAC-unrelated c-di-AMP synthetase. On the other hand, deletion of *ataC* led to increased c-di-AMP throughout the whole life cycle (Figure 6A). These data demonstrate that AtaC is an important component of c-di-AMP regulation since it is required for c-di-AMP hydrolysis *in vivo.*

To evaluate expression of AtaC and DisA, the wild type and a *disA* mutant expressing DisA-FLAG under control of the native *disA* promoter were grown and sampled under the same conditions as described for the nucleotide extraction. Whole cell lysates were obtained from samples by physical lysis and separated by SDS PAGE. The same amount of total cellular protein was loaded on the gel for each sample and verified by Coomassie staining (Appendix Figure A2) The expression of both proteins was relatively constant during the life cycle as shown with immunoblot analyses using a specific monoclonal α-FLAG antibody for detection of DisA-FLAG expressed in the *disA* mutant (Figure 6B) and a polyclonal α-AtaC antiserum for AtaC detection in the wild type (Figure 6C). The expression data correlated with the intracellular c-di-AMP measured in the wild type, suggesting that under tested conditions both DisA and AtaC are required for a balanced c-di-AMP level *in vivo*.

In summary, I have shown that DisA and AtaC are the main components of c-di-AMP regulation *in vivo*, and are expressed during the whole life cycle to maintain a basic c-di-AMP level in *S. venezuelae*.

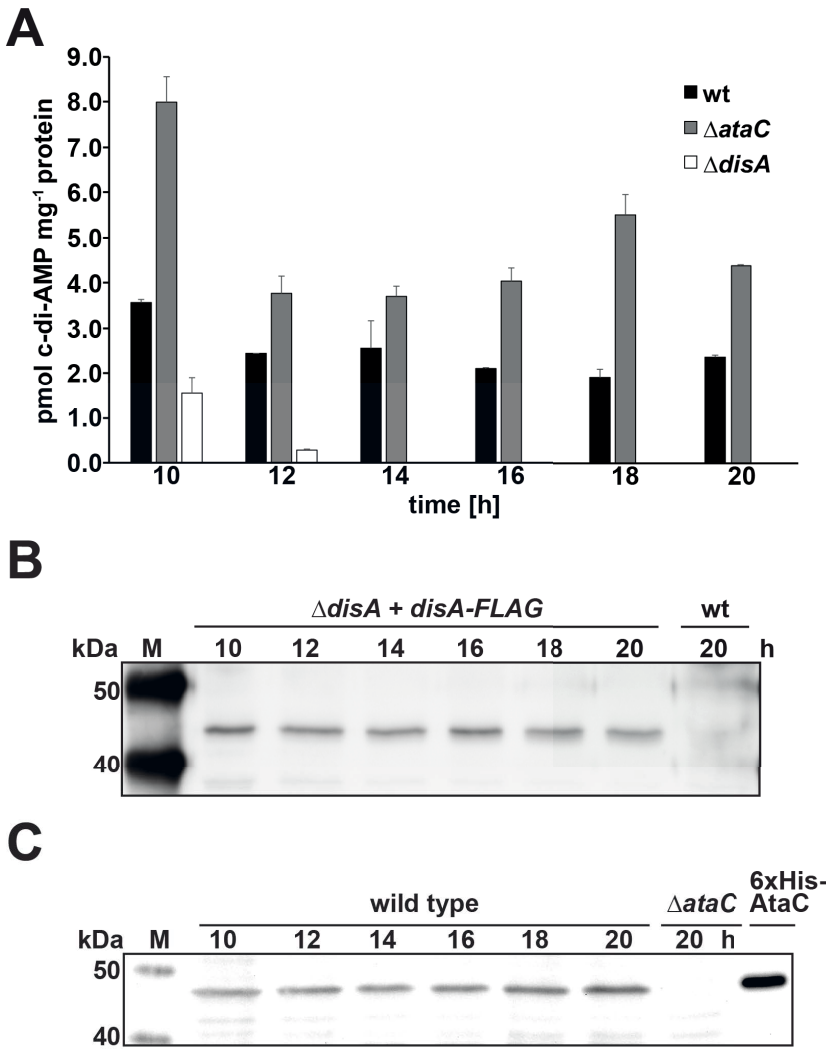


**Figure 6: Intracellular concentrations of c-di-AMP in *disA* and *ataC* mutants, and DisA-FLAG and AtaC expression in *S. venezuelae*.**

**(A)** Intracellular c-di-AMP concentrations in *S. venezuelae*. Wild type (wt), Δ*disA* and Δ*ataC* were sampled during the developmental life cycle in liquid sporulation medium. *disA* deletion led to a reduction during late vegetative growth (10 and 12 h) and disappearance of c-di-AMP upon initiation of sporulation (at 14 h). c-di-AMP was increased in all developmental stages in Δ*ataC*. Data are presented as mean ± SD of biological replicates (n = 3). **(B)** Expression of DisA-FLAG in a Δ*disA* mutant complemented with p3xFLAG-*disA* under control of the native *disA* promoter. p3xFLAG-*disA* is a pIJ10770 derivative, which integrates into the $attB_{\Phi BT1}$ site in the chromosome of *S. venezuelae*. DisA-FLAG expression was detected using a monoclonal α-FLAG antibody. Wild-type lysate was used as a negative control. **(C)** Expression of AtaC in the wild type strain. A polyclonal α-AtaC antiserum was used for detection. Δ*ataC* lysate and purified 6xHis-AtaC were used as negative and positive control, respectively. All panels were originally published in Latoscha et al. (2020) under Creative Commons Attribution-NonCommercial-NoDerivatives License 4.0 (CC BY-NC-ND) and modified here with permission.

## 4.2 Phenotypical characterization of *S. venezuelae* c-di-AMP mutants

In *B. subtilis*, DisA is involved in cellular differentiation by controlling vegetative growth, sporulation and spore germination (Bejerano-Sagie et al., 2006; Campos et al., 2014; Gándara & Alonso, 2015). Whereas $DisA_{Bsu}$ is required to delay sporulation in response to DNA damage to ensure production of viable spores, its overexpression interferes with sporulation if no stress is present (Bejerano-Sagie et al., 2006). Hence, both loss and overexpression of $DisA_{Bsu}$, which likely lead to altered intracellular c-di-AMP levels, are detrimental for differentiation in *B. subtilis*. Given the presence of a c-di-AMP-responsive riboswitch in RpfA, which is important for proper formation of exospores and efficient germination, and other potentially c-di-AMP-controlled cell wall hydrolases involved in germination and vegetative growth (Haiser et al., 2009; St-Onge et al., 2015), I hypothesized that in streptomycetes c-di-AMP produced by DisA and degraded by AtaC might adopt a similar function.

*S. venezuelae* grown on solid sporulation medium (MYM agar) provides an excellent readout for perturbations in the developmental program as the different stages of development can be distinguished on a macroscopic level. Vegetative mycelium has as a flat yellow-brown shiny colony phenotype, whereas the erected aerial hyphae turn the color to white. Finally, a polyketide pigment is produced, which provides the characteristic green color in the mature spores of *S. venezuelae*. Typical mutants impaired in differentiation are either blocked in aerial hyphae formation (*bld*, “bald”) or spore maturation (*whi*, “white”) (Tschowri, 2016). Similarly, potential influence on differentiation by alterations of intracellular c-di-AMP due to deletion or inactivation of *disA* and *ataC* should be reflected in altered phenotypes.

On the other hand, c-di-AMP produced by CdaA is important for the osmotic stress response in Firmicutes as many potassium importers are directly or indirectly regulated by c-di-AMP, which also influences expression and activity of several osmoprotectant uptake systems (Stülke & Krüger, 2020). However, CdaM in *M. pneumoniae* and CdaZ in *H. volcanii* appear to be involved in this process as well, suggesting that osmoregulation is the main function of c-di-AMP independent of the particular DAC (Blötz et al., 2017; Braun et al., 2019). Hence, I wondered whether streptomycetes employ c-di-AMP generated by DisA for a similar purpose.

Taken together, the following experiments were designed to answer the question whether c-di-AMP controls development and osmoregulation in *S. venezuelae*

### 4.2.1 Increased c-di-AMP levels interfere with differentiation and growth

Δ*disA* and Δ*ataC* colonies were grown as patches on MYM agar to evaluate the influence of altered c-di-AMP levels on development of *S. venezuelae*. Deletion of *disA*, and hence reduction of intracellular c-di-AMP, had no effect on differentiation as the strain turned green and thus produced the spore pigment like the wild type after four days of growth, indicating completed sporulation (Figure 7A, *left*). In contrast, deletion of *ataC* caused a considerable defect in development, as this strain erected aerial hyphae but failed to produce or accumulate the green spore pigment at wild-type level. Even after prolonged incubation for seven days Δ*ataC* did not become as green as the wild type (Figure 7A, *right*). This phenotype was dependent on c-di-AMP accumulation since only the wild-type allele but not the enzymatically inactive $ataC_{D269N}$ expressed under control of the native *ataC* promoter from the $attB_{\Phi BT1}$ site restored wild type-like pigmentation (Figure 7A).

To gain a more detailed insight into the developmental phenotype of Δ*ataC*, c-di-AMP mutants as well as complemented strains were sent to John Innes Centre, UK, for analysis using scanning electron microscopy (SEM). Single colonies grown on MYM agar were gathered after four or seven days and images were taken by K. C. Findlay. In agreement with the macroscopic observation of colony patches, wild type and Δ*disA* were completely differentiated and showed mature spore chains after four days (Figure 7B). On the contrary, Δ*ataC* was comprised of many undifferentiated and several plain, presumably lysed hyphae (Figure 7B, white and red arrows, respectively). Extension of growth to seven days allowed detection of sporulated hyphae, suggesting that accumulation of c-di-AMP leads to a general delay in development. However, residual undifferentiated and lysed hyphae were still present (Figure 7B).

To assess whether *ataC* deletion results in a growth defect as indicated by observation of lysed hyphae in the SEMs, I inoculated liquid MYM with spores of c-di-AMP mutants and monitored growth by measuring the optical density at 578 nm ($OD_{578}$). Indeed, the *ataC* mutant showed slower growth than wild type or Δ*disA* and required three more hours to reach the final $OD_{578}$ around 19 to 20 h of growth (Figure 7C). The growth defect on solid as well as in liquid MYM was complemented by expression of the wild-type *ataC* allele in Δ*ataC* (Figure 7 B and C).

Summarized, these data demonstrate that c-di-AMP produced by DisA is dispensable for *S. venezuelae* differentiation under standard growth conditions, but interferes with development and growth if accumulated due to *ataC* deletion.

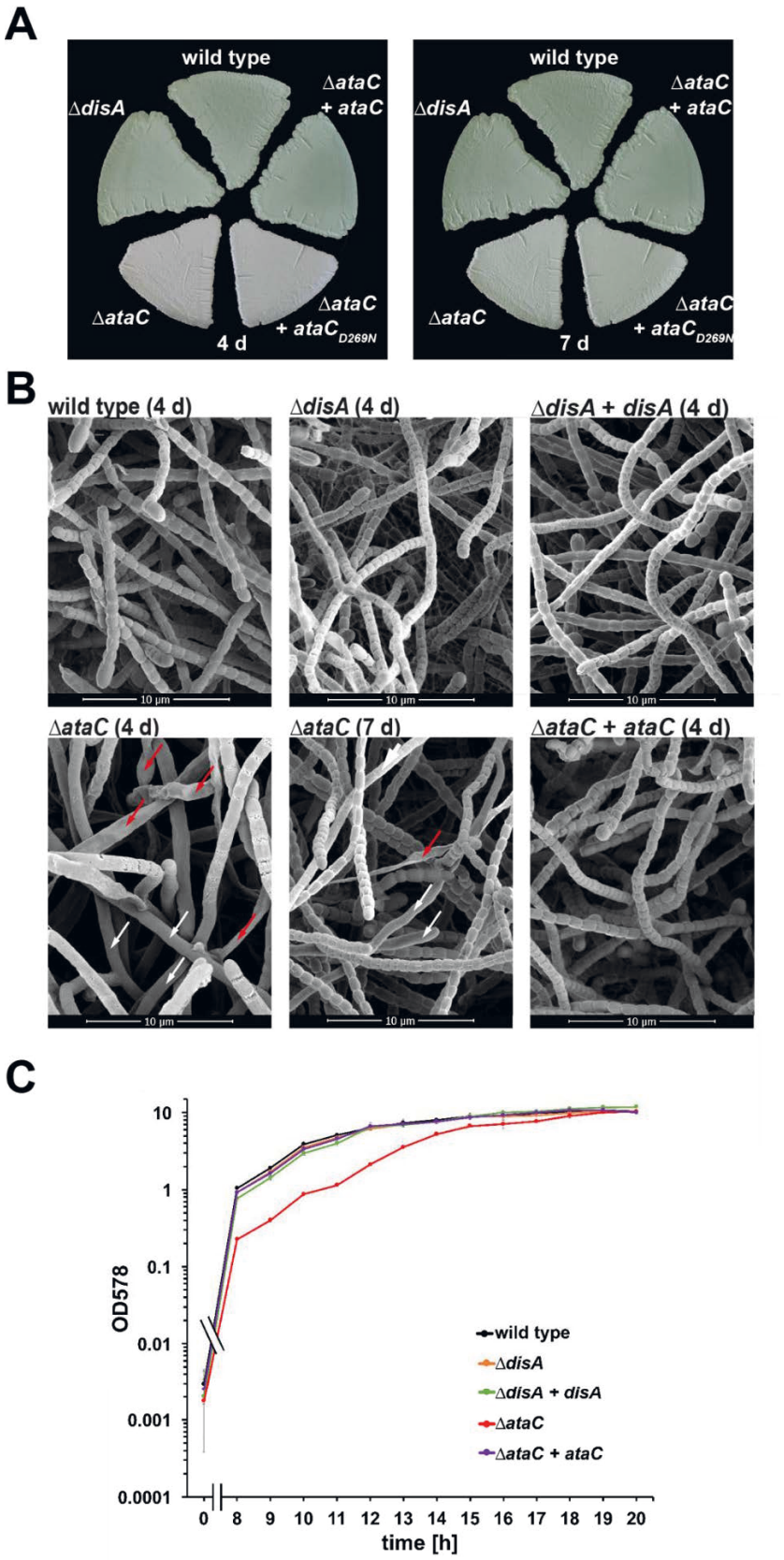


**Figure 7: Development and growth of *S. venezuelae* c-di-AMP mutants.**

The figure legend continues on page 80.

**(A)** Development of c-di-AMP mutants on MYM agar. Spores of different strains were streaked as patches on plates and incubated for the indicated times at 30 °C. Δ*disA* showed no deviation from the wild-type phenotype (*left*), whereas Δ*ataC* did not accumulate the spore pigment even after prolonged incubation for 7 days (d) (*right*). This phenotype was dependent on increased intracellular c-di-AMP since Δ*ataC* was complemented by the wild-type allele but not the inactive $ataC_{D269N}$ expressed under control of the native *ataC* promoter from the $attB_{\Phi BT1}$ site. **(B)** Scanning electron micrographs show deviant differentiation of Δ*ataC*. Unlike wild type and Δ*disA*, which were fully sporulated after 4 d, the *ataC* mutant was comprised of undifferentiated aerial hyphae and plain, likely lysed hyphae (white and red arrows, respectively). After prolonged incubation for 7 d, Δ*ataC* sporulated, but retained some undifferentiated and lysed hyphae. Complementation with the wild-type allele completely restored the developmental defect of Δ*ataC*. **(C)** Δ*ataC* showed a growth delay in liquid sporulation medium, which was complemented by wild-type *ataC*. The optical density (OD) was measured at 578 nm. Data are presented as the mean ± SD of biological replicates (n = 2).



### 4.2.2 Reduction of c-di-AMP increases susceptibility to stress by monovalent cations

As regulation of potassium homeostasis and transport of osmoprotectants appear to be the major functions of c-di-AMP in Firmicutes (Stülke & Krüger, 2020), I tested whether growth of *S. venezuelae* c-di-AMP mutants is affected by high osmolyte concentrations in the medium. To evaluate this, I serially diluted spores and spotted macrocolonies from different dilution steps on nutrient agar (NA) supplemented with 0.5 M NaCl and used untreated NA as control.

NaCl treatment led to a general growth inhibition, resulting in smaller colony size compared to the control plate (Figure 8A). Colonies of Δ*ataC* were smaller than wild-type colonies on both plates. This phenotype is likely caused by the general growth defect already observed for this strain (Figure 7 B and C) and was complemented by expression of the wild-type *ataC* allele (Figure 8A). However, colony forming units (CFUs) still appeared at the highest dilution of $10^2$ CFU, suggesting that increased intracellular c-di-AMP levels do not affect the resistance of the *ataC* mutant to NaCl.

In contrast, c-di-AMP produced by DisA was indispensable for growth at high salt conditions since both Δ*disA* and the strain expressing the enzymatically inactive $DisA_{D86A}$ were strongly inhibited and only formed macrocolonies at the highest CFU amount of $10^5$ (Figure 8A). The NaCl resistance was restored in the deletion mutant by expression of *disA* under control of its native promoter from the $attB_{\Phi BT1}$ site.

I wondered whether Δ*disA* is generally susceptible to osmotic stress. Hence, in the next experiment I included 0.5 M of sucrose as a non-ionic osmolyte and 0.5 M KCl as an additional ionic osmolyte. Sucrose had only a small effect on growth of all strains and Δ*disA* did not show stronger inhibition than the wild type (Figure 8B). Similar to inhibition by NaCl,

growth of Δ*disA* was strongly inhibited at high KCl concentrations. Interestingly, KCl exhibited an overall stronger inhibitory effect on all strains compared to NaCl, which is reflected in the longer incubation time required to form colonies of comparable size (four days on 0.5 M KCl versus two days on 0.5 M NaCl).

Altogether, these experiments demonstrate that *S. venezuelae* relies on c-di-AMP production by DisA to effectively counteract stress induced by monovalent cations.

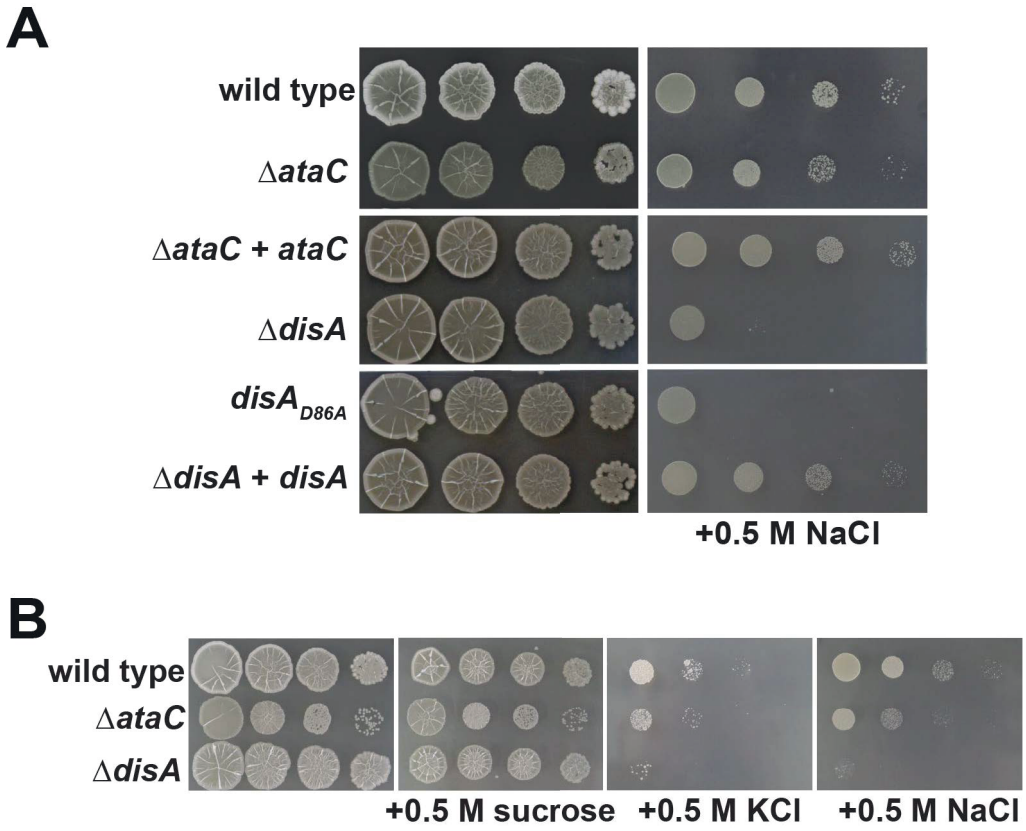


**Figure 8: Growth of c-di-AMP mutants in presence of different osmolytes.**

Spores were serially diluted and spotted on nutrient agar (NA) supplemented with the indicated concentrations of NaCl, KCl or sucrose. **(A)** Δ*disA* shows high sensitivity to increased NaCl concentration. This phenotype is dependent on c-di-AMP since the strain containing the inactive variant $disA_{D86A}$ phenocopies the deletion mutant. Resistance to NaCl was restored in Δ*disA* by complementation with wild-type *disA* expressed under control of the native *disA* promoter from the $attB_{\Phi BT1}$ site. **(B)** A high concentration of potassium but not the non-ionic osmolyte sucrose inhibited growth of Δ*disA*, suggesting that c-di-AMP is rather involved in regulation of ion homeostasis than general osmoregulation. NA supplemented with NaCl was used as a control for Δ*disA* sensitivity. Plates were incubated for 2 d at 30 °C with the exception of the KCl plate, which required incubation for 4 d.

### 4.2.3 Alterations of intracellular c-di-AMP do not affect spore viability

In *B. subtilis*, deletion of *disA* was reported to result in loss of viable spores (Bejerano-Sagie et al., 2006). My data suggest that in *S. venezuelae*, *disA* deletion does not affect spore formation, but Δ*ataC* showed a strong delay in sporulation and presumably incomplete spore maturation as indicated by defective pigmentation (Figure 7 A and B). I performed a heat shock assay, which was used in previous studies to evaluate viability of *Streptomyces* spores (Haiser et al., 2009; Molle et al., 2000; Tschowri et al., 2014). Spores of wild type, Δ*ataC*, Δ*disA* and $disA_{D86A}$ were diluted to equal concentrations and exposed for 1 h to 50 °C in a water bath. However, neither strain showed a reduced survival rate compared to the wild type, suggesting that imbalance of intracellular c-di-AMP does not directly affect the spore quality under the tested condition (Figure 9A).

Nevertheless, one of the obvious Δ*ataC* phenotypes is the incomplete spore pigmentation. Up to date little is known about the physiological role of the spore pigment in *Streptomyces*. In other bacteria and eukaryotes many different functions for pigments were suggested, including protection from UV light (El-Naggar & El-Ewasy, 2017; Narsing Rao et al., 2017; Rosa-Fraile et al., 2014). Besides that, *S. pneumoniae* PDE mutants were demonstrated to be more susceptible to UV light (Bai et al., 2013). To test if the pigment-defective *ataC* mutant is more sensitive to UV light than the fully pigmented wild type, I exposed spores to increasing intensities of light at the wavelength of 254 nm and evaluated the survival. However, no significant differences were detectable between Δ*ataC* and wild type, suggesting that under tested conditions the spore pigment is not required for spore survival (Figure 9B).

Overall, these data indicate that despite the sporulation and growth defects observed in Δ*ataC*, neither increased c-di-AMP nor abolishment of c-di-AMP production affect the spore quality and allow formation of mature spores.

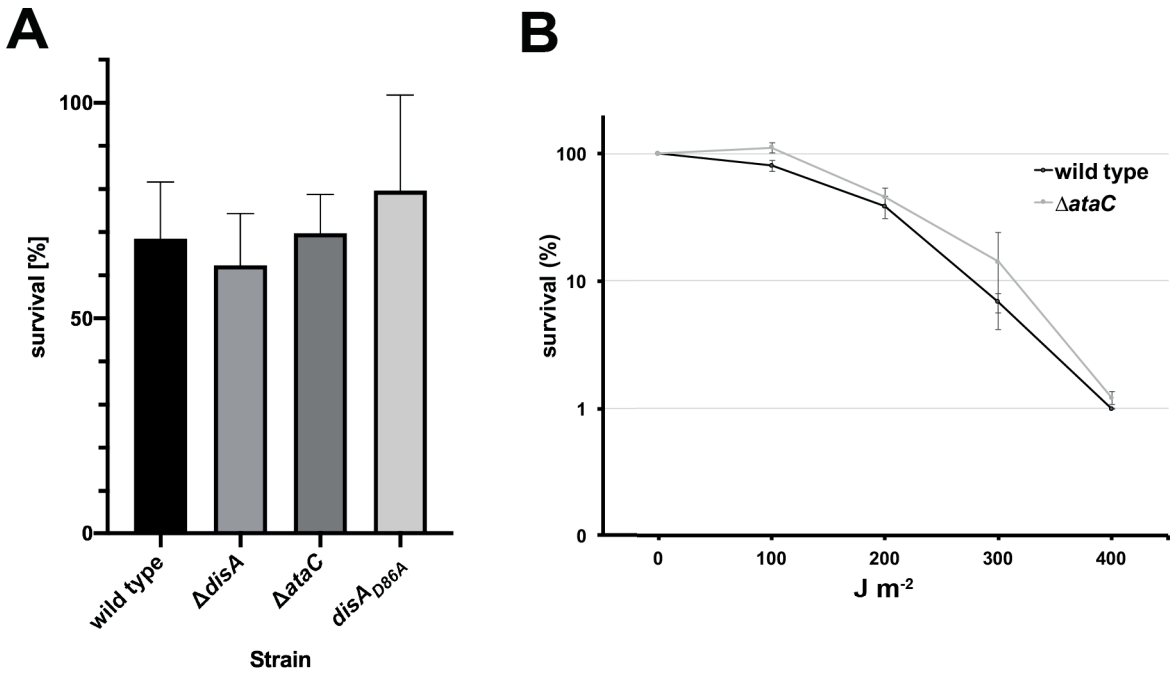


**Figure 9: Alteration of intracellular c-di-AMP levels does not affect spore quality.**

**(A)** Survival of *S. venezuelae* spores after a heat shock of 50 °C for 1 h. Spores were serially diluted and the colony forming units (CFU) were counted. Neither decrease nor accumulation of c-di-AMP affected the number of surviving CFU in the respective strains. Survival was determined as the ratio of CFU after the heat shock to CFU prior to the heat shock. Data are presented as mean ± SD of two dilution steps and are representative for three independent experiments. **(B)** Survival of Δ*ataC* spores in comparison to the wild type after exposure to indicated intensities of UV light (wavelength of 254 nm). Spores were serially diluted and the colony forming units (CFU) were counted. Survival was determined as the ratio of CFU after UV light exposure to CFU without UV light treatment. Data are presented as mean ± SD of two independent experiments.



### 4.2.4 Do other c-di-AMP metabolizing enzymes exist in *S. venezuelae*?

The detection of residual c-di-AMP in the Δ*disA* mutant (Figure 6A) was quite surprising since c-di-AMP is exclusively synthesized by the DAC domain (Figure 1A). *Streptomyces spp.* (and Actinobacteria in general) encode only DisA as the sole DAC domain protein (Corrigan & Gründling, 2013; Yin et al., 2020). Hence, *Streptomyces* appears to contain at least one novel enzyme capable of c-di-AMP synthesis independent of the DAC domain. However, this synthetase cannot compensate for the loss of a functional *disA* (Figure 8) and appears to be strongly regulated as its expression or activity is restricted to the (late) vegetative growth phase and ceases upon onset of sporulation (Figure 6A).

#### 4.2.4.1 *ataC* deletion in *disA*$_{D86A}$ suppresses the sensitivity to cation-induced stress

The salt sensitive phenotype observed for *disA* mutants (Figure 8) implicates that the c-di-AMP synthesized by the unknown synthetase cannot be deployed for the required stress response and is likely utilized for other physiological processes.

However, I wondered whether a potential increase in intracellular c-di-AMP due to the removal of the PDE AtaC might improve growth of a *disA* mutant in presence of high salt. To test this, I deleted *ataC* in the strain *disA*$_{D86A}$, which expresses the inactive DisA and shows the same NaCl-sensitive phenotype as Δ*disA* (Figure 8). The growth of resulting strain *disA*$_{D86A}$ Δ*ataC* was restored on NaCl and KCl-supplemented plates compared to the *disA*$_{D86A}$ parent strain (Figure 10). This effect was dependent on the enzymatic activity of AtaC, since expression of the enzymatically inactive AtaC$_{D269N}$ under control of the native *ataC* promoter had no effect on the salt resistance. In contrast, complementation with wild-type *ataC* increased the salt sensitivity of the resulting strain (Figure 10). These results suggest that the c-di-AMP level in *disA*$_{D86A}$ Δ*ataC* is sufficiently increased to compensate for *disA* inactivation and activate the resistance mechanism against cation-induced stress.

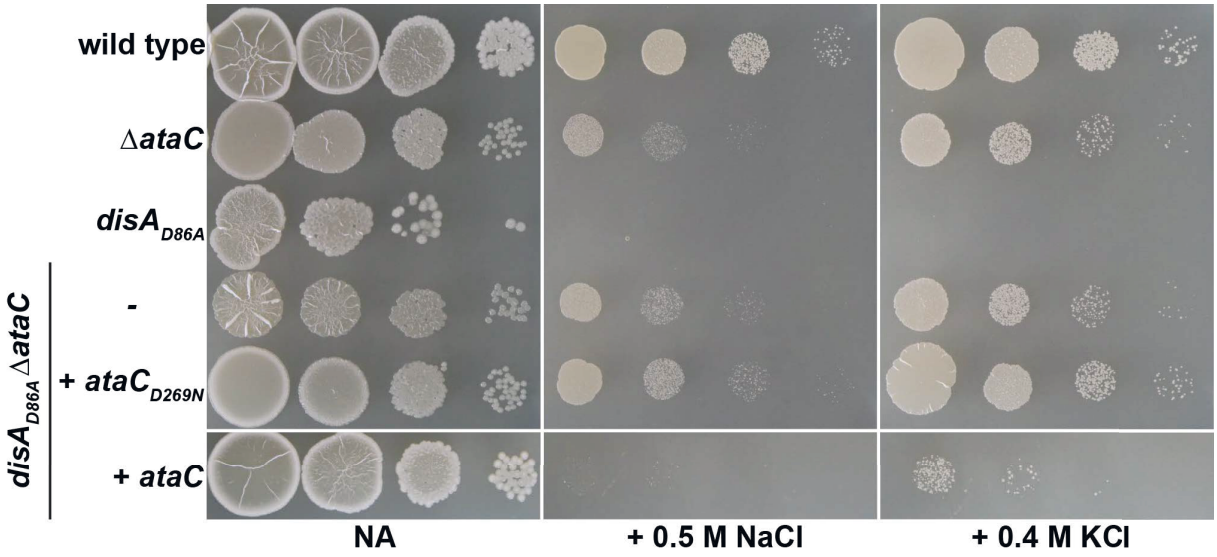


**Figure 10: Deletion of *ataC* in the *disA*$_{D86A}$ mutant suppresses the sensitivity to Na$^+$ and K$^+$ stress.**
This effect is dependent on enzymatic activity of *ataC* since complementation with wild-type *ataC* under control of the native promoter at the *attB*$_{\Phi BT1}$ site, but not inactive *ataC*$_{D269N}$ restores the susceptibility to high Na$^+$ and K$^+$ concentrations.

#### 4.2.4.2 Intracellular c-di-AMP of *disA*$_{D86A}$ Δ*ataC* is increased during vegetative growth

To evaluate c-di-AMP production in *disA*$_{D86A}$ Δ*ataC*, I grew the strain in MYM and regularly took samples for c-di-AMP quantification in cooperation with V. Kaever and H. Bähre (Hannover Medical School). The wild type and the *disA*$_{D86A}$ parent strain were used as references. Similar to Δ*disA*, a low c-di-AMP level could be observed in *disA*$_{D86A}$ during the late vegetative growth phase (until 12 h) (Figure 11). In contrast in *disA*$_{D86A}$ Δ*ataC*, c-di-AMP was increased to wild-type levels at 10 h of growth and remained detectable until 14 h of growth, demonstrating that *ataC* deletion in *disA*$_{D86A}$ indeed sufficiently increased the intracellular c-di-AMP level during early growth to allow survival on medium with high NaCl or KCl concentrations (Figure 10).

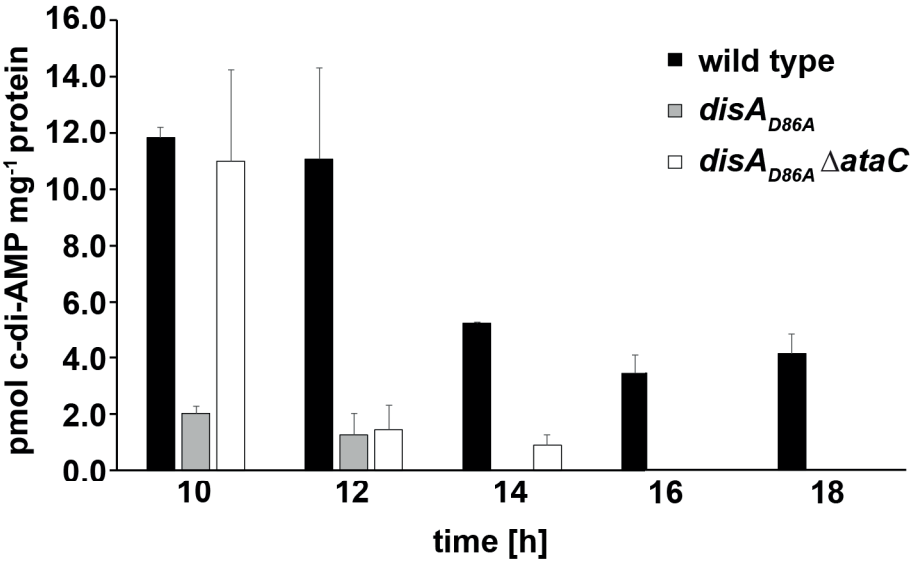


**Figure 11: Intracellular concentrations of c-di-AMP in *disA*$_{D86A}$ and *disA*$_{D86A}$ Δ*ataC*.**
Strains were sampled during the developmental life cycle in liquid sporulation medium. The inactivation of *disA* led to a reduction during late vegetative growth (10 and 12 h) and disappearance of c-di-AMP upon initiation of sporulation (at 14 h). c-di-AMP was increased in *disA*$_{D86A}$ Δ*ataC* in comparison to *disA*$_{D86A}$ and remained detectable until 14 h. Data are presented as mean ± SD of biological replicates (n = 3).

#### 4.2.4.3 Does AtaC cooperate with another PDE to cleave c-di-AMP?

Intriguingly, although deletion of *ataC* in the *disA*$_{D86A}$ increased the c-di-AMP level at 10 h growth, a drop at 12 h and disappearance of c-di-AMP in the later growth phases still occurred (Figure 11). Although the latter result could be explained with inactivation of the cryptic c-di-AMP synthase and subsequent dilution within the growing hyphae (the c-di-AMP level was normalized to the total cell protein which amount increased during growth), the c-di-AMP reduction between 10 and 12 h is too great, suggesting that the c-di-AMP produced until 10 h was actively degraded by another PDE to reach such a low level at 12 h. There is

some evidence for this hypothesis. First, although c-di-AMP is increased in the *ataC* mutant, its intracellular concentration remains constant in the later growth phases instead of accumulating (Figure 6A), which could be expected if AtaC is the single PDE in *Streptomyces*. Second, 5'-pApA, the intermediate cleavage product of c-di-AMP, is still detectable during the whole life cycle in the *ataC* mutant (Figure 12A). Interestingly, 5'-pApA is also detectable in Δ*disA* (Figure 12A) and might be a degradation product of c-di-AMP produced by the cryptic c-di-AMP synthase (Figure 6A and Figure 11).

A potential candidate for a second c-di-AMP PDE might be Vnz_31290. Similar to AtaC, Vnz_31290 belongs to the phosphodiesterase superfamily (Pfam PF01663) and appeared in the same list of PDEs, in which AtaC was found (paragraph 4.1.2). Although the cytosolic domain of Vnz_31290 shares only 23% sequence identity to AtaC, all residues predicted to be required for enzymatic activity, including D269, are conserved (Latoscha et al., 2020) (Figure 12B). However, all attempts to generate a Vnz_31290 overexpression construct failed and a *vnz_31290* deletion mutant showed wild type-like phenotypes on MYM agar and NA supplemented with salt (Figure 12 C and D). Nevertheless, it has been reported in Firmicutes encoding multiple PDEs that a single PDE deletion sometimes has only little effect on growth (Hu et al., 2020; Huynh et al., 2015; Rørvik et al., 2020). Hence, a potential role as a c-di-AMP PDE cannot be completely ruled out for Vnz_31290 at the moment.

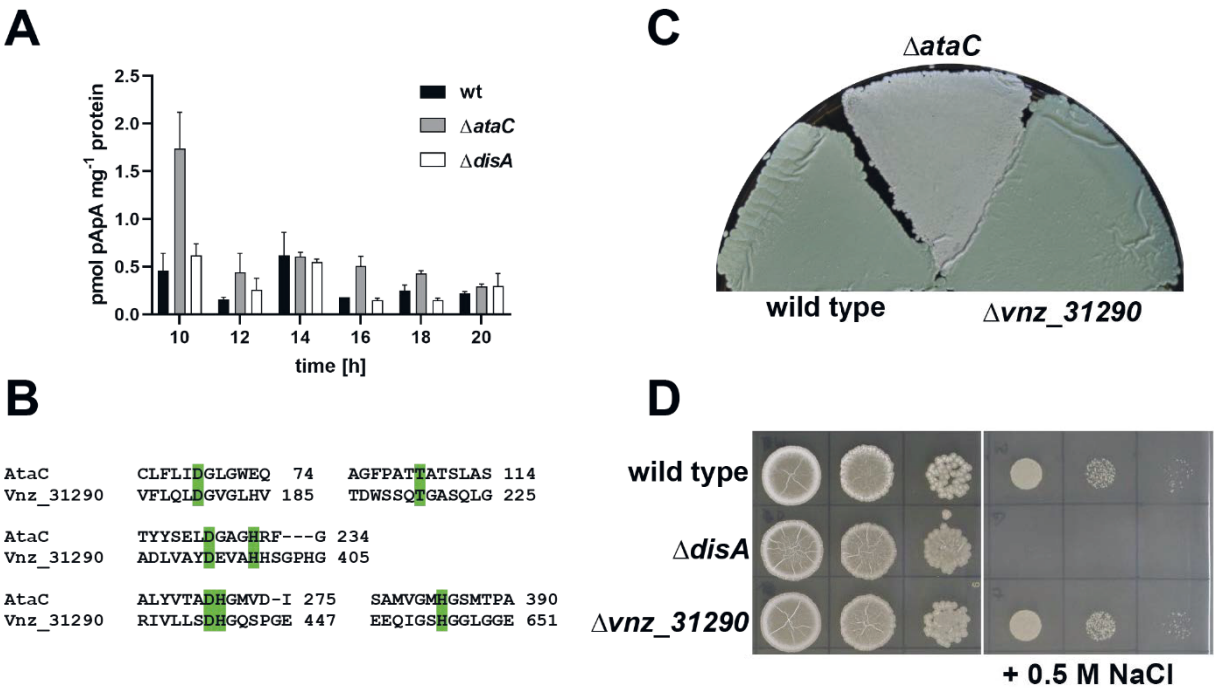


**Figure 12: Intracellular pApA levels in *S. venezuelae* c-di-AMP mutants and phenotypical characterization of the *vnz_31290* mutant.**

**(A)** Intracellular pApA concentrations in *S. venezuelae*. Wild type (wt), Δ*disA* and Δ*ataC* were sampled during the developmental life cycle in liquid sporulation medium and the quantification of pApA was performed as described for c-di-AMP. pApA is detectable in all strains. **(B)** Alignment of AtaC with the cytosolic domain of Vnz_31290 (aa 142 to 722). The alignment was cropped to the putative active site and the amino acid residues predicted to participate in enzymatic activity of AtaC were labeled in green (Latoscha et al., 2020). Numbers indicate the last amino acid position shown for each sequence part. **(C)** Development of Δ*vnz_31290* on MYM agar. Spores of indicated strains were streaked as patches on plates and incubated for 2 d at 30 °C. In contrast to Δ*ataC*, Δ*vnz_31290* showed no deviation from the wild-type phenotype. **(D)** Spores indicated strains were serially diluted and spotted on NA and NA supplemented with 0.5 M NaCl. Δ*vnz_31290* is as resistant to NaCl as the wild type.

## 4.3 Biochemical and phenotypical characterization of RCK_C domain proteins from *S. venezuelae*

The increased sensitivity of Δ*disA* to stress induced by high $Na^+$ and $K^+$ concentrations in the medium raised the question of how c-di-AMP produced by DisA modulates the cellular response. My BLAST analyses revealed that most known c-di-AMP-binding proteins are not conserved in *S. venezuelae*. There are however a few exceptions. First, Gundlach et al. (2017) identified a KimA homolog encoded by *sco6385* in *S. coelicolor.* KimA has been demonstrated to be regulated by binding of c-di-AMP to the *ydaO* riboswitch and directly to the protein (Gibhardt et al., 2019; Gundlach et al., 2017; Gundlach et al., 2019). The corresponding protein in *S. venezuelae* is Vnz_15480, which shares 42% amino acid sequence identity to *B. subtilis* KimA. Interestingly, BLAST analyses using *B. subtilis* KimA revealed a second protein, Vnz_27465, which has 38% amino acid sequence identity and is

encoded downstream of *vnz_27460* (encodes an RCK_C domain protein, see below) albeit on a different DNA strand and separated by 235 bp. However, the role of Vnz_15480 and Vnz_27465 in potassium uptake remains to be evaluated in *S. venezuelae*. Second, *S. venezuelae* encodes a KdpD homolog (Vnz_27435). However, the motif responsible for c-di-AMP binding in *S. aureus* is degenerate and likely does not bind c-di-AMP (Moscoso et al., 2016). Third, Vnz_16000 shares 45% amino acid sequence identity to OpuCA from *L. monocytogenes*, but lacks the CBS domain required for c-di-AMP binding (Huynh et al., 2016). Fourth, Vnz_12395 shares 25% amino acid sequence identity to *S. aureus* CpaA and does not encode the RCK_C domain (Corrigan et al., 2013).

Overall, the proteins described above appear to be unlikely to participate in c-di-AMP-regulated processes in *S. venezuelae* due to degenerate binding motifs or missing domains. Hence, in this part of the study I aimed to identify c-di-AMP sensors in *S. venezuelae* to understand how the appropriate response to $Na^+$ and $K^+$ stress is achieved in this model organism.

### 4.3.1 *S. venezuelae* RCK_C domain proteins possess putative c-di-AMP binding sites

In Firmicutes, proteins containing a so-called RCK_C domain (C-terminal domain of regulator of conductance of $K^+$) are involved in control of potassium homeostasis by modulating the activity or expression of several potassium importers (Commichau et al., 2018). Moreover, *in vitro*, c-di-AMP was shown to activate CpaA, an RCK_C domain-containing cation/proton antiporter in *S. aureus*, which functions as a $Na^+$ and $K^+$ exporter (Chin et al., 2015).

Since all known RCK_C domain effectors regulated by c-di-AMP are absent in *S. venezuelae*, I searched for Pfam PF02080 in the InterProScan annotated *S. venezuelae* genome and identified six novel proteins containing an RCK_C domain (Latoscha et al., 2020). A multiple sequence alignment (MSA) was performed with c-di-AMP binding RCK_C domain proteins KtrA from *S. aureus* and KtrC from *B. subtilis* (Kim et al., 2015; Rocha et al., 2019). Comparison of the putative c-di-AMP binding sites to the corresponding residues in KtrA and KtrC showed a varying degree of conservation within the *S. venezuelae* proteins (Figure 13). Two proteins, Vnz_28055 (CpeA) and Vnz_28520 (CpeD), showed the highest conservation with four well conserved residues (L104, R110, I117 and V118), two residues with conserved polarity (R108 and S116) as well as a Val at position 103, which could potentially contribute to c-di-AMP binding.

Interestingly, both proteins share 89% amino acid sequence identity and are annotated as “potassium transporter TrkA” on StrepDB. In other bacteria, TrkA consists of a double RCK domain and acts as a gating component, regulating transport activity of the unspecific monovalent cation channel TrkH in response to binding of adenosine-containing

nucleotides like ATP and ADP (Schrecker et al., 2019). Interestingly, the TrkA homolog in *S. agalactiae* (depicted as TrkH in the study) was shown to bind c-di-AMP *in vitro* (Devaux et al., 2018). However, CpeA and CpeD show a different domain architecture, consisting of an N-terminal domain of unknown function and a single C-terminal RCK_C domain (Figure 15 A and B). Further BLAST analyses showed that CpeA and CpeD share 27 and 24% amino acid sequence identity, respectively, and 50% amino acid sequence similarity to KhtT, the c-di-AMP-binding component of the KhtTU potassium efflux system in *B. subtilis* (Fujisawa et al., 2007; Gundlach et al., 2019). In support with this, a search in the Conserved Domain Database (CDD) using the amino acid sequences of CpeA and CpeD identified both proteins as members of the KhtT superfamily. According to the entry O07535 on UniprotKB, KhtT shows the same domain architecture like CpeA/CpeD, consisting of a single C-terminal RCK_C domain and an undefined N-terminal portion.

Altogether, the bioinformatic analyses suggest a potential link of CpeA and CpeD to regulation of ion homeostasis in *S. venezuelae*.

```
Sau_KtrA              TEKMAGQSIIDLDIRAQYGINIIAIK      180
Bsu_KtrC              NSRLAGNTLLDLDIRAKYGINIVAIK      180
Vnz_28055(CpeA)       HSYWNGRVLGETRMRTETGVSIVAVL      121
Vnz_28520(CpeD)       HSYWNGRVLGETRMRTEAGASIVAVL      121
Vnz_28040             GSRLHGVAVFELRLPPPAVITLLVRG      445
Vnz_14905             HSRMHGVEVAELRLPPGAAVTLVVRE      430
Vnz_27460             --AWIGHKVSRLQ-D-ETGVRVAFLT      177
Vnz_12665             GKSLDTLSKEHPEFS-SGGVYVTDVL      337
```

**Figure 13: Multiple sequence alignment (MSA) of *S. venezuelae* proteins containing the RCK_C domain.** Six proteins containing an RCK_C domain were identified and used for MSA with KtrA from *S. aureus* (Kim et al., 2015) and KtrC from *B. subtilis* (Rocha et al., 2019) using Clustal Omega (Madeira et al., 2019). The MSA was cropped to the c-di-AMP binding region. The numbers indicate the position of the last shown amino acid in the polypeptide chain. Amino acids involved in hydrophobic interactions are highlighted in yellow, and amino acids responsible for hydrophilic interactions are marked in cyan.

### 4.3.2 CpeA and CpeD bind c-di-AMP *in vitro*

Since CpeA and CpeD showed the highest conservation within the predicted c-di-AMP binding site, I hypothesized that these two proteins might function as c-di-AMP-binding effectors in *S. venezuelae.* I decided to purify 6xHis-tagged CpeA and CpeD and test them for c-di-AMP binding *in vitro*. Due to an erroneous annotation of the translational start site on StrepDB, a CpeD version was used that was truncated by five N-terminal amino acids.

First, the purified proteins were tested in nano differential scanning fluorimetry (nanoDSF) thermal shift assays, measuring the folding status of the proteins in presence of

potential nucleotide ligands. In this method, protein solutions are gradually heated and the folding status is measured by assessing the ratio of fluorescence at 350 nm to 330 nm. Each protein has characteristic inflection points (Ti), which depend on the primary amino acid sequence and the used buffer, and indicate transitions in the folding status of the protein, i. e. its unfolding. Specific binding of a ligand stabilizes the protein structure, which is reflected in a shift of the Ti to higher temperatures.

Purified CpeA was incubated with different nucleotides and applied to nanoDSF. CpeA showed a Ti upshift of 3 °C in presence of c-di-AMP indicating stabilization of CpeA upon c-di-AMP binding (Ti of 52.5 °C without nucleotides versus 55.5 °C with c-di-AMP) (Figure 14A). Interestingly, although c-di-GMP, pApA and cAMP had no effect on the Ti, addition of ATP caused an upshift of 1.4 °C to 53.9 °C, suggesting that CpeA might also bind ATP. To test this, I applied a Differential Radial Capillary Action of Ligand Assay (DRaCALA). This assay allows visualization of radiolabeled ligand binding to a protein: the bound ligand is retained as a concentrated spot or ring after the application of the protein-ligand mixture onto nitrocellulose; on the other hand, the ligand is freely diffusible if no binding or inhibition of binding to the protein occurs (Roelofs et al., 2011). Hence, I performed the DRaCALA using [$^{32}$P]-c-di-AMP in competition with different unlabeled nucleotides in high excess. CpeA-[$^{32}$P]-c-di-AMP-complex formation was significantly inhibited only in presence of unlabeled c-di-AMP. These data suggest that c-di-AMP is the physiological and specific ligand of CpeA (Figure 14C, *top*). In agreement with this finding, CpeA failed to bind [$^{32}$P]-ATP in the DRaCALA (Figure 14C, *bottom*).

In nanoDSF experiments, CpeD showed a similar behavior like CpeA: upon addition of c-di-AMP, the Ti shifted from 54.1 to 57.6 °C by 3.5 °C and led to a change in the shape of the first derivative curve (Figure 14B). c-di-GMP had only a mild effect and increased the Ti by 0.6 °C. Surprisingly, despite the high sequence similarity to CpeA, CpeD failed to bind [$^{32}$P]-c-di-AMP in DRaCALA even by increasing the used protein amount to 10 µg (Figure 14D). To exclude that proper nucleotide binding was impaired by the missing N-terminal amino acids, I purified the 6xHis-tagged full-length CpeD and applied the protein to nanoDSF under similar conditions as above. In comparison to the truncated CpeD the basal Ti was increased (57.9 °C) and addition of c-di-AMP caused a smaller upshift of 1.6 °C (Appendix Figure A3). However, incubation with c-di-GMP had no effect on full length CpeD.

In summary, two RCK_C domain proteins capable of c-di-AMP binding were identified in *S. venezuelae*. Whereas CpeA specifically bound c-di-AMP in two independent *in vitro* experiments, c-di-AMP binding by CpeD was less feasible, suggesting a lower affinity to c-di-AMP.

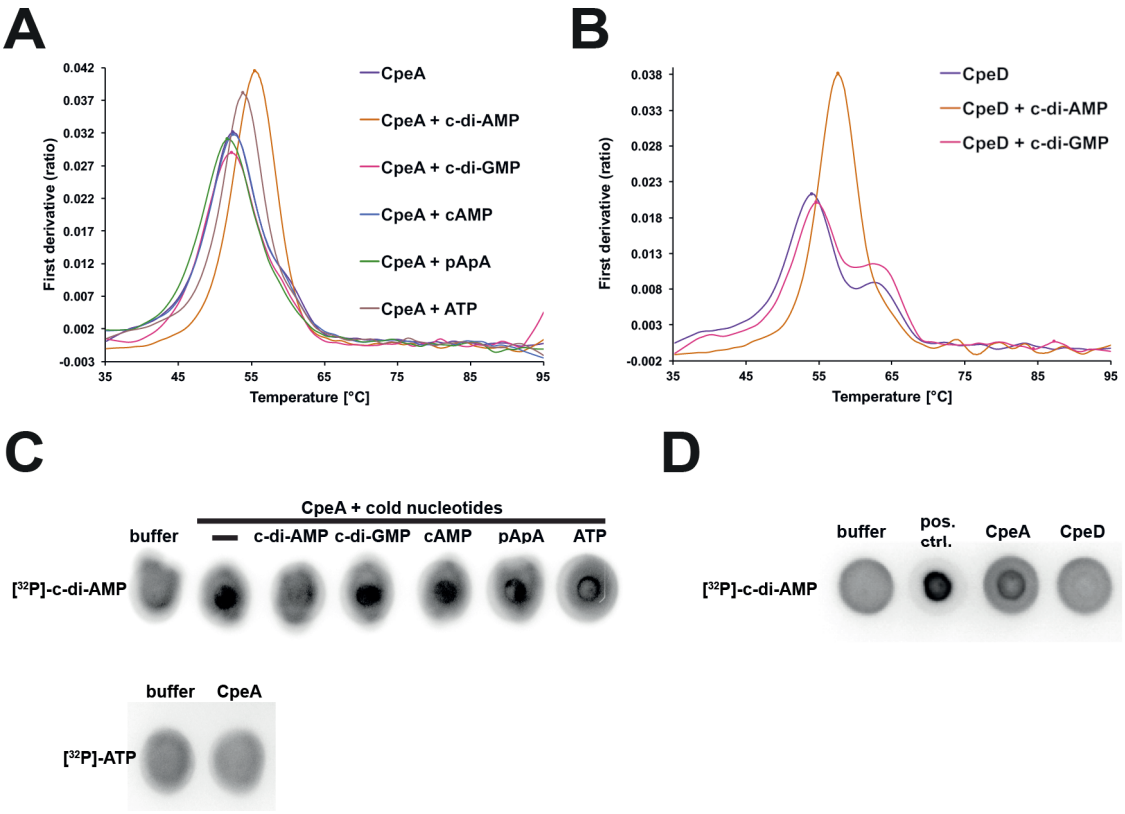


**Figure 14: *in vitro* c-di-AMP binding of purified CpeA and CpeD.**

**(A)** nano differential scanning fluorimetry (nanoDSF) of 5 µM CpeA incubated with 1 mM of different nucleotides. The thermal shift is shown as the first derivative of the unfolding curves. Addition of c-di-AMP shows highest increase of the CpeA inflection point (orange), whereas ATP has only an intermediate effect (brown) compared to the unfolding of untreated CpeA (purple). Addition of other nucleotides has no positive effect. **(B)** nanoDSF of 5 µM CpeD incubated with 1 mM c-di-AMP or c-di-GMP. Only addition of c-di-AMP caused a remarkable upshift of the CpeD inflection point (orange) compared to untreated protein (purple). **(C)** CpeA specifically binds [$^{32}$P]-c-di-AMP in Differential Radial Capillary Action of Ligand Assay (DRaCALA). 5 µg protein were incubated with 42 nM [$^{32}$P]-c-di-AMP before addition of 100 µM unlabeled nucleotides as competitors. Only c-di-AMP competed with binding of [$^{32}$P]-c-di-AMP (*top panel*). CpeA does not bind [$^{32}$P]-ATP in DRaCALA. 5 µg CpeA were incubated with 83 nM [$^{32}$P]-ATP (*bottom panel*). **(D)** CpeD does not bind [$^{32}$P]-c-di-AMP in DRaCALA. 10 µg CpeD were incubated with 42 nM [$^{32}$P]-c-di-AMP. 2 µg GST-PgpH$_{HD}$ and 10 µg CpeA were used as positive control.

Panel C was originally published in (Latoscha et al., 2020) under Creative Commons Attribution-NonCommercial-NoDerivatives License 4.0 (CC BY-NC-ND) and modified here with permission.

### 4.3.3 CpeA and CpeD are encoded in operons with predicted cation/proton exchangers

With the knowledge that CpeA and CpeD bind c-di-AMP *in vitro*, the next step was to analyze the potential function of these proteins. *cpeA* and *cpeD* are organized in putative operons with the genes *vnz_28050* (*cpeB*) and *vnz_28525* (*cpeE*), respectively, which are annotated as “cation/H$^+$ antiporter” on StrepDB (Figure 15 A and B). Protter analyses predicted the gene products CpeB and CpeE as membrane-bound proteins consisting of 13 TM domains

and a short cytosolic domain (Figure 15 C and D). CpeB and CpeE share an overall amino acid sequence identity of 85 %, which is increased to 91 % if comparing only the predicted TMs. The *cpeA* operon contains a third gene encoding a hypothetical protein, *vnz_28045* (*cpeC*), which is predicted to form 3 TM domains (Figure 15A). However, global BLAST analysis on NCBI against all available genomes revealed that Vnz_28045 is confined to 15 *Streptomyces* species. Interestingly, although *cpeAB* is conserved in *S. coelicolor*, a *cpeC* homolog is not encoded. Hence, CpeC does not seem to fulfill a conserved function.

HHpred analysis of CpeB and CpeE revealed multiple sodium/proton antiporters as structural homologs including NapA from *Thermus thermophilus* (Protein Database [PDB] code: 5BZ3), MjNhaP1 from *Methanocaldococcus jannaschii* (PDB code: 4CZB) and PaNhaP from *Pyrococcus abyssii* (PDB code: 4CZ8) as the closest hits (100% probability). These proteins have been shown to exchange sodium ions for protons, with uptake or efflux of $Na^+$ depending on the $Na^+$ and $H^+$ gradients across the cell membrane (Furrer et al., 2007; Okazaki et al., 2019; Warnau et al., 2020).

Interestingly within the first 380 amino acids of their polypeptide chains, CpeB and CpeE share 32 and 34 % amino acid sequence identity, respectively, and 54% amino acid sequence similarity to KhtU, the antiporter subunit of the KhtTU potassium efflux system in *B. subtilis* (Fujisawa et al., 2007). Additionally, a search in the CDD using the amino acid sequences of CpeB and CpeE revealed that both proteins contain a KefB domain. In gram-negative bacteria, KefGB and the related KefFC are potassium efflux transporters that exchange potassium against protons protecting bacteria against stress caused by accumulation of electrophiles (positively charged molecules) (Fujisawa et al., 2007; Healy et al., 2014; Schrecker et al., 2019).

Based on the *in silico* analyses, which strongly suggest a function in cation transport, *vnz_28055-28045* and *vnz_28520-28525* were renamed to *cpeABC* and *cpeDE* (cpe for cation/proton exchanger), respectively.

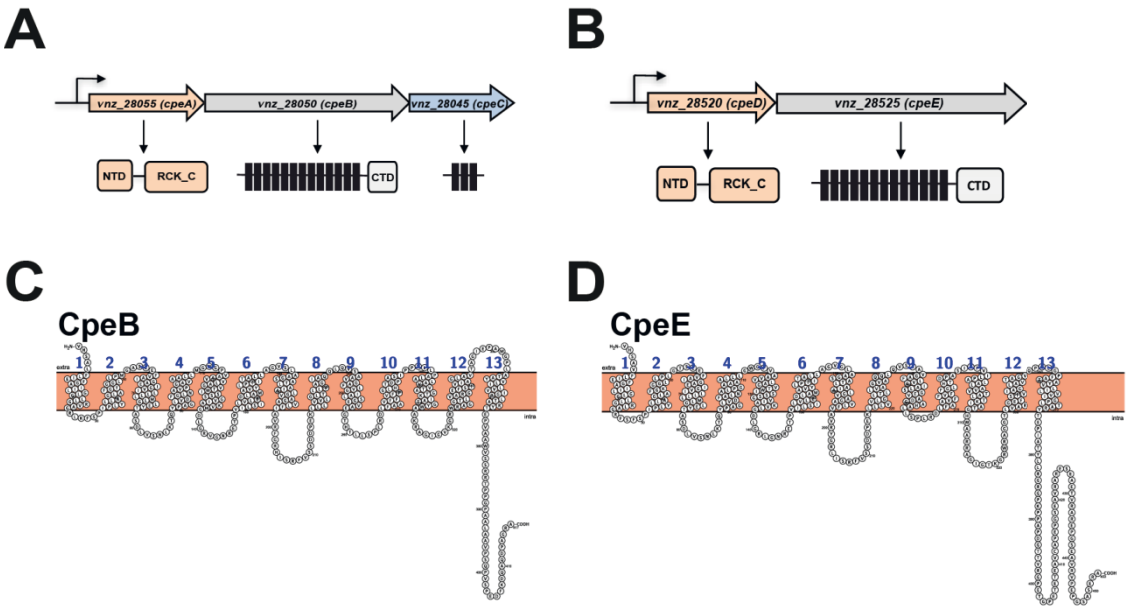


**Figure 15: *cpeA* and *cpeD* are encoded in operons with predicted cation/proton exchangers.**

**(A)** Operon structure of *cpeA* as annotated on StrepDB. *cpeA* (*vnz_28055*) forms an operon with *vnz_28050* (*cpeB*; annotated as "cation/$H^+$ antiporter") and *vnz_28045* (*cpeC*; annotated as "hypothetical protein"). **(B)** *cpeD* precedes *vnz_28525* (*cpeE*, annotated as "cation/$H^+$ antiporter"). Structural prediction of CpeB **(C)** and CpeE **(D)** via Protter suggests that both proteins are likely membrane-located and consist of 13 transmembrane (TM) domains and a short cytosolic portion.



### 4.3.4 c-di-AMP-dependent *in vivo* interaction of CpeA and CpeD with CpeB and CpeE

Soluble RCK_C domain-containing proteins like KtrA and KtrC were shown to act as so-called gating complexes, which modulate potassium import by the membrane-located pore proteins KtrB and KtrD, respectively, upon binding of nucleotide ligands (Corrigan et al., 2013; Gibhardt et al., 2019). The association of CpeA and CpeD with the predicted cation/proton antiporters CpeB and CpeE, respectively, led to the question whether CpeA and CpeD adopt a similar role as regulatory subunits for transporter activity in response to c-di-AMP binding.

To answer this question, I used the Bacterial Adenylate Cyclase Two-Hybrid (BACTH) assay, which exploits the reconstitution of the adenylate cyclase from *Bordetella pertussis* ($Cya_{Bpe}$) in a *cya*-deficient *E. coli* strain. Bait and target proteins are fused to the T25 and T18 fragments of $Cya_{Bpe}$ and interaction of fused proteins brings both fragments in close physical proximity, thus permitting adenylate cyclase activity. On a suitable medium like MacConkey agar, fermentation of maltose is enabled, and the color change of a pH indicator allows evaluation of interaction between bait and target proteins.

The predicted transporters CpeB and CpeE were fused to the T25 fragment, whereas the putative regulators CpeA and CpeD were fused to T18. To evaluate the contribution of c-di-AMP to transporter-regulator complex formation, the constructs encoding the T18 fusions were extended with *disA-FLAG* or *disA*$_{D86A}$*-FLAG* and expressed under control of a separate *lac* promoter. After 24 h of growth, a strain expressing CpeA and CpeB showed a basal interaction, which was substantially improved when DisA-FLAG was co-expressed (Figure 16A, Appendix Figure A4A). The enhancement of CpeA-CpeB interaction was solely dependent on c-di-AMP production since a strain co-expressing the inactive DisA$_{D86A}$-FLAG behaved similarly as the strain without DisA-FLAG (Figure 16A, Appendix Figure A4B). Interestingly, CpeC fused to T25 or T18 did not exhibit any interaction with CpeA or CpeB, respectively, regardless of c-di-AMP production (Appendix Figure A4C).

Similar to observations with CpeA and CpeB, c-di-AMP produced by DisA-FLAG enabled interaction of CpeD with CpeE, which however, required a longer incubation time of 45 h (Figure 16B, Appendix Figure A4A). Again, inactivation of DisA-FLAG reduced the intensity of complex formation, demonstrating that c-di-AMP stimulates interaction between regulatory and transporter subunits (Figure 16B).

Given the high amino acid sequence similarity between the CpeAB and CpeDE systems, I wondered whether the regulatory subunits can cross-interact with the transporter subunits and whether c-di-AMP might be a specificity switch for interaction. In both cases, cross-interaction was detectable and strongly enhanced by c-di-AMP production (Figure 16 C and D).

Altogether, these data demonstrate that CpeA and CpeD bind c-di-AMP *in vivo*, which stimulates interaction with the predicted cation/proton antiporters CpeB and CpeE, suggesting that CpeA and CpeD might modulate transporter activity in response to c-di-AMP binding.

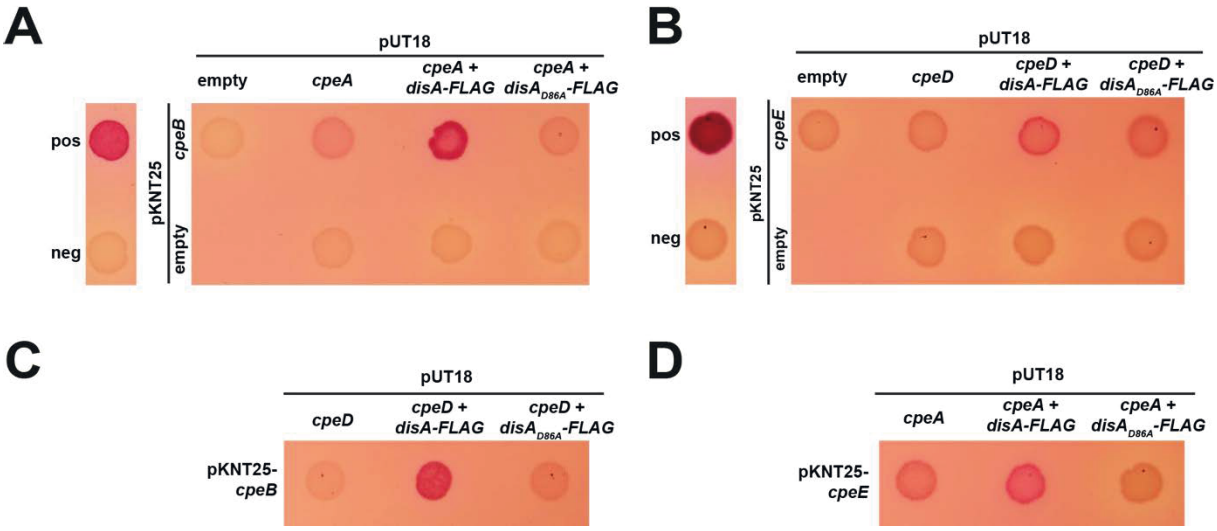


**Figure 16: CpeA and CpeD interact with CpeB and CpeE in a c-di-AMP-dependent manner.**

*E coli* W3110 Δ*cya* strains containing the indicated construct combinations were spotted on Difco MacConkey agar supplemented with 1 % maltose and incubated at 26 °C for 24 h (A, C) or 45 h (B, D). A strain containing empty vectors and a strain carrying the leucine zipper part of the yeast GCN4 protein were used as a negative and a positive control, respectively. **(A)** CpeB shows basal interaction with CpeA, which is substantially increased by co-expression of DisA-FLAG but not the inactive DisA$_{D86A}$-FLAG variant. **(B)** CpeE interacts with CpeD if DisA-FLAG is co-expressed. Inactivation of DisA-FLAG abolishes interaction of CpeE and CpeD. **(C)** CpeB shows cross-interaction with CpeD upon DisA-FLAG co-expression. **(D)** CpeE cross-interacts with CpeA in presence of DisA-FLAG.

Panel A was originally published in Latoscha et al. (2020) under Creative Commons Attribution-NonCommercial-NoDerivatives License 4.0 (CC BY-NC-ND) and modified here with permission.

### 4.3.5 Expression of CpeABC improves growth in presence of potassium in a heterologous host

Given the knowledge that CpeA binds c-di-AMP to enhance interaction of CpeA with CpeB, I sought to evaluate how c-di-AMP binding affects the activity of the CpeABC transporter. Due to structural similarity of CpeB to sodium/proton antiporters (paragraph 4.3.3) and sequence similarity of CpeAB to potassium efflux systems (paragraphs 4.3.1 and 4.3.3) I hypothesized that CpeABC might control sodium and/or potassium homeostasis in response to c-di-AMP in *S. venezuelae*.

To study these possibilities, I used the construct pUT18-*cpeA-disA-FLAG* to generate the plasmids p*cpeABC-disA-FLAG* and p*cpeABC-disA$_{D86A}$-FLAG*, replacing the T18 fragment sequence by *cpeBC*. These constructs were transformed in *E. coli* strain EP432, which is deficient in the sodium exporters *nhaA* and *nhaB* and cannot grow in presence of high sodium concentrations (Furrer et al., 2007; Lentes et al., 2014; Pinner et al., 1993). If CpeABC is an active sodium transporter as HHpred analyses in paragraph 4.3.3 suggested, its expression should restore growth of EP432 in LBon + 200 mM NaCl (LB200N). However,

expression of CpeABC did not permit growth in LB200N compared to the empty vector (pUT18) regardless of c-di-AMP production, suggesting that CpeABC cannot complement the salt sensitive phenotype of the Δ*nhaA*Δ*nhaB* mutant and thus is not primarily responsible for active sodium export from the cell (Figure 17A). Instead, both strains expressing CpeABC showed improved growth in LBK (LBon + 87 mM KCl) (Figure 17A). This finding indicated that CpeABC might be rather involved in potassium homeostasis.

In Firmicutes, activity of many potassium importers is inhibited upon c-di-AMP binding to the RCK_C domain (Stülke & Krüger, 2020). To test whether CpeABC is a potassium importer, which is inactivated by c-di-AMP, I transformed *E. coli* strain LB2003 with pUT18, p*cpeABC-disA-FLAG* and p*cpeABC-disA*$_{D86A}$*-FLAG*. LB2003 is not able to grow at potassium concentrations below 15 mM KCl in defined minimal medium since it is deficient for all native potassium importers and potassium is essential for growth. Hence, this strain was extensively used to study kinetics of potassium importers from *B. subtilis* and *L. monocytogenes* in dependence on c-di-AMP (Gibhardt et al., 2019; Gundlach et al., 2019). Similarly, CpeABC expression should restore growth of LB2003 in minimal medium (M9) supplemented with 10 mM KCl if it is a potassium importer. To investigate this, cultures were grown using a modified protocol from Gibhardt et al. (2019) (see paragraph 3.4.1.3 for details). Briefly, LB2003 strains containing pUT18, p*cpeABC-disA-FLAG* or p*cpeABC-disA*$_{D86A}$*-FLAG* were grown on LBK agar and single colonies were used to inoculate LBK pre-cultures. Interestingly, consistent with observations for EP432, pre-cultures of LB2003 strains containing the CpeABC transporter showed enhanced growth in LBK, which was highest in the strain co-expressing inactive DisA$_{D86A}$-FLAG (Figure 17B). M9 overnight pre-cultures supplemented with 50 mM KCl (M9 + 50 mM KCl) were inoculated with the LBK cultures to the same starting $OD_{578}$. The overnight cultures were diluted in fresh M9 + 50 mM KCl, grown until the exponential growth phase and washed with potassium-free M9 to remove extracellular potassium. The washed cells were finally inoculated into M9 main cultures induced with a low concentration of IPTG to stimulate expression of CpeABC and DisA-FLAG variants. Two different KCl concentrations, 10 mM (evaluation of potassium import) and 50 mM (control medium), were used to monitor growth of LB2003 strains. In both M9 media only growth of the strain expressing CpeABC in combination with the inactive DisA$_{D86A}$-FLAG was considerably improved compared to the empty vector control (Figure 17C), suggesting that CpeABC might indeed be involved in regulation of potassium homeostasis and that this activity is subject to inhibition upon c-di-AMP binding. However, there is no clear evidence whether CpeABC is a potassium importer since the growth of LB2003 p*cpeABC-disA*$_{D86A}$*-FLAG* was only very weak in M9 + 10 mM KCl compared to the much greater enhancement in M9 + 50 mM KCl (Figure 17C). Hence, CpeABC might function either as a low-affinity potassium importer or a potassium exporter since it facilitates

growth at moderate extracellular potassium concentrations. Whereas the first possibility cannot be excluded yet, the similarity of CpeB to the KhtU and KefC potassium efflux transporters would rather support the latter (see paragraph 4.3.3).

In summary, expression of CpeABC in two different *E. coli* strains provided initial evidence that this transporter directly contributes to the control of the potassium homeostasis and appears to be negatively regulated by c-di-AMP under tested conditions.

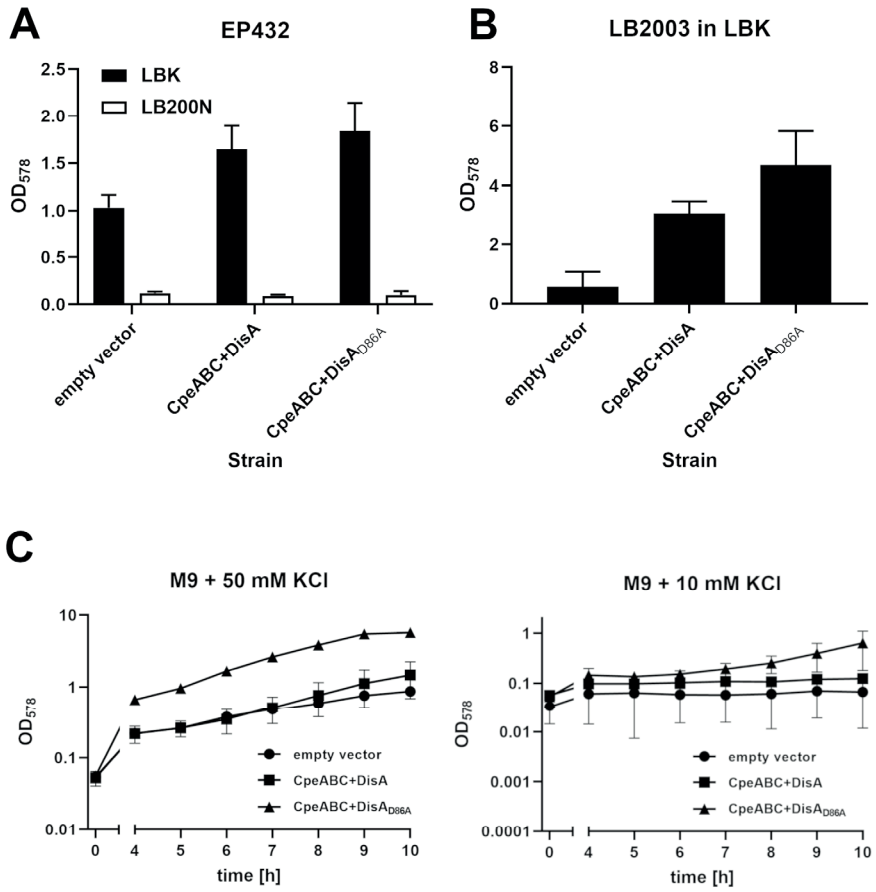


**Figure 17: Complementation of *E. coli* strains deficient in sodium exporters or potassium importers with CpeABC under control of c-di-AMP production.**

**(A)** *E. coli* EP432 is deficient for *nhaA* and *nhaB* and thus cannot grow in presence of high extracellular sodium concentrations. Complementation with CpeABC did not improve growth in LB200N containing 200 mM NaCl but in LBK, which contains 87 mM KCl. Graph shows the final $OD_{578}$ after 20 h of growth at 37 °C. Data are presented as the mean ± SD of biological replicates (n = 3). **(B)** Growth of *E. coli* LB2003 deficient for multiple potassium importers in LBK. Strains expressing CpeABC show improved growth in comparison to the empty vector. Data are presented as the mean ± SD of biological replicates (n = 3). **(C)** Growth of *E. coli* LB2003 in defined minimal medium (M9) supplemented with 50 µM IPTG and different KCl concentrations. The strain expressing CpeABC and the enzymatically inactive $DisA_{D86A}$-FLAG (triangles) showed improved growth in 50 mM KCl (*left panel*) and minor improvement at 10 mM KCl (*right panel*) compared to the other strains. Cultures were grown at 37 °C and 220 rpm and samples for $OD_{578}$ measurement were taken at indicated time points. Data are presented as the mean ± SD of biological replicates (n = 2).

### 4.3.6 Deletion and overexpression of *cpe* have no effect on sensitivity to monovalent cation stress

The c-di-AMP-dependent interaction of CpeA and CpeD with the predicted cation/proton antiporters CpeB and CpeE and improved growth of *E. coli* strains expressing CpeABC in KCl-supplemented media revealed an intriguing connection to the observed sensitivity of c-di-AMP-deficient *disA* mutants to high extracellular concentrations of monovalent cations. Hence, I hypothesized that the corresponding resistance mechanism in *Streptomyces* might be regulated via c-di-AMP, which binds to CpeA/CpeD to modulate activity of CpeB/CpeE.

To analyze whether the Cpe transporters are responsible for the Δ*disA* salt sensitivity, I generated *cpeA* and *cpeD* single deletion mutants and compared their growth to the wild type and Δ*disA* on NA supplemented with 0.5 M NaCl or 0.4 M KCl. In contrast to Δ*disA*, which was reproducibly sensitive to both salts, Δ*cpeA* and Δ*cpeD* showed wild type-like growth on both media (Figure 18). Given the high sequence similarity of CpeAB and CpeDE, which likely results in the same function, I assumed that one system might compensate for the loss of the other. Hence, I investigated the growth of the Δ*cpeA* Δ*cpeD* double mutant, which however, was still resistant to high NaCl and KCl concentrations (Figure 18). Since both KhtU and KefC are functional without the ancillary proteins (KhtT and KefF) and export potassium *in vivo* (Fujisawa et al., 2007; Healy et al., 2014), I deleted the transporter subunits *cpeB* and *cpeE* individually and in combination. Again, no mutant showed increased sensitivity to NaCl or KCl (Figure 18)

Taking into consideration that in Firmicutes c-di-AMP inhibits potassium uptake and activates potassium and sodium efflux (Stülke & Krüger, 2020), two hypotheses of how c-di-AMP might affect activity of CpeABC and CpeDE in *Streptomyces* are possible: (i) CpeB and CpeE are low-affinity potassium importers (see paragraph 4.3.5), whose potassium uptake is inhibited by interaction with c-di-AMP-bound CpeA and CpeD, respectively, or (ii) both transporters are cation exporters as indicated by similarity to potassium efflux transporters KhtTU and Kef (see paragraphs 4.3.1 and 4.3.3), which would require c-di-AMP for optimal activity. In both cases c-di-AMP produced by DisA would prevent toxic accumulation of potassium in the cytosol during growth on media with high extracellular KCl or NaCl concentrations. However, there is no experimental evidence for c-di-AMP-mediated activation of CpeABC transport activity yet and data obtained in a heterologous host rather support an inhibitory effect of c-di-AMP binding on CpeABC (Figure 17).

Hence, the first hypothesis (Cpe are potassium importers) appears to be more plausible and could explain the lack of the salt sensitivity observed in the *cpe* mutants. Since the transporters would be inactive in presence of c-di-AMP, their deletion would not further affect the salt resistance of the respective mutants. On the other hand, I hypothesized that overexpression of the transporters in Δ*disA* should be expected to increase susceptibility to

$Na^+/K^+$ because Cpe are constantly active due to lack of c-di-AMP. To test this, I cloned the *cpeABC* operon into vector pIJ10257, which allows integration of the whole resulting plasmid into the *Streptomyces* chromosome at the $attB_{\phi BT1}$ site and expression of the introduced genes under control of the strong constitutive *ermE** promoter (Hong et al., 2005). The pIJ10257 construct was conjugated into the wild type, Δ*disA* and Δ*ataC*. Serial spore dilutions were spotted on NA supplemented with different KCl concentrations: 0.25 M KCl permit growth of Δ*disA* and thus this concentration was used to test whether *cpeABC* overexpression turns Δ*disA* more susceptible to monovalent cation stress; conversely, 0.5 M KCl served to assess whether overexpressed CpeABC can improve growth of c-di-AMP-producing wild type and Δ*ataC*, which would be expected if it functions as a c-di-AMP-activated potassium efflux system. However, presence of pIJ10257-*cpeABC* did not significantly increase the $K^+$ sensitivity or resistance of all tested strains (Figure 19A). Although it seems that Δ*disA* pIJ10257-*cpeABC* and Δ*ataC* pIJ10257-*cpeABC* appeared to grow slightly better on NA supplemented with 0.4 M and 0.5 M KCl than their parent strains (Figure 19A), this is rather likely due to the reduced CFU count of Δ*disA* and Δ*ataC* spotted on the plates, as can be clearly seen on the control plate without additional KCl (Figure 19A). In agreement with this, no increased KCl or NaCl resistance was observed for Δ*disA* pIJ10257-*cpeABC* and Δ*ataC* pIJ10257-*cpeABC* after re-adjustment of the parent strain CFUs (Appendix Figure A5).

Notably, in some cases *S. venezuelae* can lose the integrated pIJ10257 if Hyg selection is removed (N. Tschowri, personal communication). To make sure that all strains retained pIJ10257-*cpeABC* after spore stock generation, spores were streaked for single colonies on NA + 16 µg/ml Hyg. The wild type with an integrated empty vector was used as a positive control. All strains grew, indicating Hyg resistance and thus presence of pIJ10257-*cpeABC*. For further analysis, single colonies of Hyg-resistant strains were picked and streaked on NA supplemented with 0.5 M NaCl and 0.4 M KCl. Δ*disA* and Δ*ataC* colonies of approximately the same size grown on NA without Hyg were used as reference. Similar to the results observed previously, there was no difference in growth of strains containing pIJ10257-*cpeABC* with wild type pIJ10257 and Δ*disA* and Δ*ataC* after incubation for 3 d (Figure 19B).

In a similar fashion, the same strains were streaked on MYM agar and MYM agar supplemented with 16 µg/ml Hyg and incubated for 4 d. On the MYM plate, the wild type and Δ*disA* derivatives developed normally and both Δ*ataC* and Δ*ataC* pIJ10257-*cpeABC* failed to accumulate the spore pigment and remained greyish as expected (Figure 19C, *left*). Interestingly, Δ*ataC* pIJ10257-*cpeABC* became slightly green when grown on MYM in presence of Hyg (Figure 19C, *right*). However, this experiment was performed only once and

needs to be repeated with an appropriate control strain (Δ*ataC* pIJ10257) to rule out that this phenotype is not solely resulting from Hyg addition.

Altogether, neither deletion nor overexpression of *cpe* genes could conclusively demonstrate the contribution of the Cpe transporters to the *Streptomyces* ion stress response, suggesting that the c-di-AMP-controlled regulatory mechanism is more sophisticated and other transporters with similar function might compensate for the loss of Cpe.

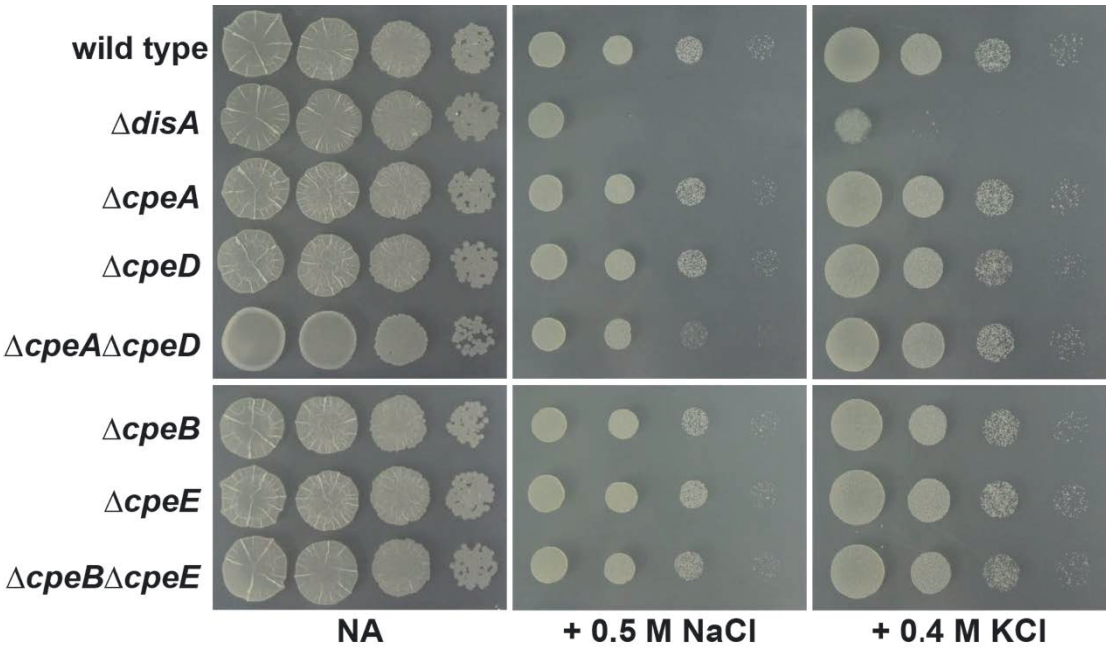


**Figure 18: Growth of different *cpe* mutants on NA supplemented with 0.5 M NaCl and 0.4 M KCl after 2 d at 30 °C.**

Spores of the indicated strains were serially diluted and spotted on NA supplemented with 0.5 M NaCl or 0.4 M KCl with subsequent incubation for 2 d at 30 °C.

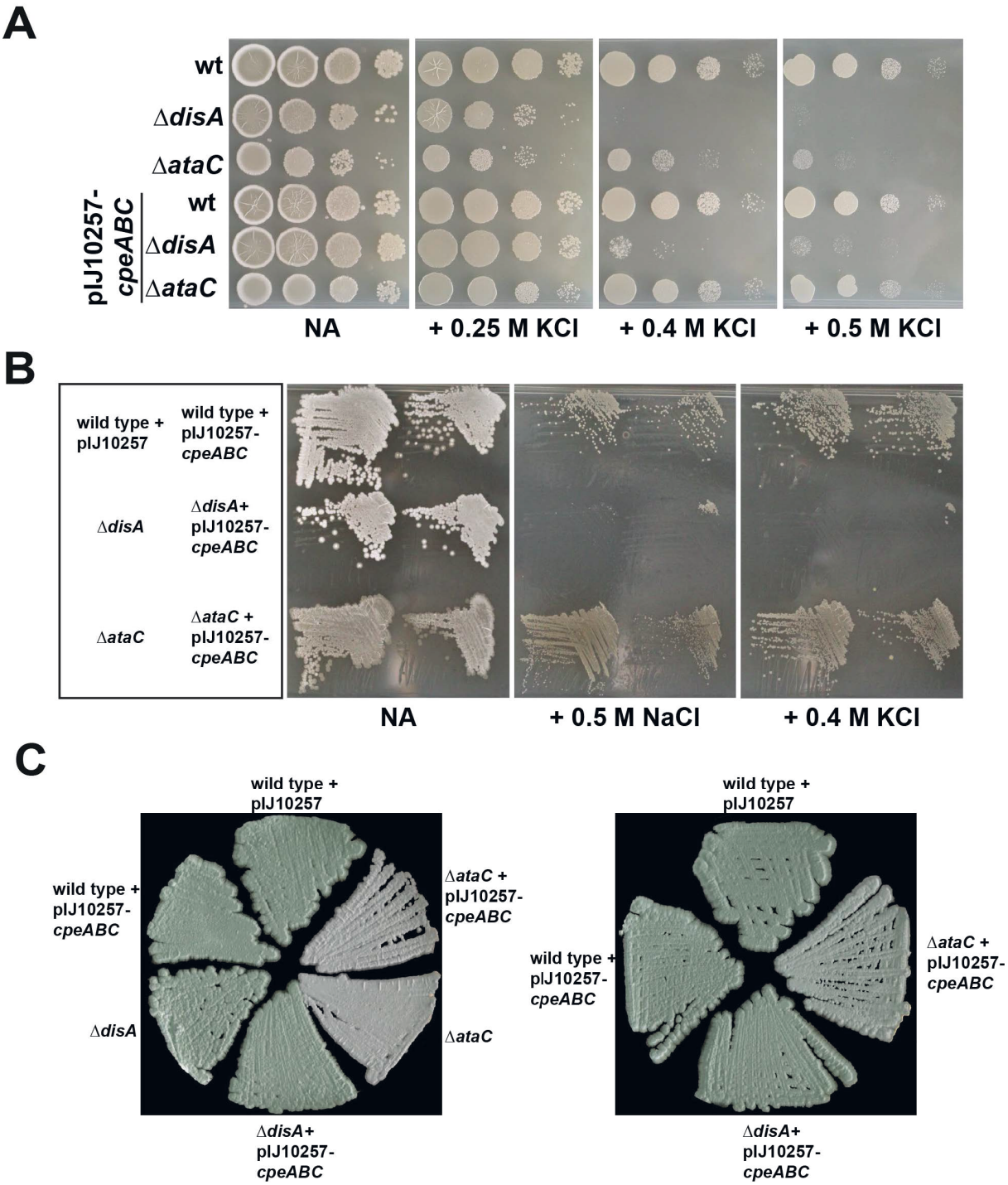


**Figure 19: Phenotypes of *S. venezuelae* strains expressing *cpeABC* under control of the constitutive promoter *ermE*p* from the *attB*$_{\Phi BT1}$ site.**

**(A)** *S. venezuelae* strains were serially diluted and spotted on NA supplemented with different KCl concentrations. **(B)** Single colonies of *S. venezuelae* strains grown for 3 d at RT on NA (Δ*disA* and Δ*ataC*) or NA supplemented with 16 µg/ml Hyg (strains containing pIJ10257 derivatives) were re-streaked on NA supplemented with NaCl or KCl and grown for 3 d at 30 °C. **(C)** Similar to (B), single colonies of indicated strains were streaked on MYM (*left*) or MYM supplemented with 16 µg/ml Hyg (*right*) and incubated for 4 d at 30 °C.

### 4.3.7 The purified RCK_C domains of Vnz_12665, Vnz_14905, Vnz_27460 and Vnz_28040 do not bind c-di-AMP *in vitro*

There are two possible explanations why it was not possible to obtain conclusive phenotypes using *cpe* mutants and overexpression strains: (i) either CpeAB and CpeDE are not responsible for the Δ*disA* phenotype or (ii) other potentially c-di-AMP-regulated transporter systems with redundant functions to the Cpe transporters exist.

Besides CpeA and CpeD, *S. venezuelae* contains four additional proteins with predicted RCK_C domains albeit with less well conserved binding residues (Figure 13). Similar to CpeB and CpeE, I performed *in silico* predictions for the remaining RCK_C domain proteins using Protter and HHpred. Vnz_28040, Vnz_14905 and Vnz_12665 were predicted to be membrane proteins (Figure 20 A, B, D), which are annotated as "$K^+/H^+$ antiporter" (Vnz_28040 and Vnz_14905) or "aspartate-alanine antiporter" (Vnz_12665) on StrepDB. Interestingly, HHpred analyses showed that the closest structural homologs for the TM domains of the three proteins were NapA (PDB code: 5BZ3) and MjNhaP1 (PDB code: 4CZB), the same sodium/proton antiporters predicted for CpeB and CpeE (paragraph 4.3.3), suggesting that Vnz_28040, Vnz_14905 and Vnz_12665 might adopt a similar function like CpeB and CpeE. In contrast, Vnz_27460 is a putative cytosolic protein and HHpred analysis identified a TrkA channel protein from *T. maritima* (PDB code: 3L4B) and a Ktr potassium uptake protein from *B. subtilis* (PDB code: 6I8V) as the closest structural homologs (Figure 20C).

To test c-di-AMP binding of all four proteins, the Protter predicted cytosolic domains, which contain the respective RCK_C domains (aa 183-380 in Vnz_12665, aa 380-507 in Vnz_14905, aa 390-506 in Vnz_28040 and full-length Vnz_27460), were purified as N-terminally GST-tagged fusion proteins. The purified proteins were tested for c-di-AMP binding using nanoDSF. All proteins showed two inflection points (Ti), indicating that the GST tag and the RCK_C containing domains likely unfold sequentially. However, neither Ti was significantly upshifted upon addition of c-di-AMP, suggesting that none of the proteins binds c-di-AMP under tested conditions (Appendix Figure A6). To confirm this finding, a DRaCALA using 10 µg of purified fusion proteins and CpeA as a positive control was performed. Although CpeA reproducibly bound [$^{32}$P]-c-di-AMP, no binding was observed for the other RCK_C domain proteins (Figure 20E).

In summary, these data show that the cytosolic domains of Vnz_12665, Vnz_14905, Vnz_27460 and Vnz_28040 do not bind c-di-AMP under tested conditions.

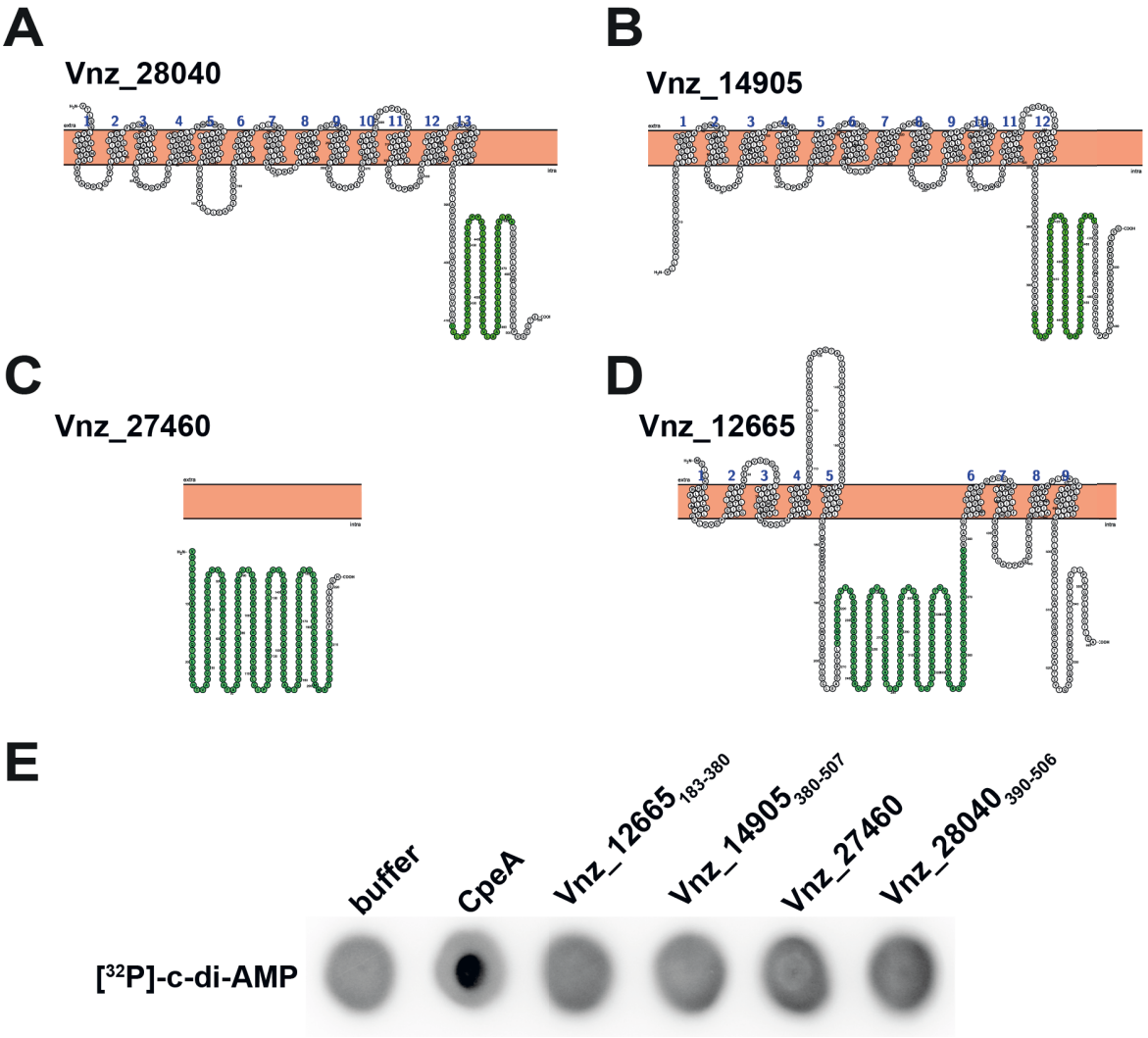


**Figure 20: Structural prediction and c-di-AMP binding of RCK_C domain containing proteins.**
**(A)** and **(B)** Vnz_28040 and Vnz_14905 are predicted membrane proteins containing 13 and 12 TMs, respectively, with the RCK_C domains likely located in the soluble cytosolic portion. **(C)** Vnz_27460 is predicted to be a cytosolic protein. **(D)** Vnz_12665 is predicted to be comprised of 9 TMs, which are interrupted by a cytosolic portion containing the RCK_C domain. **(E)** Binding of 42 nM [$^{32}$P]-c-di-AMP to 10 µg of purified cytosolic domains (aa 183-380 in Vnz_12665, aa 380-507 in Vnz_14905, aa 390-506 in Vnz_28040 and full-length Vnz_27460) of indicated RCK_C domain-containing proteins in a DRaCALA. 10 µg CpeA were used as a positive control for binding. Structural predictions were performed via Protter. RCK_C domains, as identified via HHpred, are highlighted in green in (A) to (D).

### 4.3.8 Individual deletions of membrane-associated RCK_C domain proteins have no effect on salt resistance of *S. venezuelae*

The lack of *in vitro* c-di-AMP binding observed in the previous paragraph could be the result of suboptimal experimental conditions, f. e. the cytosolic domains of tested proteins might require the respective TM domains for proper folding and thus c-di-AMP binding. This is supported by the fact that the initial 350/330 nm ratio of 0.8-0.9 is quite high (compared to

~0.55 of CpeA and CpeD), suggesting that the structure of the fusion proteins is rather disordered (Appendix Figure A6).

Hence, next I generated RCK_C deletion mutants to evaluate whether the predicted cation/proton antiporters contribute to the c-di-AMP-dependent resistance to monovalent cation stress. The genes *vnz_14905*, *vnz_28040* and *vnz_12665* were selected for individual deletion since their gene products were predicted to show high structural similarity to CpeB/CpeE and thus can be expected to adopt the same function (paragraph 4.3.7). *vnz_27460* predicted to encode a soluble protein was not further analyzed here.

I serially diluted and spotted spores of wild type, Δ*disA* and the RCK_C single mutants on NA supplemented with 0.5 M NaCl or 0.4 M KCl. However, no mutant showed similar growth inhibition like Δ*disA* (Figure 21), demonstrating that none of the tested RCK_C domain-containing proteins is solely responsible for the monovalent cation stress resistance. Hence, probably rather a combination of different factors with redundant function appears to be utilized in this mechanism.

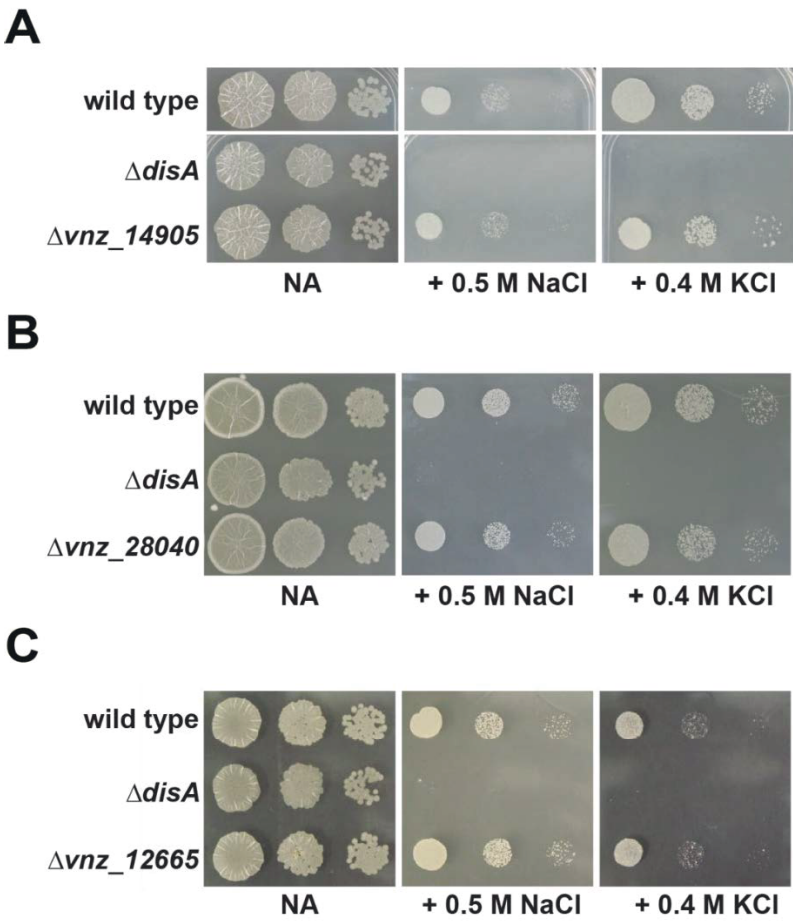


**Figure 21: *S. venezuelae* RCK_C mutants are resistant to stress by monovalent cations.**
Strains were grown on NA or NA supplemented with 0.5 M NaCl or 0.4 M KCl for 2 d at 30 °C. **(A)** Growth of Δ*vnz_14905*. **(B)** Growth of Δ*vnz_28040*. **(C)** Growth of Δ*vnz_12665*.

# 5 Discussion

## 5.1 c-di-AMP metabolism in *S. venezuelae*

In this work, I have shown that in agreement with the main principle of c-di-AMP metabolism, *S. venezuelae* utilizes a DAC domain protein and a PDE to regulate intracellular c-di-AMP. Whereas the PDE AtaC was previously unrecognized for c-di-AMP cleavage, the synthetase DisA is a typical diadenylate cyclase. Nevertheless, this work also provides evidence for presence of other non-canonical enzyme(s) involved in the c-di-AMP metabolism in *S. venezuelae* (see below).

### 5.1.1 *S. venezuelae* synthesizes c-di-AMP via DisA and an unknown DAC-independent synthetase

In a previous study, it has been shown that *S. venezuelae* is capable of DisA-dependent c-di-AMP production *in vivo* (St-Onge et al., 2015). However, evidence for direct biochemical activity of $DisA_{Sven}$ was missing. In this work, I demonstrated that $DisA_{Sven}$ is an active DAC *in vitro* and relies on an intact DGA motif for catalytic activity (Figure 4).

In agreement with DisA being the only DAC domain protein in Actinobacteria (Yin et al., 2020), *disA* deletion or inactivation abolished detectable c-di-AMP after the onset of sporulation during growth in liquid sporulation media. In contrast to previous findings (St-Onge et al., 2015), I detected c-di-AMP production during the late vegetative growth phase (Figure 6A and Figure 11). At this point a contamination of samples appears to be unlikely since c-di-AMP production was found in two independent mutants (Δ*disA* and $disA_{D86A}$) in different experiments and the detected c-di-AMP level could be enhanced in $disA_{D86A}$ upon deletion of the PDE-encoding *ataC* (Figure 11). The observed discrepancy might result from the additional thorough physical cell lysis using silica beads in this work (paragraph 3.8.2), which likely increases the overall nucleotide yield compared to the previous study. Hence, my data provide evidence for presence of at least one DAC-unrelated c-di-AMP synthetase which produces c-di-AMP exclusively during the (late) vegetative growth phase.

In contrast to most c-di-AMP-producing bacteria and archaea, which do not permit deletion of DAC proteins in rich media (Stülke & Krüger, 2020; Yin et al., 2020), *disA* is not essential and could be readily deleted in *S. venezuelae* (St-Onge et al., 2015) (this thesis). It would be interesting to study whether the cryptic c-di-AMP synthetase in *S. venezuelae* is the reason why *disA* can be deleted since a certain amount of c-di-AMP would still be retained in the cytosol at least during vegetative growth. Interestingly, activity of this synthetase cannot compensate the requirement of DisA-produced c-di-AMP during growth at monovalent cation stress if AtaC is present (Figure 10), suggesting that it controls a distinct cellular process

during vegetative growth, which could however explain why DisA is dispensable for proper growth in rich media (Figure 7). Hence, it will be important to identify the obscure c-di-AMP synthetase and determine the physiological function its c-di-AMP in *S. venezuelae* in future studies.

What might be the nature of this synthetase? Recently, Hallberg et al. (2016) described the so-called hybrid, promiscuous GGDEF enzyme HyprA in *Geobacter sulfurreducens*, which is capable of c-di-AMP production under certain conditions *in vitro*. The natural Ser variation of a conserved Asp residue (corresponding to D344 in *Caulobacter crescentus* PleD) allows binding of ATP and GTP to the active site of HyprA, and thus synthesis of cGAMP, c-di-AMP or c-di-GMP (Hallberg et al., 2016). However, my BLAST analyses revealed that all GGDEF-containing enzymes possess the conserved Asp at this position, suggesting that none of these proteins is involved in cryptic c-di-AMP production in *S. venezuelae.*

There are several possibilities how the c-di-AMP synthetase could be identified in *S. venezuelae*. A convenient method would be the employment of pulldown assays of proteins from *S. venezuelae* Δ*disA* cell lysate using immobilized c-di-AMP as binding matrix, with subsequent protein identification by mass spectrometry. This approach was frequently applied in other bacteria to identify c-di-AMP-binding proteins, including a PDE (Bai et al., 2014; Blötz et al., 2017; Gundlach, Dickmanns, et al., 2015; Stülke & Krüger, 2020; Sureka et al., 2014). Usage of Δ*disA* cell lysate should avoid saturation of proteins with endogenous c-di-AMP and binding of DisA to the matrix. However, this method would require some improvements in future studies since my preliminary attempts to pull down c-di-AMP binding proteins failed. Alternatively, candidate *S. venezuelae* cyclases from a list generated using an *in silico* analysis (M. M. Al-Bassam and N. Tschowri, unpublished) could be analyzed for c-di-AMP production. Similar to DisA, purified candidate proteins can be tested for c-di-AMP production in radioactive cyclase assays coupled to TLC and by measurements of intracellular c-di-AMP after deletion of candidate genes in the $disA_{D86A}$ mutant. A c-di-AMP synthetase will generate a reaction product which migrates at the same size as c-di-AMP synthesized by DisA in the TLC, whereas deletion of its gene should abolish detectable c-di-AMP in combination with the $disA_{D86A}$ mutation.

Independent of the used approach, identification and characterization of the cryptic c-di-AMP synthetase will be crucial to fully understand the role of c-di-AMP in *S. venezuelae*.

### 5.1.2 The novel PDE AtaC degrades c-di-AMP in Actinobacteria

With a few exceptions, most Actinobacteria do not encode the canonical GdpP-, DhhP- or PgpH-type PDEs and the degradation of c-di-AMP in this phylum remained widely mysterious (Yin et al., 2020). A combination of bioinformatic and biochemical methods led to

identification of AtaC as a novel c-di-AMP-specific PDE (Figure 5). Similar to some DhhP-type PDEs, AtaC cleaves c-di-AMP to pApA and AMP (Figure 5) (Bai et al., 2013; Bowman et al., 2016; Latoscha et al., 2020). In cooperation with G. Witte's group (LMU Munich), the biochemical and biophysical properties of AtaC were further characterized. The structural model of AtaC based on its close structural homolog PhnA revealed that Asp269 is required for manganese coordination and we demonstrated that a D269N mutation abolishes metal binding and enzymatic activity *in vitro* (Latoscha et al., 2020). Furthermore, AtaC shows similar enzymatic kinetics as the canonical c-di-AMP PDEs. For example, the catalytic constants of purified AtaC and *B. subtilis* GdpP are 0.2 $s^{-1}$ and 0.55 $s^{-1}$, respectively, and are comparable to each other (Latoscha et al., 2020; Rao et al., 2010). The dissociation constant of 0.9 µM of the inactive $AtaC_{D269N}$ is similar to the values of 0.3-0.4 µM measured for *L. monocytogenes* PgpH (Huynh et al., 2015; Latoscha et al., 2020).

Although AtaC homologs are not restricted to Actinobacteria, the vast majority (~88%) is encoded in Actinobacterial genomes (Latoscha et al., 2020). To evaluate whether c-di-AMP cleavage is a conserved function within AtaC homologs, I selected the proteins from the Firmicute *C. botulinum* and from the Actinobacteria *M. tuberculosis* and *M. luteus* (Latoscha et al., 2020). The purified proteins were tested for c-di-AMP cleavage and only *M. luteus* AtaC showed clear and specific activity, whereas the other proteins generated barely detectable degradation products (Figure 5 and Figure A1). However, $AtaC_{Mtub}$ was largely insoluble during purification, probably resulting in a too low protein concentration for demonstration of enzymatic activity. In contrast to *S. venezuelae* and *M. luteus*, *M. tuberculosis* contains a soluble DhhP homolog, and GdpP- and PgpH-type PDEs are encoded *C. botulinum* (Manikandan et al., 2014; Yang et al., 2014), permitting the possibility that $AtaC_{Mtub}$ and $AtaC_{Cbo}$ may exhibit a different enzymatic function. For example, in many bacteria, which contain multiple c-di-AMP PDEs, the DhhP-type PDE often uses 5'-pApA as the preferred or even exclusive substrate (Bai et al., 2013; Bowman et al., 2016; Konno et al., 2018). Given that $AtaC_{Sven}$ shows a high hydrolysis activity for 5'-pApA *in vitro* (Latoscha et al., 2020), it is feasible to speculate whether $AtaC_{Mtub}$ and $AtaC_{Cbo}$ might be rather pApA-specific PDEs. Since $AtaC_{Cbo}$ shows only a very low amino acid sequence identity of 21% compared to $AtaC_{Sven}$, it is however conceivable that this protein might prefer a completely different substrate than c-di-AMP or pApA.

However, in *S. venezuelae*, AtaC likely functions primarily as a c-di-AMP PDE *in vivo* since intracellular c-di-AMP levels are increased in an *ataC* mutant (Figure 6A). Interestingly during the late growth phases, c-di-AMP remains constantly elevated but does not further accumulate in the *ataC* mutant. Increased but constant c-di-AMP might be achieved in two ways in Δ*ataC*: (i) post-translational down regulation of c-di-AMP synthesis activity in response to the high c-di-AMP level or (ii) due to cleavage activity by another PDE(s).

However, in contrast to diguanylate cyclases, which produce the related but distinct molecule c-di-GMP and are often allosterically inhibited by c-di-GMP binding to a specific inhibitory site (Hengge et al., 2019), a similar mechanism has not been described for DACs up to date. On the other hand, degradation of c-di-AMP in *disA*$_{D86A}$ Δ*ataC* and detection of intracellular pApA in Δ*ataC* suggests the possibility of activity of a second c-di-AMP PDE in *S. venezuelae* (Figure 11 and Figure 12A). The candidate PDE Vnz_31290 contains the residues predicted to constitute the active site in AtaC, but could not be tested for c-di-AMP cleavage *in vitro* and the respective mutant did not show any phenotype (Figure 12 C and D). However, a potential role in *S. venezuelae* c-di-AMP metabolism cannot be excluded yet since it has been reported that in some bacteria containing multiple PDEs deletion of a single PDE is sometimes insufficient to result in a detectable phenotype (Huynh et al., 2015; Rørvik et al., 2020). For example, neither *gdpP* nor *pgpH* single deletion has an effect on growth of *L. monocytogenes* in broth or during infection, but a double PDE mutant is impaired (Huynh et al., 2015). In *S. mitis*, a *gdpP* deletion mutant has no phenotype, whereas deletion of *dhhP* impairs growth in broth and leads to formation of colonies with reduced size on solid medium (Rørvik et al., 2020). Hence, in future studies a cleavage activity of Vnz_31290 towards c-di-AMP should be evaluated. Alternatively, the pulldown method suggested in paragraph 5.1.1 could be applied for identification of a novel PDE as well since a similar approach was successful in identification of the *L. monocytogenes* PgpH as c-di-AMP-binding protein (Sureka et al., 2014).

Taken together, *S. venezuelae* and probably Actinobacteria in general utilize an enzymatic set for c-di-AMP regulation that substantially differs from Firmicutes. Whereas I could demonstrate that DisA and AtaC are the main components for c-di-AMP synthesis and degradation *in vivo*, respectively, it is likely that novel enzymes involved in *Streptomyces* c-di-AMP metabolism will be identified in future studies.

## 5.2 c-di-AMP regulates growth, development and ion homeostasis in *S. venezuelae*

One of the main aims of this PhD project was the identification of c-di-AMP-regulated physiological functions in *S. venezuelae*. By deleting or inactivating *ataC* and *disA*, and subsequent analysis of growth and development, I could show that deregulation of intracellular c-di-AMP leads to distinct and exclusive phenotypes, demonstrating that c-di-AMP is responsible for multiple cellular functions in *S. venezuelae* (see below).

In *S. venezuelae*, c-di-AMP generated by DisA is expendable for development and growth on rich media (MYM and NA), but impedes both processes when it is increased due to *ataC* deletion (Figure 7). On the other hand, loss of c-di-AMP produced by DisA leads to susceptibility to high concentrations of NaCl and KCl of the respective mutants (Figure 8).

Particularly, the *ataC* mutant was delayed in sporulation and failed to accumulate sufficient green spore pigment (Figure 7 A and B). Moreover, it formed smaller colonies on solid medium and showed slower growth in liquid sporulation medium (Figure 8 and Figure 7C). Similarly, growth defects in rich medium were reported frequently in PDE mutants of Firmicutes (Hu et al., 2020; Huynh et al., 2015; Konno et al., 2018; Mehne et al., 2013; Rørvik et al., 2020). This is likely caused by reduced potassium and compatible solute uptake due to transporter inhibition by increased c-di-AMP levels, which is reflected in sensitivity to increased osmolyte concentrations in most PDE mutants (Corrigan et al., 2013; Devaux et al., 2018; Huynh et al., 2016; Pham et al., 2018; Teh et al., 2019). In contrast, the *ataC* mutant is as resistant as the wild type to both non-ionic and monovalent cation osmotic stress in rich medium (Figure 8). However, *S. venezuelae disA* mutants were strongly inhibited by high concentrations of $Na^+$ and $K^+$, but not sucrose (Figure 8). Effects on osmotic resistance of cyclase mutants were rarely studied, but similar to my results, deletion of the non-essential *cdaA* in *S. pyogenes* abolished growth of the respective mutant in medium with elevated NaCl and KCl concentrations (Fahmi et al., 2019). Interestingly reminiscent of the *ataC* mutant, *S. pyogenes* PDE mutants were reported to be not affected under the same conditions (Fahmi et al., 2019). On the other hand, in Firmicutes encoding essential DACs, conditional depletion of *cdaA* in *L. monocytogenes* leads to increased resistance to NaCl and sorbitol, and addition of NaCl or KCl enables growth of *L. monocytogenes* and *S. aureus cdaA* deletion mutants in rich medium (Huynh et al., 2016; Whiteley et al., 2017; Zeden et al., 2020; Zeden et al., 2018).

Altogether, these findings suggest that the similar process of ion homeostasis is likely differently regulated in bacteria where DAC proteins are not essential. This indeed appears to be the case for *S. venezuelae* since the majority of c-di-AMP-regulated effectors involved in potassium or osmolyte uptake is not encoded in the genome or lacks critical domains for c-di-AMP binding (paragraph 4.3). In contrast, I identified the two novel RCK_C domain proteins CpeA and CpeD able to bind c-di-AMP *in vitro* and interact with predicted cation/proton antiporters, CpeB and CpeE, in response to c-di-AMP binding *in vivo* (Figure 14 and Figure 16). Although the exact function and the effect of c-di-AMP binding on activity could not be elucidated, the Cpe transporters might contribute to the salt sensitivity of Δ*disA* and growth defect of Δ*ataC* due to mis-regulation of intracellular $K^+$ ion and proton concentrations (discussed in more detail in paragraph 5.3).

Alternatively, potential down regulation of several cell wall remodeling enzymes could contribute to the growth defects observed in the *ataC* mutant. *S. venezuelae* encodes six genes preceded by an *ydaO*-like riboswitch. In *S. coelicolor*, RpfA (Vnz_14255 in *S. venezuelae*), SwlA (Vnz_04045), SwlB (Vnz_36100) and SwlC (Vnz_31850) were confirmed as cell wall lytic enzymes and studied in detail (Haiser et al., 2009; St-Onge et al., 2015). For

RpfA, c-di-AMP-dependent down regulation of expression has been demonstrated in *S. coelicolor* and *S. venezuelae*, and can be expected for the other genes as well (St-Onge et al., 2015). Remarkably, RpfA and SwlA are required for proper spore germination, whereas SwlB and SwlC are involved in hyphae branching during vegetative growth (Haiser et al., 2009). Hence, cumulative down regulation of all of these proteins via increased c-di-AMP in Δ*ataC* could lead to a delay in germination and possibly slower increase of the optical density during vegetative growth due to lack of hyphae branches, resulting in the observed growth defect (Figure 7). However, individual deletions in the four cell wall hydrolases result in formation of defective, heat-sensitive spores in *S. coelicolor* (Haiser et al., 2009), whereas *S. venezuelae* Δ*ataC* produces spores that are as heat-resistant as wild type spores (Figure 9). On the other hand, this discrepancy might as well arise from species-specific differences in spore morphogenesis. It would be interesting to determine via quantitative real-time PCR how low or high c-di-AMP in Δ*disA* and Δ*ataC*, respectively, influences the expression of each of the six riboswitch-regulated cell wall hydrolases. Depending on the outcome, phenotypes of *S. venezuelae* cell wall hydrolase deletion or overexpression strains could be evaluated in comparison to Δ*disA* and Δ*ataC* to determine their potential contribution to the respective phenotypes.

Production of the polyketide spore pigment is one of the last steps in the *Streptomyces* developmental cycle and is considered as a trait of mature spores (McCormick & Flärdh, 2012). However, the *ataC* mutant failed to accumulate sufficient spore pigment after prolonged incubation when differentiated spores were detectable in the wild type (Figure 7 A and B). This phenotype was at least partially independent of the growth defect since the colonies did not become as green as the wild type even after incubation for three weeks (data not shown). In contrast to the classical *whi* mutants, which remain white because they do not sporulate or produce the spore pigment (Latoscha et al., 2019), the color of the *ataC* mutant appeared to be rather greyish-green on solid medium and pale green in the spore stock. In comparison, wild-type and Δ*disA* colonies and spores were dark green after 2-3 days on sporulation medium (Figure 7A). This suggests that increased c-di-AMP either interferes with the expression of the *whiE* locus or maybe directly inhibits activity of one or more components of the pigment synthesis machinery. The first possibility is not unprecedented since c-di-GMP indirectly controls *whiE* expression via complex formation of the sigma factor WhiG with the anti-sigma factor RsiG in *S. venezuelae* (Gallagher et al., 2020). However, how c-di-AMP influences spore pigmentation remains to be elucidated and could be achieved by RNAseq analyses in Δ*ataC* and *in vitro* binding assays with purified WhiE proteins.

In summary, c-di-AMP is involved in different physiological and developmental processes in *S. venezuelae* and is required for correct growth and pigmentation, and survival under monovalent cation stress conditions.

## 5.3 Biological function of the Cpe transporters

The c-di-AMP-dependent interaction of the RCK_C domain proteins CpeA and CpeD with the predicted cation/proton antiporters CpeB and CpeE implied a reasonable connection to the NaCl and KCl-sensitive phenotype observed in Δ*disA* (Figure 16). CpeB and CpeE are structurally related to different sodium/proton antiporters, share decent sequence homology to KhtU, part of the potassium efflux transporter KhtTU from *B. subtilis*, and possess a KefB domain, which is involved in potassium efflux in gram-negative bacteria (paragraph 4.3.3).

However, neither deletions of the RCK_C domain proteins or transporter subunits in the wild type nor overexpression of *cpeABC* in c-di-AMP mutants resulted in a significant phenotype, keeping the exact function of the Cpe transporters enigmatic in *S. venezuelae* (Figure 18 and Figure 19). Several explanations for these results are feasible: (i) CpeABC and CpeDE are not involved in the DisA-dependent stress response under tested conditions, but may be used under different conditions; (ii) if Cpe transporters are potassium uptake systems, which are active in the *disA* mutant due to lack of inhibition via c-di-AMP and thus accumulate intracellular potassium to a toxic level, their loss would have no effect in the wild-type strain; or (iii) other c-di-AMP regulated proteins have a redundant function and can compensate for the loss of both Cpe transporters.

In support of possibility (i), a study has shown that in *S. venezuelae* co-cultivated with *Saccharomyces cerevisiae* on YPD agar, expression of CpeBC, CpeE and Vnz_28040 is upregulated under alkaline conditions, which was suggested to aid *S. venezuelae* survival by increased proton uptake (Jones et al., 2017). In agreement with this, KhtTU and KefFC showed increased potassium efflux activity at alkaline pH *in vitro* (Fujisawa et al., 2007). Interestingly, CpeA and CpeD, which are the first genes in the predicted *cpeB* and *cpeE* operons, respectively, were not upregulated (Jones et al., 2017).

However, expression of the CpeABC transporter in two different *E. coli* strains showed growth improvement at KCl concentrations above 50 mM, whereas growth at 200 mM NaCl was not observed (Figure 17). The remaining question is whether potassium uptake or efflux is responsible for this effect. Whereas expression of potassium importers from Firmicutes allows growth of *E. coli* LB2003 at extracellular potassium concentration of 10 mM and below (Bai et al., 2014; Gibhardt et al., 2019; Gundlach et al., 2019), only co-expression of CpeABC with $DisA_{D86A}$-FLAG (no c-di-AMP production) marginally improved growth under similar conditions (Figure 17C). This finding suggests that CpeABC might exhibit an activity as a low-affinity potassium uptake system, which is inhibited by c-di-AMP

and would be in good agreement with the common regulation of potassium importers by c-di-AMP (Stülke & Krüger, 2020). Nevertheless, CpeABC-induced growth improvement of *E. coli* EP432, which possesses the native potassium uptake systems, is somewhat counterintuitive in a medium containing sufficient KCl for growth. On the other hand, the parent strain of LB2003 and EP432, *E. coli* K-12, can accumulate intracellular potassium ions to a concentration of more than 200 mM during exponential growth (Schultz & Solomon, 1961; Stumpe & Bakker, 1997; Weiden et al., 1967). Hence, expression of an additional potassium uptake system could be beneficial to achieve these concentrations faster and thus facilitate growth. Altogether, if Cpe transporters are potassium uptake systems, which are inhibited by c-di-AMP binding as suggested by the data obtained from heterologous expression in *E. coli*, neither deletion of the RCK_C domain proteins nor of the transporters would lead to a salt-sensitive phenotype as observed in Figure 18. Consequently, overexpression of CpeABC in Δ*disA* would be expected to increase sensitivity to KCl, which was not the case under conditions tested (Figure 19). However due to lack of specific antibodies, it could not be assessed whether CpeABC is properly expressed.

On the other hand, *in silico* analyses suggest that the Cpe transporters might be involved in potassium efflux (paragraph 4.3.3). KhtTU and Kef transporters have been both characterized as potassium efflux systems, and Kef is important to counteract toxic effects of accumulated positively charged molecules by the acidification of the cytosol due to $H^+$ uptake (Fujisawa et al., 2007; Healy et al., 2014). Similar to CpeB/CpeE, both KhtU and KefC are encoded in operons with cytosolic proteins KhtT and KefF, respectively, and complex formation of the transporter subunit with the cytosolic proteins is required for potassium efflux activity *in vitro* (Fujisawa et al., 2007). Additionally, an *E. coli* KefFC complex shows a higher rate of potassium export *in vivo* than KefC alone (Healy et al., 2014). This indicates that binding of the cytosolic ancillary proteins to the transporters stimulates the potassium efflux activity. Intriguingly, c-di-AMP facilitates interaction of CpeA/CpeD with CpeB/CpeE *in vivo* (Figure 16), which could be interpreted as transporter activation. Whereas binding of c-di-AMP to KhtT has been demonstrated, the consequences for the transport activity were not studied yet (Gundlach et al., 2019). However, $Na^+$ and $K^+$ export by CpaA from *S. aureus* is stimulated *in vitro* by c-di-AMP binding to the RCK_C domain within its polypeptide chain (Chin et al., 2015). A function of Cpe as c-di-AMP-activated potassium efflux systems would be an elegant explanation for most of the phenotypes observed in the c-di-AMP mutants. First, in medium with increased KCl concentrations, lack of c-di-AMP in Δ*disA* would lead to accumulation of potassium to toxic levels in the cytosol. Second, it would abolish the exchange of potassium ions for protons, and thus reduction of intracellular pH, resulting in an inability to counteract the toxicity of sodium ions. Interestingly, a KefFC complex shows also some sodium/proton antiport activity *in vitro* (Fujisawa et al., 2007), hence a contribution of

CpeB/CpeE to sodium efflux via their KefC-related KefB domain cannot be fully excluded yet. Third, increased c-di-AMP in Δ*ataC* would constantly keep Cpe in an active state, thus acidifying the cytosol, which could result in disruption of the proton motive force and cause the observed growth defects. Nevertheless, although the data obtained in *E. coli* LB2003 do not support the model of CpeABC activation by c-di-AMP, they neither exclude the possibility of CpeABC general function as a potassium exporter (Figure 17). A future study using an *E. coli* strain deficient for *kefB* and *kefC* (Healy et al., 2014) for CpeABC/DisA-FLAG and CpeABC/$DisA_{D86A}$-FLAG expression might bring insight whether CpeABC is a potassium efflux system. Alternatively, *in vitro* systems for evaluation of antiporter activity have been established. For example, Chin et al. (2015) and colleagues reconstituted *S. aureus* CpaA in phosphatidylcholine proteoliposomes and measured transport activity in dependence on c-di-AMP by applying high external potassium or sodium concentrations. This created an inward cation gradient, resulting in exchange of cations for protons. Alkalization of the proteoliposomes due to proton efflux was monitored by alteration of the fluorescence of the hydrophilic pH-sensitive dye pyranine contained within the proteoliposomes (Chin et al., 2015). A similar method was applied to characterize the potassium efflux activity of the KhtTU and KefFC (Fujisawa et al., 2007). Here, the transporters were overexpressed in an antiporter-deficient *E. coli* strain, which was used to prepare everted membrane vesicles. The vesicles were loaded with acridine orange, which became fluorescent by the alkalization of the vesicle when potassium/proton activity was initiated by high external KCl concentrations (Fujisawa et al., 2007). Both methods might be helpful to determine whether Cpe transporters exhibit a potassium (or other ion) efflux activity. Alternatively, ion content in c-di-AMP and *cpe* mutants could be measured directly to understand if and how c-di-AMP imbalance influences intracellular ion concentrations in *S. venezuelae* (Gundlach et al., 2017). Although my preliminary potassium measurements in wild type and Δ*ataC* in cooperation with D. Hertel (Georg-August-Universität Göttingen) were not successful, they could provide valuable results after some methodical optimization in future studies.

However, if the Cpe systems are required in *S. venezuelae* for active potassium export and coping with stress induced by monovalent cations (or electrophiles in general), why does the deletion of both transporters not show any phenotype in presence of high NaCl or KCl concentrations? *S. venezuelae* encodes additional predicted transporter proteins containing RCK_C domains within their polypeptide chain. Vnz_12665, Vnz_14905 and Vnz_28040 are structurally similar to CpeB and CpeE (paragraph 4.3.7), suggesting that they might adopt a similar function and potentially compensate for the loss of both Cpe systems. However, purified RCK_C domains of these proteins failed to bind c-di-AMP *in vitro*, which could be a result from low conservation of the putative c-di-AMP-binding site (Figure 20E and Figure 13). On the other hand, all RCK_C domain proteins from Firmicutes tested up to date

were shown to bind c-di-AMP, suggesting that regulation of RCK_C by c-di-AMP is universal in this phylum (Bai et al., 2014; Corrigan et al., 2013; Devaux et al., 2018; Gundlach et al., 2019). For the only exception, the chloride channel EriC from *S. agalactiae*, from which only the RCK_C domain could be expressed in *E. coli*, the authors suggested that it might require the respective TMs for c-di-AMP binding (Devaux et al., 2018). A similar situation is plausible for the RCK_C domains of Vnz_12665, Vnz_14905 and Vnz_28040 since they were insoluble as 6xHis-tagged versions (data not shown) and nanoDSF measurements suggested that the respective GST fusion proteins were disordered in solution (Appendix Figure A6). Hence, it cannot be excluded that c-di-AMP binding will be possible to properly folded full-length proteins in *E. coli* lysates as shown for *B. subtilis* CpaA (Gundlach et al., 2019).

To evaluate whether one of the RCK_C domain proteins is responsible for the potassium and sodium sensitivity of Δ*disA*, I deleted the respective genes in *S. venezuelae*. Similar to the *cpe* mutants, no deletion was sufficient to achieve the Δ*disA* phenotype (Figure 21). These results suggest that the c-di-AMP-dependent regulation of ion homeostasis in *S. venezuelae* is a complex mechanism and probably multiple combined deletions of RCK_C domain proteins will be required to figure out which components are involved in this process. Alternatively, screening of Δ*disA* suppressors, i. e. *disA* mutants with spontaneously restored salt resistance due to secondary mutations within the chromosome, might bring more insight in this mechanism. Nevertheless, it is important to keep in mind that such suppressors can also restore growth in a c-di-AMP-independent manner (Gundlach et al., 2017; Whiteley et al., 2017). The first Δ*disA* suppressors were isolated towards the end of this study and their chromosomes will be analyzed in cooperation with F. M. Commichau (BTU Cottbus-Senftenberg) in future studies.

To summarize, the first discovered c-di-AMP effector proteins CpeA and CpeD are likely involved in regulation of intracellular potassium levels in *S. venezuelae* via interaction with the transporter subunits CpeB and CpeE. Although the exact nature of the Cpe transporters remains to be elucidated, they provide a promising link to the sodium and potassium sensitivity of Δ*disA* and the growth defect in Δ*ataC*. However, other so far unidentified c-di-AMP-dependent components contribute to these phenotypes and wait to be discovered in future.

## 5.4 The c-di-AMP signaling network in *S. venezuelae*

The model in Figure 22 summarizes the knowledge about c-di-AMP signaling in *S. venezuelae* obtained from previous findings and results from this work. In *S. venezuelae*, the DAC DisA and the novel PDE AtaC are expressed throughout the whole life cycle to maintain a basic level of c-di-AMP (St-Onge et al., 2015) (this thesis). At least one additional non-DAC

synthetase contributes to the c-di-AMP pool, which is degraded by AtaC probably in cooperation with other PDE(s) (Figure 22). In streptomycetes, c-di-AMP appears to regulate (at least) two different processes: (i) inhibition of expression of RpfA and likely other cell wall hydrolases (St-Onge & Elliot, 2017; St-Onge et al., 2015), suggesting involvement in peptidoglycan remodeling which is essential for germination and for hyphae branching during vegetative growth (Haiser et al., 2009) and (ii) activation of the cell response to monovalent cation stress (this thesis) (Figure 22). Since c-di-AMP produced by the unidentified synthetase is exclusively detectable during vegetative growth and cannot compensate for loss *disA* during growth at high sodium and potassium concentrations, it is tempting to speculate that the cryptic synthetase might be rather involved in a cellular process distinct from DisA-regulated monovalent cation stress response. How the latter is achieved by DisA remains to be elucidated, but data obtained during this study suggest that c-di-AMP produced by DisA directly controls activity of the predicted cation/proton antiporters CpeB and CpeE by facilitating interaction with the cytosolic c-di-AMP-binding effectors CpeA and CpeD (Figure 22). c-di-AMP-driven association into the complexes CpeAB(C) and CpeDE appears to result in inhibition of transporter activity of CpeABC expressed in *E. coli*. These findings suggest a model in which Cpe transporters constitutively import potassium in exchange for protons and are inhibited by c-di-AMP once a certain intracellular potassium concentration is achieved (Figure 22). This mechanism would fail in the *disA* mutant, which produces insufficient c-di-AMP, leading to toxic accumulation of potassium. On the other hand, similarity of Cpe transporters to the characterized potassium efflux systems KhtTU and Kef indicate that they might adopt a similar function. In this model, CpeB and CpeE would be inactive until c-di-AMP-mediated interaction with CpeA and CpeD occurs, which would activate efflux of potassium in exchange for protons to prevent toxic accumulation of potassium during growth under high potassium concentrations. However, experimental data obtained in this study do not support c-di-AMP-dependent activation of Cpe and further studies will be required to finally understand the function of these transporters. Nevertheless, other c-di-AMP-responsive components with redundant functions must be involved into the stress response to monovalent cations since *cpe* deletions show no phenotype comparable to Δ*disA*. Hence, I postulate that in addition to Cpe likely other ion transporters are regulated by c-di-AMP and can compensate the loss of *cpe* due to redundant functions (Figure 22). As soil-dwelling bacteria, streptomycetes are often challenged by alterations in osmotic pressure due to desiccation or rainfall. Expression of multiple transporters with redundant functions would be a fail-safe mechanism to ensure an adequate cellular response to changes in extracellular cation abundance.

In summary, this thesis significantly increased our knowledge about c-di-AMP signaling Streptomycetes. The enzymatic set involved in c-di-AMP maintenance was

extended by the previously unrecognized AtaC as the major c-di-AMP-cleaving PDE in Actinobacteria and a potentially novel class of c-di-AMP synthetases. Mutational analyses showed that c-di-AMP is involved in many physiological processes in *S. venezuelae* including growth, differentiation and ion stress resistance. Biochemical characterization of the c-di-AMP-binding proteins CpeA and CpeD and physiological studies of the putative potassium transporter CpeABC provided first insights in the regulation of the latter and promise more fascinating findings in future studies.

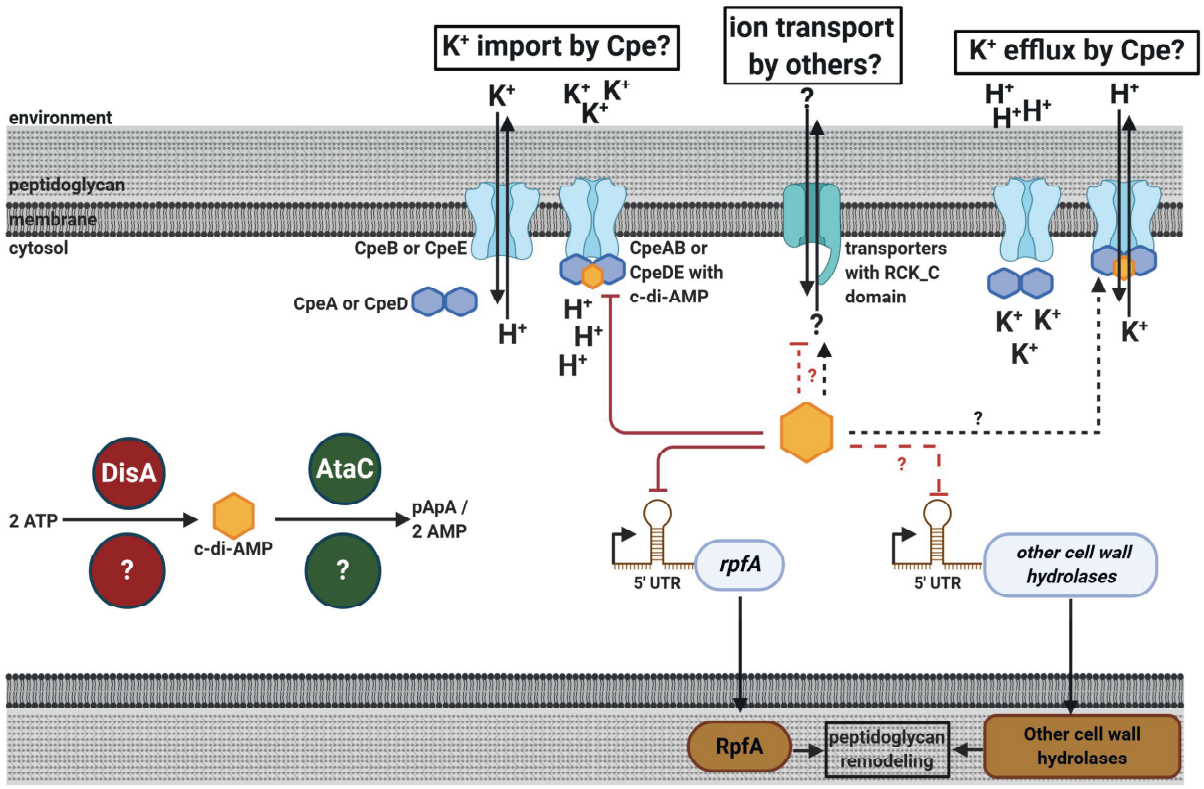


**Figure 22: Model of c-di-AMP metabolism and signaling in *Streptomyces*.**
The canonical DAC DisA and an unknown synthetase (question mark in red circle) use two ATP molecules to synthesize c-di-AMP, which is cleaved by the novel Actinobacterial PDE AtaC and likely another PDE (question mark in green circle) to 5'-pApA and/or two AMP. In *S. venezuelae*, c-di-AMP regulates the activity of Cpe transporters and probably other ion transporters containing a cytosolic RCK_C domain within their polypeptide chains. In Cpe transporters, c-di-AMP binds to the RCK_C domain proteins CpeA and CpeD and stimulates interaction with the antiporter subunits CpeB and CpeE, which presumably results in modulation of antiport activity and regulation of ion homeostasis. Experimental evidence in *E. coli* suggests that c-di-AMP inhibits potassium uptake by CpeABC, but potassium efflux mediated by Cpe transporters cannot be excluded yet in *S. venezuelae*. For simplicity, CpeC was omitted from the model. Additionally, c-di-AMP binding to a riboswitch in the 5' UTR transcript regions inhibits expression of RpfA and likely other cell wall hydrolases, involved in cell wall remodeling during germination, vegetative growth and sporulation in *S. coelicolor* (Haiser et al., 2009; St-Onge & Elliot, 2017; St-Onge et al., 2015). Arrows indicate positive regulation and lines with a bar show inhibition. Dashed lines indicate assumed regulation, which was not shown experimentally yet.

# 6 References


Agostoni, M., Logan-Jackson, A. R., Heinz, E. R., Severin, G. B., Bruger, E. L., Waters, C. M., & Montgomery, B. L. (2018). Homeostasis of Second Messenger Cyclic-di-AMP Is Critical for Cyanobacterial Fitness and Acclimation to Abiotic Stress. *Front Microbiol*, *9*, 1121. https://doi.org/10.3389/fmicb.2018.01121

Al-Bassam, M. M., Haist, J., Neumann, S. A., Lindenberg, S., & Tschowri, N. (2018). Expression Patterns, Genomic Conservation and Input Into Developmental Regulation of the GGDEF/EAL/HD-GYP Domain Proteins in *Streptomyces*. *Front Microbiol*, *9*, 2524. https://doi.org/10.3389/fmicb.2018.02524

Andrade, W. A., Firon, A., Schmidt, T., Hornung, V., Fitzgerald, K. A., Kurt-Jones, E. A., Trieu-Cuot, P., Golenbock, D. T., & Kaminski, P. A. (2016). Group B *Streptococcus* Degrades Cyclic-di-AMP to Modulate STING-Dependent Type I Interferon Production. *Cell Host Microbe*, *20*(1), 49-59. https://doi.org/10.1016/j.chom.2016.06.003

Bai, Y., Yang, J., Eisele, L. E., Underwood, A. J., Koestler, B. J., Waters, C. M., Metzger, D. W., & Bai, G. (2013). Two DHH subfamily 1 proteins in *Streptococcus pneumoniae* possess cyclic di-AMP phosphodiesterase activity and affect bacterial growth and virulence. *J Bacteriol*, *195*(22), 5123-5132. https://doi.org/10.1128/JB.00769-13

Bai, Y., Yang, J., Zarrella, T. M., Zhang, Y., Metzger, D. W., & Bai, G. (2014). Cyclic di-AMP impairs potassium uptake mediated by a cyclic di-AMP binding protein in *Streptococcus pneumoniae*. *J Bacteriol*, *196*(3), 614-623. https://doi.org/10.1128/JB.01041-13

Bai, Y., Yang, J., Zhou, X., Ding, X., Eisele, L. E., & Bai, G. (2012). *Mycobacterium tuberculosis* Rv3586 (DacA) is a diadenylate cyclase that converts ATP or ADP into c-di-AMP. *PLoS One*, *7*(4), e35206. https://doi.org/10.1371/journal.pone.0035206

Bejerano-Sagie, M., Oppenheimer-Shaanan, Y., Berlatzky, I., Rouvinski, A., Meyerovich, M., & Ben-Yehuda, S. (2006). A checkpoint protein that scans the chromosome for damage at the start of sporulation in *Bacillus subtilis*. *Cell*, *125*(4), 679-690. https://doi.org/10.1016/j.cell.2006.03.039

Blötz, C., Treffon, K., Kaever, V., Schwede, F., Hammer, E., & Stülke, J. (2017). Identification of the Components Involved in Cyclic Di-AMP Signaling in *Mycoplasma pneumoniae*. *Front Microbiol*, *8*, 1328. https://doi.org/10.3389/fmicb.2017.01328

Bobek, J., Smidova, K., & Cihak, M. (2017). A Waking Review: Old and Novel Insights into the Spore Germination in *Streptomyces*. *Front Microbiol*, *8*, 2205. https://doi.org/10.3389/fmicb.2017.02205

Borovok, I., Gorovitz, B., Yanku, M., Schreiber, R., Gust, B., Chater, K., Aharonowitz, Y., & Cohen, G. (2004). Alternative oxygen-dependent and oxygen-independent ribonucleotide reductases in *Streptomyces*: cross-regulation and physiological role in response to oxygen limitation. *Mol Microbiol*, *54*(4), 1022-1035. https://doi.org/10.1111/j.1365-2958.2004.04325.x

Bowman, L., Zeden, M. S., Schuster, C. F., Kaever, V., & Gründling, A. (2016). New Insights into the Cyclic Di-adenosine Monophosphate (c-di-AMP) Degradation Pathway and the Requirement of the Cyclic Dinucleotide for Acid Stress Resistance in *Staphylococcus aureus*. *J Biol Chem*, *291*(53), 26970-26986. https://doi.org/10.1074/jbc.M116.747709

Braun, F., Thomalla, L., van der Does, C., Quax, T. E. F., Allers, T., Kaever, V., & Albers, S. V. (2019). Cyclic nucleotides in archaea: Cyclic di-AMP in the archaeon *Haloferax volcanii* and its putative role. *Microbiologyopen*, *8*(9), e00829. https://doi.org/10.1002/mbo3.829

Bremer, E., & Krämer, R. (2019). Responses of Microorganisms to Osmotic Stress. *Annu Rev Microbiol*, *73*, 313-334. https://doi.org/10.1146/annurev-micro-020518-115504

Brückner, R., & Titgemeyer, F. (2002). Carbon catabolite repression in bacteria: choice of the carbon source and autoregulatory limitation of sugar utilization. *FEMS Microbiol Lett*, *209*(2), 141-148. https://doi.org/10.1111/j.1574-6968.2002.tb11123.x

Bursy, J., Kuhlmann, A. U., Pittelkow, M., Hartmann, H., Jebbar, M., Pierik, A. J., & Bremer, E. (2008). Synthesis and uptake of the compatible solutes ectoine and 5-hydroxyectoine by *Streptomyces coelicolor* A3(2) in response to salt and heat stresses. *Appl Environ Microbiol*, *74*(23), 7286-7296. https://doi.org/10.1128/AEM.00768-08

Bush, M. J., Tschowri, N., Schlimpert, S., Flärdh, K., & Buttner, M. J. (2015). c-di-GMP signalling and the regulation of developmental transitions in streptomycetes. *Nat Rev Microbiol*, *13*(12), 749-760. https://doi.org/10.1038/nrmicro3546

Campos, S. S., Ibarra-Rodriguez, J. R., Barajas-Ornelas, R. C., Ramirez-Guadiana, F. H., Obregon-Herrera, A., Setlow, P., & Pedraza-Reyes, M. (2014). Interaction of apurinic/apyrimidinic endonucleases Nfo and ExoA with the DNA integrity scanning protein DisA in the processing of oxidative DNA damage during *Bacillus subtilis* spore outgrowth. *J Bacteriol*, *196*(3), 568-578. https://doi.org/10.1128/JB.01259-13

Chater, K. F. (2016). Recent advances in understanding *Streptomyces*. *F1000Res*, *5*, 2795. https://doi.org/10.12688/f1000research.9534.1

Chin, K. H., Liang, J. M., Yang, J. G., Shih, M. S., Tu, Z. L., Wang, Y. C., Sun, X. H., Hu, N. J., Liang, Z. X., Dow, J. M., Ryan, R. P., & Chou, S. H. (2015). Structural Insights into the Distinct Binding Mode of Cyclic Di-AMP with SaCpaA_RCK. *Biochemistry*, *54*(31), 4936-4951. https://doi.org/10.1021/acs.biochem.5b00633

Choi, P. H., Sureka, K., Woodward, J. J., & Tong, L. (2015). Molecular basis for the recognition of cyclic-di-AMP by PstA, a PII-like signal transduction protein. *Microbiologyopen*, *4*(3), 361-374. https://doi.org/10.1002/mbo3.243

Choi, P. H., Vu, T. M. N., Pham, H. T., Woodward, J. J., Turner, M. S., & Tong, L. (2017). Structural and functional studies of pyruvate carboxylase regulation by cyclic di-AMP in lactic acid bacteria. *Proc Natl Acad Sci U S A*, *114*(35), E7226-E7235. https://doi.org/10.1073/pnas.1704756114

Christen, M., Christen, B., Folcher, M., Schauerte, A., & Jenal, U. (2005). Identification and characterization of a cyclic di-GMP-specific phosphodiesterase and its allosteric control by GTP. *J Biol Chem*, *280*(35), 30829-30837. https://doi.org/10.1074/jbc.M504429200

Commichau, F. M., Gibhardt, J., Halbedel, S., Gundlach, J., & Stülke, J. (2018). A Delicate Connection: c-di-AMP Affects Cell Integrity by Controlling Osmolyte Transport. *Trends Microbiol*, *26*(3), 175-185. https://doi.org/10.1016/j.tim.2017.09.003

Commichau, F. M., Heidemann, J. L., Ficner, R., & Stülke, J. (2019). Making and Breaking of an Essential Poison: the Cyclases and Phosphodiesterases That Produce and Degrade the Essential Second Messenger Cyclic di-AMP in Bacteria. *J Bacteriol*, *201*(1). https://doi.org/10.1128/JB.00462-18

Corrigan, R. M., Abbott, J. C., Burhenne, H., Kaever, V., & Gründling, A. (2011). c-di-AMP is a new second messenger in *Staphylococcus aureus* with a role in controlling cell size and envelope stress. *PLoS Pathog*, *7*(9), e1002217. https://doi.org/10.1371/journal.ppat.1002217

Corrigan, R. M., Campeotto, I., Jeganathan, T., Roelofs, K. G., Lee, V. T., & Gründling, A. (2013). Systematic identification of conserved bacterial c-di-AMP receptor proteins. *Proc Natl Acad Sci U S A*, *110*(22), 9084-9089. https://doi.org/10.1073/pnas.1300595110

Corrigan, R. M., & Gründling, A. (2013). Cyclic di-AMP: another second messenger enters the fray. *Nat Rev Microbiol*, *11*(8), 513-524. https://doi.org/10.1038/nrmicro3069

Costantino, N., & Court, D. L. (2003). Enhanced levels of lambda Red-mediated recombinants in mismatch repair mutants. *Proc Natl Acad Sci U S A*, *100*(26), 15748-15753. https://doi.org/10.1073/pnas.2434959100

Cox, C. D., Bavi, N., & Martinac, B. (2018). Bacterial Mechanosensors. *Annu Rev Physiol*, *80*, 71-93. https://doi.org/10.1146/annurev-physiol-021317-121351

Datsenko, K. A., & Wanner, B. L. (2000). One-step inactivation of chromosomal genes in *Escherichia coli* K-12 using PCR products. *Proc Natl Acad Sci U S A*, *97*(12), 6640-6645. https://doi.org/10.1073/pnas.120163297

Davies, B. W., Bogard, R. W., Young, T. S., & Mekalanos, J. J. (2012). Coordinated regulation of accessory genetic elements produces cyclic di-nucleotides for *V. cholerae* virulence. *Cell*, *149*(2), 358-370. https://doi.org/10.1016/j.cell.2012.01.053

Derouaux, A., Halici, S., Nothaft, H., Neutelings, T., Moutzourelis, G., Dusart, J., Titgemeyer, F., & Rigali, S. (2004). Deletion of a cyclic AMP receptor protein homologue diminishes germination and affects morphological development of *Streptomyces coelicolor*. *J Bacteriol*, *186*(6), 1893-1897. https://doi.org/10.1128/jb.186.6.1893-1897.2004

Devaux, L., Sleiman, D., Mazzuoli, M. V., Gominet, M., Lanotte, P., Trieu-Cuot, P., Kaminski, P. A., & Firon, A. (2018). Cyclic di-AMP regulation of osmotic homeostasis is essential in Group B *Streptococcus*. *PLoS Genet*, *14*(4), e1007342. https://doi.org/10.1371/journal.pgen.1007342

El-Naggar, N. E., & El-Ewasy, S. M. (2017). Bioproduction, characterization, anticancer and antioxidant activities of extracellular melanin pigment produced by newly isolated microbial cell factories *Streptomyces glaucescens* NEAE-H. *Sci Rep*, *7*, 42129. https://doi.org/10.1038/srep42129

Epstein, W. (2003). The roles and regulation of potassium in bacteria. *Prog Nucleic Acid Res Mol Biol*, *75*, 293-320. https://doi.org/10.1016/s0079-6603(03)75008-9

Fahmi, T., Faozia, S., Port, G. C., & Cho, K. H. (2019). The Second Messenger c-di-AMP Regulates Diverse Cellular Pathways Involved in Stress Response, Biofilm Formation, Cell Wall Homeostasis, SpeB Expression, and Virulence in *Streptococcus pyogenes*. *Infect Immun*, *87*(6). https://doi.org/10.1128/IAI.00147-19

Fujisawa, M., Ito, M., & Krulwich, T. A. (2007). Three two-component transporters with channel-like properties have monovalent cation/proton antiport activity. *Proc Natl Acad Sci U S A*, *104*(33), 13289-13294. https://doi.org/10.1073/pnas.0703709104

Furrer, E. M., Ronchetti, M. F., Verrey, F., & Pos, K. M. (2007). Functional characterization of a NapA Na(+)/H(+) antiporter from *Thermus thermophilus*. *FEBS Lett*, *581*(3), 572-578. https://doi.org/10.1016/j.febslet.2006.12.059

Gallagher, K. A., Schumacher, M. A., Bush, M. J., Bibb, M. J., Chandra, G., Holmes, N. A., Zeng, W., Henderson, M., Zhang, H., Findlay, K. C., Brennan, R. G., & Buttner, M. J. (2020). c-di-GMP Arms an Anti-sigma to Control Progression of Multicellular Differentiation in *Streptomyces*. *Mol Cell*, *77*(3), 586-599 e586. https://doi.org/10.1016/j.molcel.2019.11.006

Gándara, C., & Alonso, J. C. (2015). DisA and c-di-AMP act at the intersection between DNA-damage response and stress homeostasis in exponentially growing *Bacillus subtilis* cells. *DNA Repair (Amst)*, *27*, 1-8. https://doi.org/10.1016/j.dnarep.2014.12.007

Gándara, C., de Lucena, D. K. C., Torres, R., Serrano, E., Altenburger, S., Graumann, P. L., & Alonso, J. C. (2017). Activity and in vivo dynamics of *Bacillus subtilis* DisA are affected by RadA/Sms and by Holliday junction-processing proteins. *DNA Repair (Amst)*, *55*, 17-30. https://doi.org/10.1016/j.dnarep.2017.05.002

Gibhardt, J., Heidemann, J. L., Bremenkamp, R., Rosenberg, J., Seifert, R., Kaever, V., Ficner, R., & Commichau, F. M. (2020). An extracytoplasmic protein and a moonlighting enzyme modulate synthesis of c-di-AMP in *Listeria monocytogenes*. *Environ Microbiol*, *22*(7), 2771-2791. https://doi.org/10.1111/1462-2920.15008

Gibhardt, J., Hoffmann, G., Turdiev, A., Wang, M., Lee, V. T., & Commichau, F. M. (2019). c-di-AMP assists osmoadaptation by regulating the *Listeria monocytogenes* potassium transporters KimA and KtrCD. *J Biol Chem*, *294*(44), 16020-16033. https://doi.org/10.1074/jbc.RA119.010046

Gomelsky, M. (2011). cAMP, c-di-GMP, c-di-AMP and now cGMP: bacteria use them all! *Mol Microbiol*, *79*(3), 562-565. https://doi.org/10.1111/j.1365-2958.2010.07514.x

Gundlach, J., Dickmanns, A., Schröder-Tittmann, K., Neumann, P., Kaesler, J., Kampf, J., Herzberg, C., Hammer, E., Schwede, F., Kaever, V., Tittmann, K., Stülke, J., & Ficner, R. (2015). Identification, characterization, and structure analysis of the cyclic di-AMP-binding PII-like signal transduction protein DarA. *J Biol Chem*, *290*(5), 3069-3080. https://doi.org/10.1074/jbc.M114.619619

Gundlach, J., Herzberg, C., Kaever, V., Gunka, K., Hoffmann, T., Weiss, M., Gibhardt, J., Thurmer, A., Hertel, D., Daniel, R., Bremer, E., Commichau, F. M., & Stülke, J. (2017). Control of potassium homeostasis is an essential function of the second messenger cyclic di-AMP in *Bacillus subtilis*. *Sci Signal*, *10*(475). https://doi.org/10.1126/scisignal.aal3011

Gundlach, J., Krüger, L., Herzberg, C., Turdiev, A., Poehlein, A., Tascon, I., Weiss, M., Hertel, D., Daniel, R., Hänelt, I., Lee, V. T., & Stülke, J. (2019). Sustained sensing in potassium homeostasis: Cyclic di-AMP controls potassium uptake by KimA at the levels of expression and activity. *J Biol Chem*, *294*(24), 9605-9614. https://doi.org/10.1074/jbc.RA119.008774

Gundlach, J., Mehne, F. M., Herzberg, C., Kampf, J., Valerius, O., Kaever, V., & Stülke, J. (2015). An Essential Poison: Synthesis and Degradation of Cyclic Di-AMP in *Bacillus subtilis*. *J Bacteriol*, *197*(20), 3265-3274. https://doi.org/10.1128/JB.00564-15

Gust, B., Challis, G. L., Fowler, K., Kieser, T., & Chater, K. F. (2003). PCR-targeted *Streptomyces* gene replacement identifies a protein domain needed for biosynthesis of the sesquiterpene soil odor geosmin. *Proc Natl Acad Sci U S A*, *100*(4), 1541-1546. https://doi.org/10.1073/pnas.0337542100

Gust, B., Chandra, G., Jakimowicz, D., Yuqing, T., Bruton, C. J., & Chater, K. F. (2004). Lambda red-mediated genetic manipulation of antibiotic-producing *Streptomyces*. *Adv Appl Microbiol*, *54*, 107-128. https://doi.org/10.1016/S0065-2164(04)54004-2

Haiser, H. J., Yousef, M. R., & Elliot, M. A. (2009). Cell wall hydrolases affect germination, vegetative growth, and sporulation in *Streptomyces coelicolor*. *J Bacteriol*, *191*(21), 6501-6512. https://doi.org/10.1128/JB.00767-09

Hallberg, Z. F., Wang, X. C., Wright, T. A., Nan, B., Ad, O., Yeo, J., & Hammond, M. C. (2016). Hybrid promiscuous (Hypr) GGDEF enzymes produce cyclic AMP-GMP (3', 3'-cGAMP). *Proc Natl Acad Sci U S A*, *113*(7), 1790-1795. https://doi.org/10.1073/pnas.1515287113

Hayashi, K., Morooka, N., Yamamoto, Y., Fujita, K., Isono, K., Choi, S., Ohtsubo, E., Baba, T., Wanner, B. L., Mori, H., & Horiuchi, T. (2006). Highly accurate genome sequences of *Escherichia coli* K-12 strains MG1655 and W3110. *Mol Syst Biol*, *2*, 2006 0007. https://doi.org/10.1038/msb4100049

He, J., Yin, W., Galperin, M. Y., & Chou, S. H. (2020). Cyclic di-AMP, a second messenger of primary importance: tertiary structures and binding mechanisms. *Nucleic Acids Res*, *48*(6), 2807-2829. https://doi.org/10.1093/nar/gkaa112

Healy, J., Ekkerman, S., Pliotas, C., Richard, M., Bartlett, W., Grayer, S. C., Morris, G. M., Miller, S., Booth, I. R., Conway, S. J., & Rasmussen, T. (2014). Understanding the structural requirements for activators of the Kef bacterial potassium efflux system. *Biochemistry*, *53*(12), 1982-1992. https://doi.org/10.1021/bi5001118

Heidemann, J. L., Neumann, P., Dickmanns, A., & Ficner, R. (2019). Crystal structures of the c-di-AMP-synthesizing enzyme CdaA. *J Biol Chem*, *294*(27), 10463-10470. https://doi.org/10.1074/jbc.RA119.009246

Hengge, R. (2009). Principles of c-di-GMP signalling in bacteria. *Nat Rev Microbiol*, *7*(4), 263-273. https://doi.org/10.1038/nrmicro2109

Hengge, R., Häussler, S., Pruteanu, M., Stülke, J., Tschowri, N., & Turgay, K. (2019). Recent Advances and Current Trends in Nucleotide Second Messenger Signaling in Bacteria. *J Mol Biol*, *431*(5), 908-927. https://doi.org/10.1016/j.jmb.2019.01.014

Herbst, S., Lorkowski, M., Sarenko, O., Nguyen, T. K. L., Jaenicke, T., & Hengge, R. (2018). Transmembrane redox control and proteolysis of PdeC, a novel type of c-di-GMP phosphodiesterase. *EMBO J*, *37*(8). https://doi.org/10.15252/embj.201797825

Hesketh, A., Chen, W. J., Ryding, J., Chang, S., & Bibb, M. (2007). The global role of ppGpp synthesis in morphological differentiation and antibiotic production in *Streptomyces coelicolor* A3(2). *Genome Biol*, *8*(8), R161. https://doi.org/10.1186/gb-2007-8-8-r161

Hildebrand, A., Remmert, M., Biegert, A., & Söding, J. (2009). Fast and accurate automatic structure prediction with HHpred. *Proteins*, *77 Suppl 9*, 128-132. https://doi.org/10.1002/prot.22499

Hong, H. J., Hutchings, M. I., Hill, L. M., & Buttner, M. J. (2005). The role of the novel Fem protein VanK in vancomycin resistance in *Streptomyces coelicolor*. *J Biol Chem*, *280*(13), 13055-13061. https://doi.org/10.1074/jbc.M413801200

Hu, J., Zhang, G., Liang, L., Lei, C., & Sun, X. (2020). Increased Excess Intracellular Cyclic di-AMP Levels Impair Growth and Virulence of *Bacillus anthracis*. *J Bacteriol*, *202*(9). https://doi.org/10.1128/JB.00653-19

Huynh, T. N., Choi, P. H., Sureka, K., Ledvina, H. E., Campillo, J., Tong, L., & Woodward, J. J. (2016). Cyclic di-AMP targets the cystathionine beta-synthase domain of the osmolyte transporter OpuC. *Mol Microbiol*, *102*(2), 233-243. https://doi.org/10.1111/mmi.13456

Huynh, T. N., Luo, S., Pensinger, D., Sauer, J. D., Tong, L., & Woodward, J. J. (2015). An HD-domain phosphodiesterase mediates cooperative hydrolysis of c-di-AMP to affect bacterial growth and virulence. *Proc Natl Acad Sci U S A*, *112*(7), E747-756. https://doi.org/10.1073/pnas.1416485112

Jones, S. E., Ho, L., Rees, C. A., Hill, J. E., Nodwell, J. R., & Elliot, M. A. (2017). *Streptomyces* exploration is triggered by fungal interactions and volatile signals. *Elife*, *6*. https://doi.org/10.7554/eLife.21738

Kim, H., Youn, S. J., Kim, S. O., Ko, J., Lee, J. O., & Choi, B. S. (2015). Structural Studies of Potassium Transport Protein KtrA Regulator of Conductance of K+ (RCK) C Domain in Complex with Cyclic Diadenosine Monophosphate (c-di-AMP). *J Biol Chem*, *290*(26), 16393-16402. https://doi.org/10.1074/jbc.M115.641340

Kol, S., Merlo, M. E., Scheltema, R. A., de Vries, M., Vonk, R. J., Kikkert, N. A., Dijkhuizen, L., Breitling, R., & Takano, E. (2010). Metabolomic characterization of the salt stress response in *Streptomyces coelicolor*. *Appl Environ Microbiol*, *76*(8), 2574-2581. https://doi.org/10.1128/AEM.01992-09

Konno, H., Yoshida, Y., Nagano, K., Takebe, J., & Hasegawa, Y. (2018). Biological and Biochemical Roles of Two Distinct Cyclic Dimeric Adenosine 3',5'-Monophosphate- Associated Phosphodiesterases in *Streptococcus mutans*. *Front Microbiol*, *9*, 2347. https://doi.org/10.3389/fmicb.2018.02347

Latoscha, A., Drexler, D. J., Al-Bassam, M. M., Bandera, A. M., Kaever, V., Findlay, K. C., Witte, G., & Tschowri, N. (2020). c-di-AMP hydrolysis by the phosphodiesterase AtaC promotes differentiation of multicellular bacteria. *Proc Natl Acad Sci U S A*, *117*(13), 7392-7400. https://doi.org/10.1073/pnas.1917080117

Latoscha, A., Drexler, D. J., Witte, G., & Tschowri, N (2021). Assessment of Diadenylate Cyclase and c-di-AMP-phosphodiesterase Activities Using Thin-layer and Ion Exchange Chromatography. *Bio Protoc*, 11(1):e3870. https://doi.org/10.21769/BioProtoc.3870

Latoscha, A., Wörmann, M. E., & Tschowri, N. (2019). Nucleotide second messengers in *Streptomyces*. *Microbiology (Reading)*, *165*(11), 1153-1165. https://doi.org/10.1099/mic.0.000846

Lentes, C. J., Mir, S. H., Boehm, M., Ganea, C., Fendler, K., & Hunte, C. (2014). Molecular characterization of the Na+/H+-antiporter NhaA from *Salmonella* Typhimurium. *PLoS One*, *9*(7), e101575. https://doi.org/10.1371/journal.pone.0101575

Liu, G., Chater, K. F., Chandra, G., Niu, G., & Tan, H. (2013). Molecular regulation of antibiotic biosynthesis in *streptomyces*. *Microbiol Mol Biol Rev*, *77*(1), 112-143. https://doi.org/10.1128/MMBR.00054-12

Lu, S., Wang, J., Chitsaz, F., Derbyshire, M. K., Geer, R. C., Gonzales, N. R., Gwadz, M., Hurwitz, D. I., Marchler, G. H., Song, J. S., Thanki, N., Yamashita, R. A., Yang, M., Zhang, D., Zheng, C., Lanczycki, C. J., & Marchler-Bauer, A. (2020). CDD/SPARCLE: the conserved domain database in 2020. *Nucleic Acids Res*, *48*(D1), D265-D268. https://doi.org/10.1093/nar/gkz991

Madeira, F., Park, Y. M., Lee, J., Buso, N., Gur, T., Madhusoodanan, N., Basutkar, P., Tivey, A. R. N., Potter, S. C., Finn, R. D., & Lopez, R. (2019). The EMBL-EBI search and sequence analysis tools APIs in 2019. *Nucleic Acids Res*, *47*(W1), W636-W641. https://doi.org/10.1093/nar/gkz268

Manikandan, K., Sabareesh, V., Singh, N., Saigal, K., Mechold, U., & Sinha, K. M. (2014). Two-step synthesis and hydrolysis of cyclic di-AMP in *Mycobacterium tuberculosis*. *PLoS One*, *9*(1), e86096. https://doi.org/10.1371/journal.pone.0086096

McCormick, J. R., & Flärdh, K. (2012). Signals and regulators that govern *Streptomyces* development. *FEMS Microbiol Rev*, *36*(1), 206-231. https://doi.org/10.1111/j.1574-6976.2011.00317.x

Mehne, F. M., Gunka, K., Eilers, H., Herzberg, C., Kaever, V., & Stülke, J. (2013). Cyclic di-AMP homeostasis in *Bacillus subtilis*: both lack and high level accumulation of the nucleotide are detrimental for cell growth. *J Biol Chem*, *288*(3), 2004-2017. https://doi.org/10.1074/jbc.M112.395491

Mehne, F. M., Schröder-Tittmann, K., Eijlander, R. T., Herzberg, C., Hewitt, L., Kaever, V., Lewis, R. J., Kuipers, O. P., Tittmann, K., & Stülke, J. (2014). Control of the diadenylate cyclase CdaS in *Bacillus subtilis*: an autoinhibitory domain limits cyclic di-AMP production. *J Biol Chem*, *289*(30), 21098-21107. https://doi.org/10.1074/jbc.M114.562066

Molle, V., Palframan, W. J., Findlay, K. C., & Buttner, M. J. (2000). WhiD and WhiB, homologous proteins required for different stages of sporulation in *Streptomyces coelicolor* A3(2). *J Bacteriol*, *182*(5), 1286-1295. https://doi.org/10.1128/jb.182.5.1286-1295.2000

Moscoso, J. A., Schramke, H., Zhang, Y., Tosi, T., Dehbi, A., Jung, K., & Gründling, A. (2016). Binding of Cyclic Di-AMP to the *Staphylococcus aureus* Sensor Kinase KdpD Occurs via the Universal Stress Protein Domain and Downregulates the Expression of the Kdp Potassium Transporter. *J Bacteriol*, *198*(1), 98-110. https://doi.org/10.1128/JB.00480-15

Müller, M., Deimling, T., Hopfner, K. P., & Witte, G. (2015). Structural analysis of the diadenylate cyclase reaction of DNA-integrity scanning protein A (DisA) and its inhibition by 3'-dATP. *Biochem J*, *469*(3), 367-374. https://doi.org/10.1042/BJ20150373

Narsing Rao, M. P., Xiao, M., & Li, W. J. (2017). Fungal and Bacterial Pigments: Secondary Metabolites with Wide Applications. *Front Microbiol*, *8*, 1113. https://doi.org/10.3389/fmicb.2017.01113

Nelson, J. W., Sudarsan, N., Furukawa, K., Weinberg, Z., Wang, J. X., & Breaker, R. R. (2013). Riboswitches in eubacteria sense the second messenger c-di-AMP. *Nat Chem Biol*, *9*(12), 834-839. https://doi.org/10.1038/nchembio.1363

Okazaki, K. I., Wöhlert, D., Warnau, J., Jung, H., Yildiz, Ö., Kühlbrandt, W., & Hummer, G. (2019). Mechanism of the electroneutral sodium/proton antiporter PaNhaP from transition-path shooting. *Nat Commun*, *10*(1), 1742. https://doi.org/10.1038/s41467-019-09739-0

Omasits, U., Ahrens, C. H., Müller, S., & Wollscheid, B. (2014). Protter: interactive protein feature visualization and integration with experimental proteomic data. *Bioinformatics*, *30*(6), 884-886. https://doi.org/10.1093/bioinformatics/btt607

Paget, M. S., Chamberlin, L., Atrih, A., Foster, S. J., & Buttner, M. J. (1999). Evidence that the extracytoplasmic function sigma factor sigmaE is required for normal cell wall structure in *Streptomyces coelicolor* A3(2). *J Bacteriol*, *181*(1), 204-211. http://www.ncbi.nlm.nih.gov/pubmed/9864331

Pham, H. T., Nhiep, N. T. H., Vu, T. N. M., Huynh, T. N., Zhu, Y., Huynh, A. L. D., Chakrabortti, A., Marcellin, E., Lo, R., Howard, C. B., Bansal, N., Woodward, J. J., Liang, Z. X., & Turner, M. S. (2018). Enhanced uptake of potassium or glycine betaine or export of cyclic-di-AMP restores osmoresistance in a high cyclic-di-AMP *Lactococcus lactis* mutant. *PLoS Genet*, *14*(8), e1007574. https://doi.org/10.1371/journal.pgen.1007574

Pinner, E., Kotler, Y., Padan, E., & Schuldiner, S. (1993). Physiological role of *nhaB*, a specific Na+/H+ antiporter in *Escherichia coli*. *J Biol Chem*, *268*(3), 1729-1734. https://www.ncbi.nlm.nih.gov/pubmed/8093613

Quintana, I. M., Gibhardt, J., Turdiev, A., Hammer, E., Commichau, F. M., Lee, V. T., Magni, C., & Stülke, J. (2019). The KupA and KupB Proteins of *Lactococcus lactis* IL1403 Are Novel c-di-AMP Receptor Proteins Responsible for Potassium Uptake. *J Bacteriol*, *201*(10). https://doi.org/10.1128/JB.00028-19

Rao, F., Ji, Q., Soehano, I., & Liang, Z. X. (2011). Unusual heme-binding PAS domain from YybT family proteins. *J Bacteriol*, *193*(7), 1543-1551. https://doi.org/10.1128/JB.01364-10

Rao, F., See, R. Y., Zhang, D., Toh, D. C., Ji, Q., & Liang, Z. X. (2010). YybT is a signaling protein that contains a cyclic dinucleotide phosphodiesterase domain and a GGDEF domain with ATPase activity. *J Biol Chem*, *285*(1), 473-482. https://doi.org/10.1074/jbc.M109.040238

Rocha, R., Teixeira-Duarte, C. M., Jorge, J. M. P., & Morais-Cabral, J. H. (2019). Characterization of the molecular properties of KtrC, a second RCK domain that regulates a Ktr channel in *Bacillus subtilis*. *J Struct Biol*, *205*(3), 34-43. https://doi.org/10.1016/j.jsb.2019.02.002

Roelofs, K. G., Wang, J., Sintim, H. O., & Lee, V. T. (2011). Differential radial capillary action of ligand assay for high-throughput detection of protein-metabolite interactions. *Proc Natl Acad Sci U S A*, *108*(37), 15528-15533. https://doi.org/10.1073/pnas.1018949108

Rørvik, G. H., Liskiewicz, K. A., Kryuchkov, F., Naemi, A. O., Aasheim, H. C., Petersen, F. C., Kuntziger, T. M., & Simm, R. (2020). Cyclic Di-adenosine Monophosphate Regulates Metabolism and Growth in the Oral Commensal *Streptococcus mitis*. *Microorganisms*, *8*(9). https://doi.org/10.3390/microorganisms8091269

Rosa-Fraile, M., Dramsi, S., & Spellerberg, B. (2014). Group B streptococcal haemolysin and pigment, a tale of twins. *FEMS Microbiol Rev*, *38*(5), 932-946. https://doi.org/10.1111/1574-6976.12071

Rubin, B. E., Huynh, T. N., Welkie, D. G., Diamond, S., Simkovsky, R., Pierce, E. C., Taton, A., Lowe, L. C., Lee, J. J., Rifkin, S. A., Woodward, J. J., & Golden, S. S. (2018). High-throughput interaction screens illuminate the role of c-di-AMP in cyanobacterial nighttime survival. *PLoS Genet*, *14*(4), e1007301. https://doi.org/10.1371/journal.pgen.1007301

Sadeghi, A., Soltani, B. M., Nekouei, M. K., Jouzani, G. S., Mirzaei, H. H., & Sadeghizadeh, M. (2014). Diversity of the ectoines biosynthesis genes in the salt tolerant *Streptomyces* and evidence for inductive effect of ectoines on their accumulation. *Microbiol Res*, *169*(9-10), 699-708. https://doi.org/10.1016/j.micres.2014.02.005

Saito, N., Xu, J., Hosaka, T., Okamoto, S., Aoki, H., Bibb, M. J., & Ochi, K. (2006). EshA accentuates ppGpp accumulation and is conditionally required for antibiotic production in *Streptomyces coelicolor* A3(2). *J Bacteriol*, *188*(13), 4952-4961. https://doi.org/10.1128/JB.00343-06

Schlimpert, S., Wasserstrom, S., Chandra, G., Bibb, M. J., Findlay, K. C., Flärdh, K., & Buttner, M. J. (2017). Two dynamin-like proteins stabilize FtsZ rings during *Streptomyces* sporulation. *Proc Natl Acad Sci U S A*, *114*(30), E6176-E6183. https://doi.org/10.1073/pnas.1704612114

Schrecker, M., Wunnicke, D., & Hänelt, I. (2019). How RCK domains regulate gating of K+ channels. *Biol Chem*, *400*(10), 1303-1322. https://doi.org/10.1515/hsz-2019-0153

Schultz, S. G., & Solomon, A. K. (1961). Cation transport in *Escherichia coli*. I. Intracellular Na and K concentrations and net cation movement. *J Gen Physiol*, *45*, 355-369. https://doi.org/10.1085/jgp.45.2.355

Schuster, C. F., Bellows, L. E., Tosi, T., Campeotto, I., Corrigan, R. M., Freemont, P., & Gründling, A. (2016). The second messenger c-di-AMP inhibits the osmolyte uptake system OpuC in *Staphylococcus aureus*. *Sci Signal*, *9*(441), ra81. https://doi.org/10.1126/scisignal.aaf7279

Shao, Z., Deng, W., Li, S., He, J., Ren, S., Huang, W., Lu, Y., Zhao, G., Cai, Z., & Wang, J. (2015). GlnR-Mediated Regulation of *ectABCD* Transcription Expands the Role of the GlnR Regulon to Osmotic Stress Management. *J Bacteriol*, *197*(19), 3041-3047. https://doi.org/10.1128/JB.00185-15

St-Onge, R. J., & Elliot, M. A. (2017). Regulation of a muralytic enzyme-encoding gene by two non-coding RNAs. *RNA Biol*, *14*(11), 1592-1605. https://doi.org/10.1080/15476286.2017.1338241

St-Onge, R. J., Haiser, H. J., Yousef, M. R., Sherwood, E., Tschowri, N., Al-Bassam, M., & Elliot, M. A. (2015). Nucleotide second messenger-mediated regulation of a muralytic enzyme in *Streptomyces*. *Mol Microbiol*, *96*(4), 779-795. https://doi.org/10.1111/mmi.12971

Stülke, J., & Krüger, L. (2020). Cyclic di-AMP Signaling in Bacteria. *Annu Rev Microbiol*, *74*, 159-179. https://doi.org/10.1146/annurev-micro-020518-115943

Stumpe, S., & Bakker, E. P. (1997). Requirement of a large K+-uptake capacity and of extracytoplasmic protease activity for protamine resistance of *Escherichia coli*. *Arch Microbiol*, *167*(2-3), 126-136. https://www.ncbi.nlm.nih.gov/pubmed/9133319

Stuttard, C. (1982) Temperate phages of *Streptomyces venezuelae*: lysogeny and host specificity shown by phages SV1 and SV2. *Microbiology* 128, 115-121.
Sun, J., Hesketh, A., & Bibb, M. (2001). Functional analysis of *relA* and *rshA*, two relA/spoT homologues of *Streptomyces coelicolor* A3(2). *J Bacteriol*, *183*(11), 3488-3498. https://doi.org/10.1128/JB.183.11.3488-3498.2001
Sureka, K., Choi, P. H., Precit, M., Delince, M., Pensinger, D. A., Huynh, T. N., Jurado, A. R., Goo, Y. A., Sadilek, M., Iavarone, A. T., Sauer, J. D., Tong, L., & Woodward, J. J. (2014). The cyclic dinucleotide c-di-AMP is an allosteric regulator of metabolic enzyme function. *Cell*, *158*(6), 1389-1401. https://doi.org/10.1016/j.cell.2014.07.046
Süsstrunk, U., Pidoux, J., Taubert, S., Ullmann, A., & Thompson, C. J. (1998). Pleiotropic effects of cAMP on germination, antibiotic biosynthesis and morphological development in *Streptomyces coelicolor*. *Mol Microbiol*, *30*(1), 33-46. https://doi.org/10.1046/j.1365-2958.1998.01033.x
Teh, W. K., Dramsi, S., Tolker-Nielsen, T., Yang, L., & Givskov, M. (2019). Increased Intracellular Cyclic di-AMP Levels Sensitize *Streptococcus gallolyticus* subsp. gallolyticus to Osmotic Stress and Reduce Biofilm Formation and Adherence on Intestinal Cells. *J Bacteriol*, *201*(6). https://doi.org/10.1128/JB.00597-18
Thomason, L. C., Sawitzke, J. A., Li, X., Costantino, N., & Court, D. L. (2014). Recombineering: genetic engineering in bacteria using homologous recombination. *Curr Protoc Mol Biol*, *106*, 1 16 11-39. https://doi.org/10.1002/0471142727.mb0116s106
Torres, R., Carrasco, B., Gándara, C., Baidya, A. K., Ben-Yehuda, S., & Alonso, J. C. (2019). *Bacillus subtilis* DisA regulates RecA-mediated DNA strand exchange. *Nucleic Acids Res*, *47*(10), 5141-5154. https://doi.org/10.1093/nar/gkz219
Tosi, T., Hoshiga, F., Millership, C., Singh, R., Eldrid, C., Patin, D., Mengin-Lecreulx, D., Thalassinos, K., Freemont, P., & Gründling, A. (2019). Inhibition of the *Staphylococcus aureus* c-di-AMP cyclase DacA by direct interaction with the phosphoglucosamine mutase GlmM. *PLoS Pathog*, *15*(1), e1007537. https://doi.org/10.1371/journal.ppat.1007537
Townsley, L., Yannarell, S. M., Huynh, T. N., Woodward, J. J., & Shank, E. A. (2018). Cyclic di-AMP Acts as an Extracellular Signal That Impacts *Bacillus subtilis* Biofilm Formation and Plant Attachment. *mBio*, *9*(2). https://doi.org/10.1128/mBio.00341-18
Tschowri, N. (2016). Cyclic Dinucleotide-Controlled Regulatory Pathways in *Streptomyces* Species. *J Bacteriol*, *198*(1), 47-54. https://doi.org/10.1128/JB.00423-15
Tschowri, N., Schumacher, M. A., Schlimpert, S., Chinnam, N. B., Findlay, K. C., Brennan, R. G., & Buttner, M. J. (2014). Tetrameric c-di-GMP mediates effective transcription factor dimerization to control *Streptomyces* development. *Cell*, *158*(5), 1136-1147. https://doi.org/10.1016/j.cell.2014.07.022
Wang, X., Cai, X., Ma, H., Yin, W., Zhu, L., Li, X., Lim, H. M., Chou, S. H., & He, J. (2019). A c-di-AMP riboswitch controlling *kdpFABC* operon transcription regulates the potassium transporter system in *Bacillus thuringiensis*. *Commun Biol*, *2*, 151. https://doi.org/10.1038/s42003-019-0414-6
Warnau, J., Wöhlert, D., Okazaki, K. I., Yildiz, Ö., Gamiz-Hernandez, A. P., Kaila, V. R. I., Kühlbrandt, W., & Hummer, G. (2020). Ion Binding and Selectivity of the Na(+)/H(+) Antiporter MjNhaP1 from Experiment and Simulation. *J Phys Chem B*, *124*(2), 336-344. https://doi.org/10.1021/acs.jpcb.9b08552
Weiden, P. L., Epstein, W., & Schultz, S. G. (1967). Cation transport in *Escherichia coli*. VII. Potassium requirement for phosphate uptake. *J Gen Physiol*, *50*(6), 1641-1661. https://doi.org/10.1085/jgp.50.6.1641
Whiteley, A. T., Eaglesham, J. B., de Oliveira Mann, C. C., Morehouse, B. R., Lowey, B., Nieminen, E. A., Danilchanka, O., King, D. S., Lee, A. S. Y., Mekalanos, J. J., & Kranzusch, P. J. (2019). Bacterial cGAS-like enzymes synthesize diverse nucleotide signals. *Nature*, *567*(7747), 194-199. https://doi.org/10.1038/s41586-019-0953-5
Whiteley, A. T., Garelis, N. E., Peterson, B. N., Choi, P. H., Tong, L., Woodward, J. J., & Portnoy, D. A. (2017). c-di-AMP modulates *Listeria monocytogenes* central metabolism to regulate growth, antibiotic resistance and osmoregulation. *Mol Microbiol*, *104*(2), 212-233. https://doi.org/10.1111/mmi.13622
Witte, C. E., Whiteley, A. T., Burke, T. P., Sauer, J. D., Portnoy, D. A., & Woodward, J. J. (2013). Cyclic di-AMP is critical for *Listeria monocytogenes* growth, cell wall homeostasis, and establishment of infection. *mBio*, *4*(3), e00282-00213. https://doi.org/10.1128/mBio.00282-13
Witte, G., Hartung, S., Büttner, K., & Hopfner, K. P. (2008). Structural biochemistry of a bacterial checkpoint protein reveals diadenylate cyclase activity regulated by DNA recombination intermediates. *Mol Cell*, *30*(2), 167-178.
Woodward, J. J., Iavarone, A. T., & Portnoy, D. A. (2010). c-di-AMP secreted by intracellular *Listeria monocytogenes* activates a host type I interferon response. *Science*, *328*(5986), 1703-1705. https://doi.org/10.1126/science.1189801
Wooten, A. K., Shenoy, A. T., Arafa, E. I., Akiyama, H., Martin, I. M. C., Jones, M. R., Quinton, L. J., Gummuluru, S., Bai, G., & Mizgerd, J. P. (2020). Unique Roles for *Streptococcus pneumoniae* Phosphodiesterase 2 in Cyclic di-AMP Catabolism and Macrophage Responses. *Front Immunol*, *11*, 554. https://doi.org/10.3389/fimmu.2020.00554
Yang, J., Bai, Y., Zhang, Y., Gabrielle, V. D., Jin, L., & Bai, G. (2014). Deletion of the cyclic di-AMP phosphodiesterase gene (cnpB) in *Mycobacterium tuberculosis* leads to reduced virulence in a mouse model of infection. *Mol Microbiol*, *93*(1), 65-79. https://doi.org/10.1111/mmi.12641

Ye, M., Zhang, J. J., Fang, X., Lawlis, G. B., Troxell, B., Zhou, Y., Gomelsky, M., Lou, Y., & Yang, X. F. (2014). DhhP, a cyclic di-AMP phosphodiesterase of *Borrelia burgdorferi*, is essential for cell growth and virulence. *Infect Immun*, *82*(5), 1840-1849. https://doi.org/10.1128/IAI.00030-14

Yin, W., Cai, X., Ma, H., Zhu, L., Zhang, Y., Chou, S. H., Galperin, M. Y., & He, J. (2020). A decade of research on the second messenger c-di-AMP. *FEMS Microbiol Rev*, *44*(6), 701-724. https://doi.org/10.1093/femsre/fuaa019

Zarrella, T. M., Yang, J., Metzger, D. W., & Bai, G. (2020). Bacterial Second Messenger Cyclic di-AMP Modulates the Competence State in *Streptococcus pneumoniae*. *J Bacteriol*, *202*(4). https://doi.org/10.1128/JB.00691-19

Zeden, M. S., Kviatkovski, I., Schuster, C. F., Thomas, V. C., Fey, P. D., & Gründling, A. (2020). Identification of the main glutamine and glutamate transporters in *Staphylococcus aureus* and their impact on c-di-AMP production. *Mol Microbiol*, *113*(6), 1085-1100. https://doi.org/10.1111/mmi.14479

Zeden, M. S., Schuster, C. F., Bowman, L., Zhong, Q., Williams, H. D., & Gründling, A. (2018). Cyclic di-adenosine monophosphate (c-di-AMP) is required for osmotic regulation in *Staphylococcus aureus* but dispensable for viability in anaerobic conditions. *J Biol Chem*, *293*(9), 3180-3200. https://doi.org/10.1074/jbc.M117.818716

Zhang, L., & He, Z. G. (2013). Radiation-sensitive gene A (RadA) targets DisA, DNA integrity scanning protein A, to negatively affect cyclic Di-AMP synthesis activity in *Mycobacterium smegmatis*. *J Biol Chem*, *288*(31), 22426-22436. https://doi.org/10.1074/jbc.M113.464883

Zhang, L., Li, W., & He, Z. G. (2013). DarR, a TetR-like transcriptional factor, is a cyclic di-AMP-responsive repressor in *Mycobacterium smegmatis*. *J Biol Chem*, *288*(5), 3085-3096. https://doi.org/10.1074/jbc.M112.428110

Zheng, C., Ma, Y., Wang, X., Xie, Y., Ali, M. K., & He, J. (2015). Functional analysis of the sporulation-specific diadenylate cyclase CdaS in *Bacillus thuringiensis*. *Front Microbiol*, *6*, 908. https://doi.org/10.3389/fmicb.2015.00908

Zhu, Y., Pham, T. H., Nhiep, T. H., Vu, N. M., Marcellin, E., Chakrabortti, A., Wang, Y., Waanders, J., Lo, R., Huston, W. M., Bansal, N., Nielsen, L. K., Liang, Z. X., & Turner, M. S. (2016). Cyclic-di-AMP synthesis by the diadenylate cyclase CdaA is modulated by the peptidoglycan biosynthesis enzyme GlmM in *Lactococcus lactis*. *Mol Microbiol*, *99*(6), 1015-1027. https://doi.org/10.1111/mmi.13281

Zimmermann, L., Stephens, A., Nam, S. Z., Rau, D., Kübler, J., Lozajic, M., Gabler, F., Söding, J., Lupas, A. N., & Alva, V. (2018). A Completely Reimplemented MPI Bioinformatics Toolkit with a New HHpred Server at its Core. *J Mol Biol*, *430*(15), 2237-2243. https://doi.org/10.1016/j.jmb.2017.12.007

# Appendix

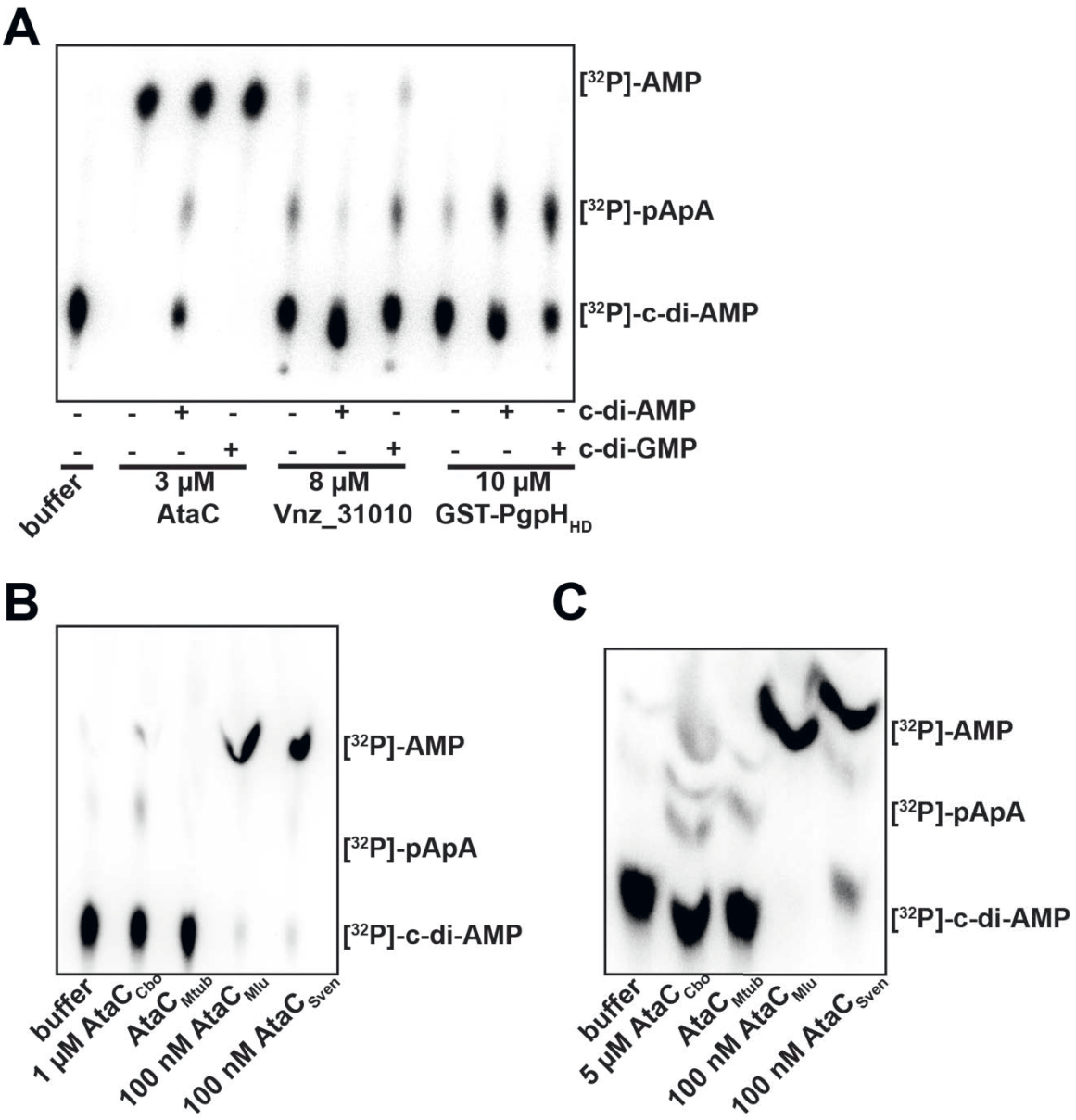


**Figure A1: PDE activity of Vnz_31010 and different AtaC orthologues.**

Indicated protein concentrations were used in the assays. For $AtaC_{Mtub}$, a concentration measurement was not possible, hence 19.5 µl of dialyzed protein were used. The buffer lanes show migration of [$^{32}$P]-c-di-AMP. **(A)** Cleavage of [$^{32}$P]-c-di-AMP in competition with 100 µM unlabeled nucleotides. Unlabeled nucleotides were added on ice before starting the reaction with 4 nM [$^{32}$P]-c-di-AMP. Only unlabeled c-di-AMP significantly interfered with cleavage of [$^{32}$P]-c-di-AMP by AtaC, demonstrating c-di-AMP specificity. Also, cleavage by 8 µM Vnz_31010 was inhibited only by c-di-AMP. **(B)** and **(C)** PDE activity of AtaC orthologues using different protein concentrations ($AtaC_{Cbo}$) or purifications ($AtaC_{Mtub}$). $AtaC_{Cbo}$ and $AtaC_{Mtub}$ show only low activity towards 2 nM [$^{32}$P]-c-di-AMP, whereas $AtaC_{Mlu}$ has a similar activity like $AtaC_{Sven}$, which was used as a positive control.

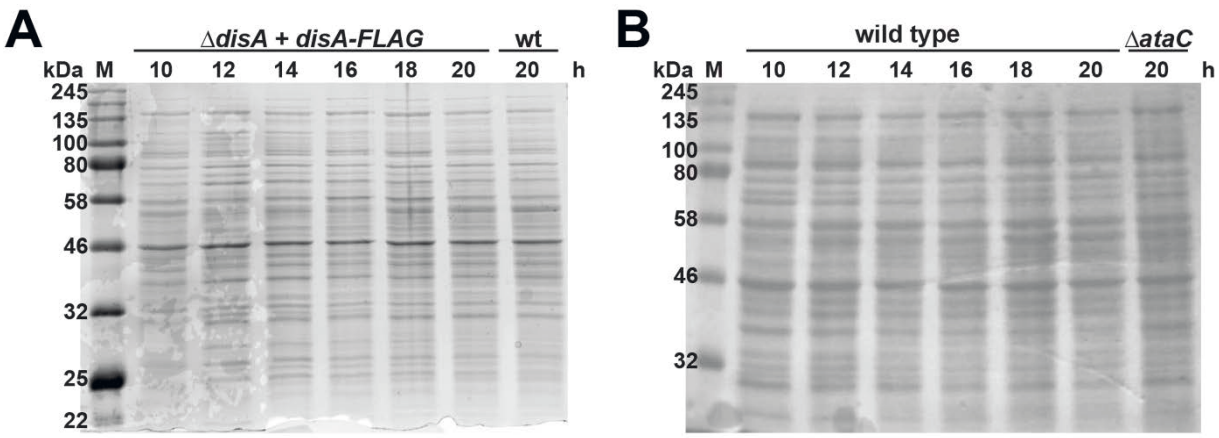


**Figure A2: Loading controls for Western blot analysis of DisA-FLAG and AtaC expression patterns in Figure 6 B and C, respectively.**

**(A)** A Δ*disA* strain was complemented with the integrative pIJ10770 vector containing C-terminally FLAG-tagged *disA* allowing expression under control of the *disA* native promoter from the $attB_{\Phi BT1}$ integration site. **(B)** AtaC expression was analyzed in *S. venezuelae* wild type. Samples were taken regularly (every 2 hours) during growth in liquid sporulation medium (MYM) at 30 °C. Wild type and Δ*ataC* samples at 20 h of growth were included as negative controls for the respective Western Blots. For DisA-FLAG and AtaC detection, 5 and 10 µg whole cell lysates were used, respectively. For each immunoblot detection, samples were loaded on two different SDS PAGE gels and separated at 50 mA for 40-50 min. Gels dedicated as control for loading control (A and B) were stained with Coomassie, whereas the second gels were Western Blotted and developed using α-FLAG (Figure 6B) or α-AtaC antiserum (Figure 6C) as the primary antibodies, respectively.

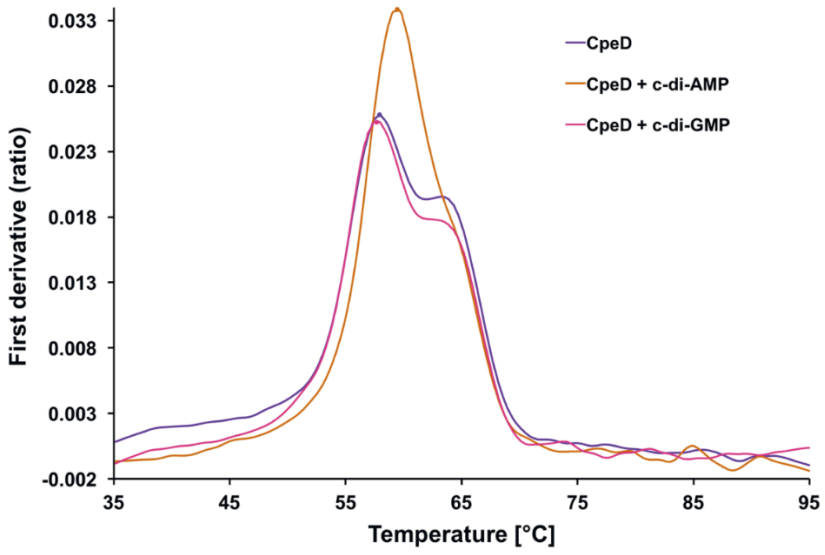


**Figure A3: nanoDSF of full-length CpeD.**

Data are presented as the first derivative of the unfolding curve of 5 µM full-length CpeD without ligands (purple) and supplemented with 1 mM c-di-AMP (orange) or c-di-GMP (pink). Only addition of c-di-AMP increases the inflection point Ti (59.5 °C with c-di-AMP vs. 57.9 °C) whereas c-di-GMP has no effect (57.7 °C with c-di-GMP vs. 57.9 °C), suggesting that CpeD preferentially binds c-di-AMP.

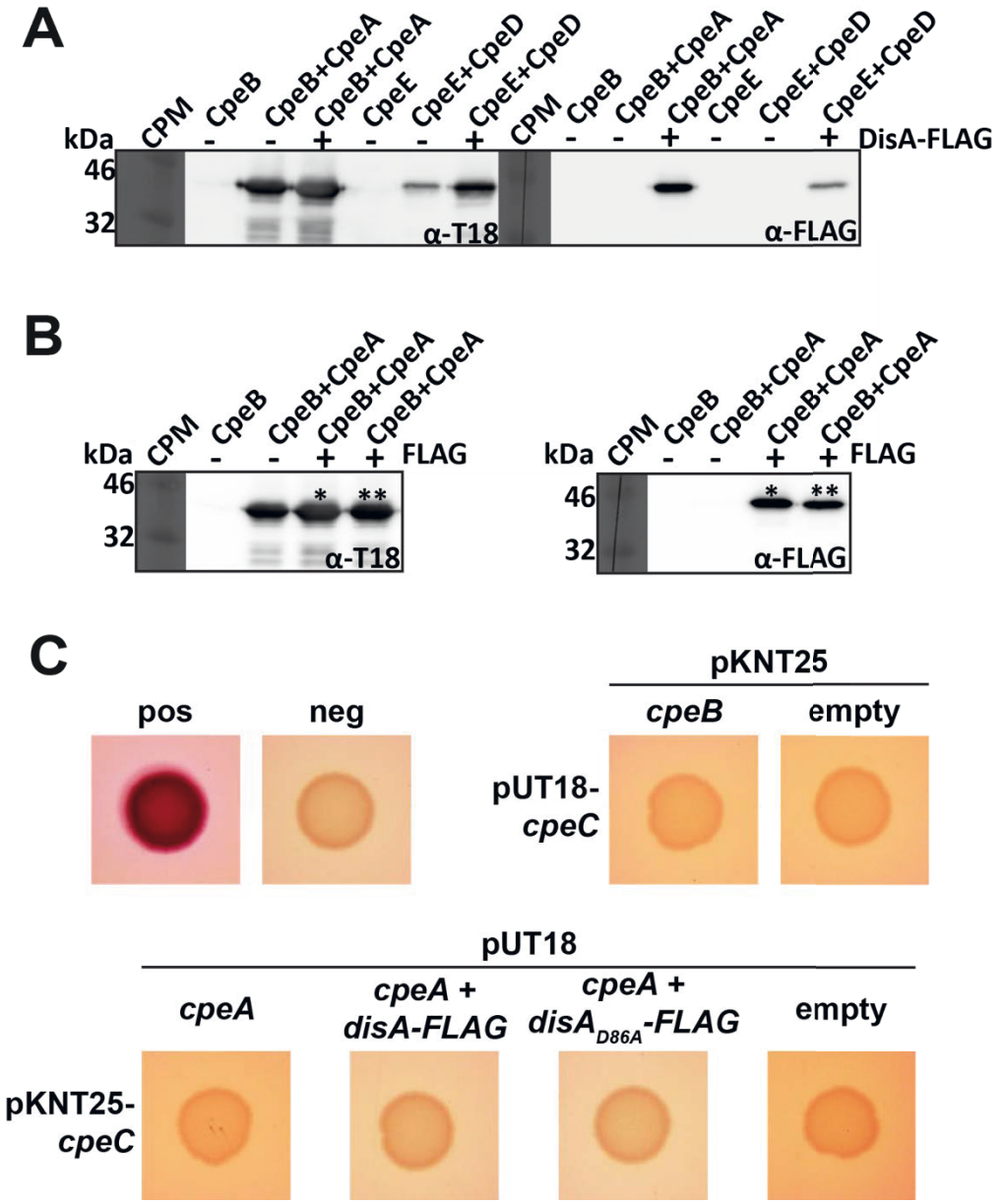


**Figure A4: Expression of T18 fusion proteins and FLAG-tagged DisA variants, and *in vivo* interaction studies with CpeC.**

**(A)** and **(B)** Detection of CpeA-T18, CpeD-T18, DisA-FLAG and $DisA_{D86A}$-FLAG in *E. coli* W3110 Δ*cya* strains. 2 µg total protein were separated on 12% SDS gels, SemyDry Western blotted and protein expression was detected. To detect T18-fusions, the monoclonal 3D1 mouse antibody was used. Detection of FLAG-tagged DisA (*) or $DisA_{D86A}$ (**) was performed with a monoclonal mouse α-FLAG antibody. Strains containing only pKNT25-*cpeB* or pKNT25-*cpeE* were used as negative controls. **(C)** *E coli* W3110 Δ*cya* strains containing the indicated construct combinations were spotted on Difco MacConkey agar supplemented with 1 % maltose and incubated at 26 °C for 48 h. A strain containing empty vectors was used as negative control and a strain carrying the leucine zipper part of the yeast GCN4 protein was used as a positive control. CpeC did not interact with CpeB or CpeA.

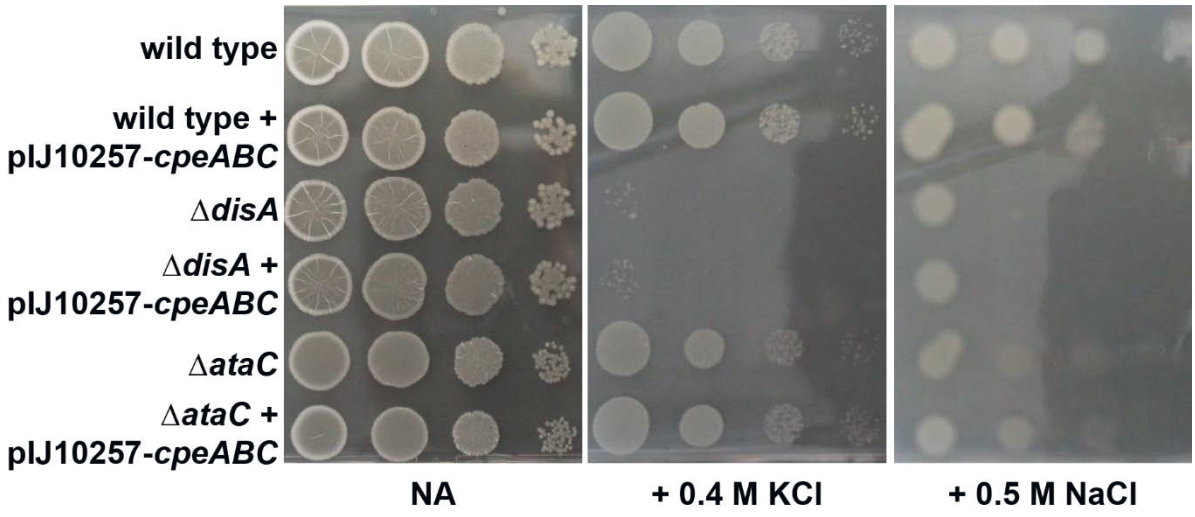


**Figure A5: Growth of *S. venezuelae* strains expressing *cpeABC* under control of the strong constitutive promoter *ermE*p* from the *attB*$_{\Phi BT1}$ site on NA supplemented with 0.4 M KCl or 0.5 M NaCl.**

CFU of Δ*disA* and Δ*ataC* were re-adjusted (in comparison to Figure 19A) and serially diluted before spotting on plates. No differences in growth compared to control strains (without pIJ10257-cpeABC) could be observed. Note that the plate supplemented with 0.5 M NaCl is slightly out of focus.

**A**

| # | Capillary label | Ti#1 | Ti#2 | Ti#3 | Initial Ratio | Δ Ratio | Sample Brightness |
|---|---|---|---|---|---|---|---|
| 1 | 12665 | 51.4 | 61.5 | | 0.8626 | 0.0502 | 152.2 |
| 2 | 12665 + c-di-AMP | 51.4 | 61.9 | | 0.8788 | 0.0347 | 100.1 |
| 3 | 14905 | 52.3 | 62.7 | 87.7 | 0.8454 | 0.0605 | 208.1 |
| 4 | 14905 + c-di-AMP | 50.9 | 62.6 | | 0.8591 | 0.0574 | 137 |
| 5 | 27460 | 55.4 | 65.4 | | 0.7977 | 0.1119 | 723.5 |
| 6 | 27460 + c-di-AMP | 55.3 | 65.3 | | 0.8008 | 0.1092 | 492.1 |

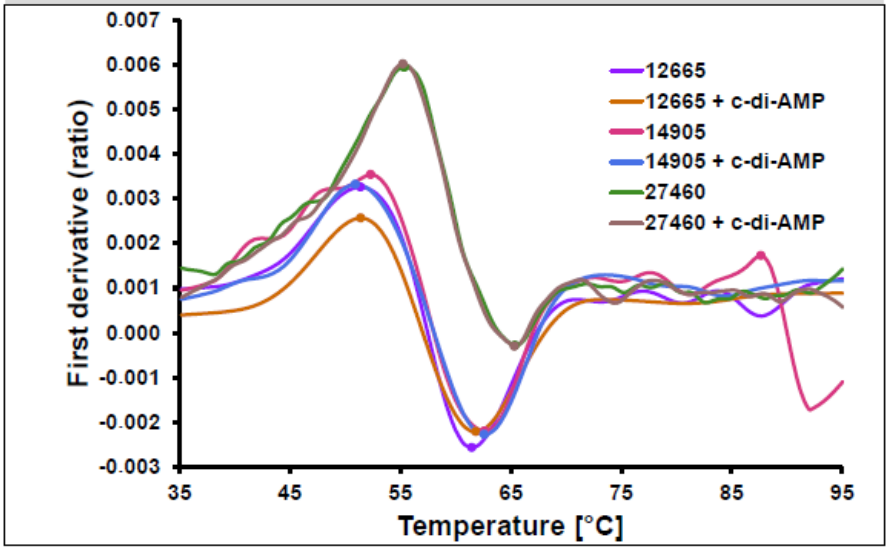


**B**

| # | Capillary label | Ti#1 | Ti#2 | Ti#3 | Initial Ratio | Δ Ratio | Sample Brightness |
|---|---|---|---|---|---|---|---|
| 1 | 28040 | 53.6 | 64.4 | | 0.8641 | 0.0212 | 78.9 |
| 2 | 28040 + c-di-AMP | 54.2 | 64.8 | | 0.9011 | -0.0192 | 53.9 |

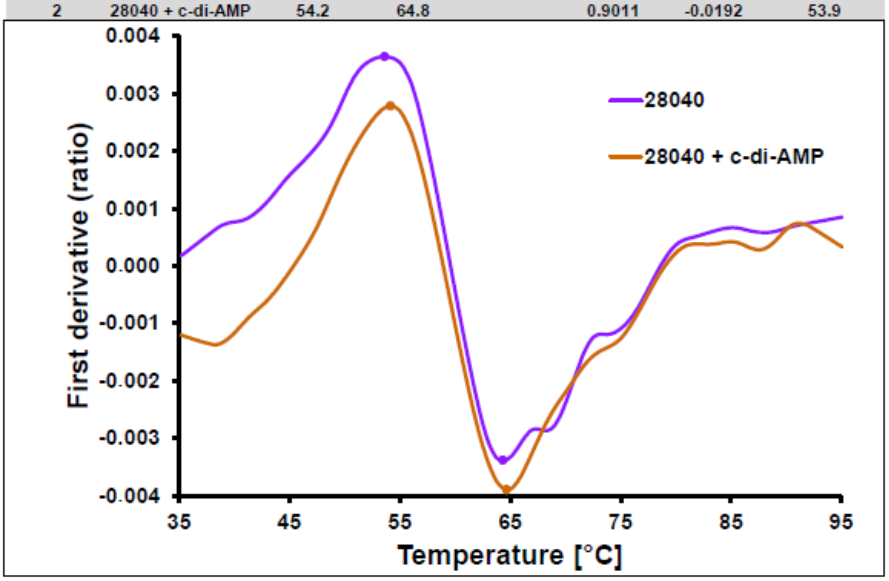


**Figure A6: nanoDSF of predicted cytosolic domains from *S. venezuelae* RCK_C domain proteins.**
**(A)** 5 µM Vnz_12665$_{183-380}$, Vnz_14905$_{380-507}$ and Vnz_27460 were incubated with 1 mM c-di-AMP. Addition of c-di-AMP has no positive effect on the inflection points (Ti) compared to untreated samples. **(B)** 5 µM Vnz_28040$_{390-506}$ were incubated with 1 mM c-di-AMP. Addition of c-di-AMP has no significant positive effect on the inflection points (Ti) compared to untreated sample. The first derivatives of the unfolding curves are shown.

# Declaration

I hereby declare that I completed the doctoral thesis independently based on the stated resources and aids.

I have not applied for a doctoral degree elsewhere and do not have a corresponding doctoral degree.

I have not submitted the doctoral thesis, or parts of it, to another academic institution and the thesis has not been accepted or rejected.

I declare that I have acknowledged the Doctoral Degree Regulations which underlie the procedure of the Faculty of Life Sciences of Humboldt-Universität zu Berlin, as amended on 5th March 2015.

Furthermore, I declare that no collaboration with commercial doctoral degree supervisors took place, and that the principles of Humboldt-Universität zu Berlin for ensuring good academic practice were abided by.

Berlin, 15.12.2020 Andreas Latoscha